ANALYSIS OF PERFORMANCE DATA AND COMPUTER MODELING OF SOLAR ENERGY SYSTEMS

by

DAVID K. LUICK

A thesis submitted in partial fulfillment of the
requirements for the degree of

MASTER OF SCIENCE
(Mechanical Engineering)

at the

UNIVERSITY OF WISCONSIN-MADISON

1987

ANALYSIS OF PERFORMANCE DATA AND COMPUTER MODELING OF SOLAR ENERGY SYSTEMS

by David Luick

Under the Supervision of Professor William A. Beckman

Once installed many solar energy systems do not perform as well as simulation programs predict. This work studies two residential, active solar energy systems to try and determine reasons why predicted and experimental results differ. The two systems studied had been instrumented and data recorded over a years time as part of the National Solar Data Network program (NSDN). This work also looked at the experimental data to determine how useful the data was since over 200 hundred different residential sites have been instrumented and data recorded.

The major problems encountered when using the experimental data was a lack of documentation on the system components (i.e. pump and pipe sizes, heat exchanger specifications, etc.). This made it very difficult to compare simulation results against the experimental data, since someone running a simulation program would have only the factory specifications on the system components. Without the factory specifications many parameters had to be estimated. Also problems were encountered with the data itself. Energy balances on the main storage tank did not balance for either system. This occurred in one system due to a faulty temperature sensor; however, the other system was supposed to have worked well, and it could not be determined why the energy balances did not close.

Since the tank energy balances did not close the experimental data was used to calculate the ASHRAE test parameters ($F_R(\tau\alpha)_n$, F_RU_L, and b_o) to determine how well the ASHRAE test results would predict the field performance of the collector. The results indicated that ASHRAE parameters would underpredict the performance of the system. These results put further doubt on the experimental data since the installed

systems usually performing below expectations, not above them.

Two main conclusions were drawn from this work. First, due to the lack of documentation on many of the NSDN systems and other problems encountered, it is not recommended that the data be used if other data is available. Second, when trying to make comparisons between actual and predicted performance either accurate data must be available with documentation on all of the system components or else the data should be measured at the same time as the system is modeled so that when differences arise the experimental sensors can be checked to be sure that they are not causing the problems. Otherwise it is nearly impossible to determine why differences occur between the experimental and predicted results since the errors could be due to inaccurate data.

APPROVED:

July 21, 1987
Date

William A Beckman
William Beckman, Professor
Mechanical Engineering

ACKNOWLEDGEMENTS

Thanks go to Professors Duffie, Beckman, Klein, and Mitchell for giving me the opportunity to work in the Solar Lab and for always being ready to answer questions. I would especially like to thank Professors Duffie and Beckman for their guidance on my project.

Special thanks go to the students in the lab without whom the lab would have been a very dreary place. Without their listening ability, many suggestions, and happy faces I would never have gotten through this thesis. They also deserve many thanks for putting up with me.

Funding for this project was provided by the Solar Energy Research Institute (SERI). Thanks for your support.

As a final note, the results and conclusions presented in this thesis do not even begin to show what I have learned during my stay in the lab. The problems encountered while completing my thesis has taught me a lot about research, people, and life in general. Thanks to all who made it possible.

TABLE OF CONTENTS

LIST OF FIGURES

LIST OF TABLES

NOMENCLATURE

Note: symbols which appear only once in the text and are defined locally are not defined here.

A_c	collector area
b_o	incidence angle modifier coefficient (one of the three parameters used to describe the collector's characteristics)
C_p	heat capacity of a fluid
F_RU_L	one of the three parameters used to describe the collector's characteristics
$F_R(\tau\alpha)$	one of the three parameters used to describe the collector's characteristics
G_{test}	flow rate through the collector per collector area during the ASHRAE test
I	solar radiation
$K_{\tau\alpha}$	incidence angle modifier
$\dot{m}$	fluid flow rate
OP	operating point
P	pump
Q	energy term
T	temperature

GREEK

α	absorptance
ε	effectiveness
θ	beam radiation incidence angle
η	collector efficiency
τ	transmittance

SUBSCRIPTS

a	ambient
c	cold
coil	inside the heat exchanger coil
col	collector
env	environment
exp	experimental
h	hot
i	inlet
max	maximum
min	minimum
mon	over a months time
n	normal
o	outlet
T	tilted surface
u	useful

I. INTRODUCTION

I.1 BACKGROUND

As part of the Department of Energy's (DOE) active heating and cooling (AHAC) program the National Solar Data Network (NSDN) was developed to monitor the performance of installed, operating solar heating systems. Within this program over 200 different residential solar heating systems were instrumented and data collected in an attempt to improve the understanding of energy systems, develop criteria used to evaluate system performance, look at ways to improve the overall system or components, and estimate the fuel savings that would occur using solar energy systems.

As the data was collected the performance of the systems were analyzed by calculating the energy flows through the system in order to determine the system performance, including the amount of energy supplied by the solar energy system to the load and the fuel savings incurred. This was done on all of the systems and gave information as to how the systems performed. All site instrumentation, data collection, and analysis was performed by Vitro Corp. located in Silver Spring, Maryland.

I.2 PURPOSE

It has been shown (e.g. Vitro Report 0802-84/01, "Actual Versus Design Performance of Solar Systems in the NSDN, 9/84") that a large majority of installed, active solar energy systems perform well below predictions; therefore, the purpose of this study was to model some of the NSDN solar energy systems using TRNSYS [1], a modular simulation program, making comparisons between the system and

component model results and the experimental data results. This was done to determine reasons for any differences between the model and experimental results. The purpose of this work was also to determine the usefulness of the NSDN data for this study and future projects.

I.3 OVERVIEW OF REMAINING CHAPTERS

Chapter 2 describes the experimental data detailing how the NSDN data was collected, validated, and analyzed. General problems with the data are also presented. Chapter 3 presents the simulation program (TRNSYS) used to model the systems, how the data was "fixed" so that it was compatible with TRNSYS, and the collector model program (used to study the collector performance). Chapter 4 covers collector model theory, including the ASHRAE 93-77 test and two different methods used to calculate the collector model parameters from the experimental data. Chapters 5 and 6 present the results from the analysis done on the Trident and Honeywell solar energy systems. The first three sections of both chapters contain similar sections that describe the system, give an analysis of the experimental data, and present the results of the collector model comparisons with the experimental data. An immersed heat exchanger model was developed for the Trident system with the development and results presented in the last section of Chapter 5. The last section of Chapter 6 presents results from a TRNSYS model of the Honeywell system. Chapter 7 presents the conclusions and recommendations for the two systems and for the usefulness of the NSDN data.

II. EXPERIMENTAL DATA

II.1 NSDN DATA

Each site monitored in the NSDN program was instrumented with temperature sensors, fluid flow meters, insolation meters, and other miscellaneous sensors. An example of the sensor types and locations can be seen in figure (5.3.1) and are described in table (5.1.1) of section (V.1.1). Every 5 minutes 20 seconds a micro-processor data logger, referred to as the Site Data Acquisition System (SDAS), records all of the sensor readings in a data "record". Each record contains the month, day, time, miscellaneous site information, and all of the data sensor readings that occurred at that moment and during the previous timestep. The SDAS reads an analog voltage input from each channel (one sensor per channel), converts it into a digital signal which is then recorded on a cassette tape. It was possible for the SDAS to take up to 10 samples of a particular variable during each timestep and average the results. This was always done for the solar radiation readings but in most cases the other data readings were the instantaneous values read at the end of each time interval.

The site recorded data was transmitted to the Central Data Processing System (CDPS), located at Vitro, over voice-grade telephone lines through a modem. The CDPS simply dials the SDSA and has it transmit the data. The data transmission took approximately fifteen minutes. During the time data was being transmitted to the CDPS no data measurements could be made at the site; therefore, a data gap of two to three timesteps always occurred during each data transfer. This was originally done once each day, but as the number of sites being monitored decreased this was changed to once every two days since a certain amount of data had to be received before processing could begin.

The CDPS converted the digital information into engineering units (EU) and then

recorded it to await further processing. Once enough data had been recorded, the data were analyzed using a set of site specific equations that calculate the energy flow through the system. The program computed the various performance factors on an hourly, daily, and monthly basis.

II.2 GENERAL PROBLEMS WITH THE DATA

II.2.1 Data Validation

Vitro performed two types of data validation 1) informal and 2) formal. Informal data validation is done by the analyst and is based on the analyst's experience. For example, if a flow reading was six gpm in a loop containing a four gpm pump, something is obviously wrong. A more subtle example would be if the energy delivered to the tank from the collector seems high or low when compared to other days or weeks. Formal validation is done by calculating energy balances on the various subsystems and components and making sure they balance within the expected data accuracy. The energy flows can also be compared to the flows predicted by theory.

Other miscellaneous checks done by Vitro include:

- ♦ comparing two temperature readings from sensors located in the same pipe or duct when no energy flows or transfers are occuring to determine if the sensors are reading accurately;

- ♠ comparing the temperature increase or decrease between two temperature sensors when an amount of energy has been added or subtracted from the fluid between the sensors;

- ♥ checking heat exchanger effectiveness;

- comparing environmental data with other sites and/or weather stations in the same area.

When errors or discrepancies were found the sensor was checked out if possible and fixed or replaced. Any "bad" data readings were usually left on the data tape, but a note was made of it in the significant events and/or sensor work-around sheets which contain a listing of all the sensor and general system problems. Appendix (1) contains these lists for the Trident and Honeywell systems.

II.2.2 Missing Data

The main problem with using the NSDN data is that during all of the months there are some data missing. By data missing, it is meant that the entire record of data was not recorded and is not written on the data tape. (The explanation given in this subsection does not include times when a pump broke or a temperature sensor went bad. In those cases (as explained in the previous section) whatever reading was recorded is still put on the data tape. The discussion in this subsection refers only to times when entire data records are missing.) As an example, table (2.1.2) could represent the data file during a day where each line represents a data record (for simplicity in this example assume that the data readings occur at 5 minute intervals). From the table it can be seen that a single data reading (where a "reading" means that all of the sensors were recorded in a data record) was missed at 12:15 and 5 readings were missed between 12:30 and 13:00. Each of these gaps demonstrates what is meant by missing data. There are no "place holders" or markers (i.e. zeros or blank lines) inserted into the data file to replace the missing records. The only way to tell when a data gap has occurred is to calculate the time interval between successive records in the data file.

TABLE 2.1.2 Example of a data file with missing records.

data file line number	time
1	12:00 pm
2	12:05
3	12:10
4	12:20
5	12:25
6	12:30
7	13:00
etc.	

The data gaps can be attributed to one of the following reasons:

1) data is being transmitted from the SDAS tape drive to the CDPS computer (no site measurements are taken when transmission is occuring);

2) reason #1 and the SDAS tape drive locked up after transmitting the stored data to the CDPS;

3) power failure or system controller errors causing the solar energy system to shut down.

The first problem occurs every time the temporarily stored site data is transmitted back to the CDPS. When the data is being transmitted the SDAS does not record any site data. Depending on which system was being monitored this could occur every day or every two days. It is easy to spot this in the data since the data dump occurred at the same time of the day and usually caused two or three data readings to be missed. The second problem was caused by the SDAS itself. Sometimes after transmitting the

stored data from its tape drive the SDAS would lock up, and the only way to start it again would be to manually push the reset button located on the machine. Since the monitored houses were unoccupied this was not always done right away. Also it was not always known right away that the SDAS had locked up. This problem is inherent in the data logger used and there was no way to fix it except to push the reset button. The third reason refers to times when the entire solar energy system shut down due to a power failure or if an error occurred in the system controller that caused the entire solar energy system to shut down. In the case of a power failure the reset button on the data logger would have to be pushed before more data could be recorded even if the power returned and the solar system restarted. In the case where the entire system shut down the data recorded would be meaningless since only stagnation temperatures would have been recorded.

II.2.3 INACCURACIES IN THE MEASUREMENTS

Obtaining accurate measurements of the air flow rate and temperature in ducts was a problem during collection of the NSDN data. To accurately measure the air temperature in a duct, the temperature profile of the duct cross section must be made and the sensor placed at the point where the average profile temperature is found. A similar procedure must be carried out to determine the velocity of the air and should be done in a long straight duct or a duct using flow straighteners. Although Vitro performed these two types of measurements with care, the results still showed significant errors. This error can be determined by calculating energy balances across a water-to-air heat exchanger. Using the water and air temperature and flow measurements the energy lost by the fluid on one side and the energy gain by the fluid on the other can be calculated using:

$$Q = \sum_{month} \dot{m} C_p (T_{out} - T_{in}) \qquad (2.3.1)$$

This was done for the Trident systems space heating loop for February through March with the monthly totals given in table (2.3.1). The results consistently show a large discrepancy between the water and air sides and Vitro recommends in their reports that when calculating energy balances and energy flows, water side measurements should be used whenever possible.

TABLE 2.3.1 Monthly energy transfer across the space heating loop water-to-air heat exchanger calculated using the water side and air side temperature and flow measurements. (Trident)

	Q_{water} (Btu)	Q_{air} (Btu)
Feb	51,400	6,300
Mar	12,000	8,000
Apr	22,000	13,600
May	20,600	12,800

III. SYSTEM MODELING

Computer simulation programs are very useful for designing solar energy systems. It is possible to simulate many different system configurations to determine which one will give the best performance. This eliminates the need to actually build the systems, saving both time and money. This chapter describes the simulation program used, and the problems overcome using experimental data to drive it.

III.1 SIMULATION PROGRAM

This study uses a modular, transient simulation program called TRNSYS [1]. It is a versatile program allowing the user to model many different types of energy systems in many different configurations. Presently the program can be used to model active and passive solar energy systems, HVAC systems, and some power plant systems.

The main advantage of TRNSYS is its modularity. Instead of modeling a system as a single large complex program, TRNSYS models the system as a set of subroutines where each subroutine numerically describes the performance of a single component of the system. The subroutines are interconnected through an executive program. This makes it very easy for the user to change the system configuration by adding or by removing components or rerouting their inputs and outputs.

The simulation runs by inputting a forcing function, which for solar systems usually consists of meteorological data. These values are read in at a predetermined, constant time interval. Although the driving data is input at a specified time interval, the executive program does not have to step through the simulation at this same time interval as it solves the equations defining the system. The time interval used to step

through the simulation is called a timestep and is determined by the user.

An interesting capability of TRNSYS is that the timestep used for numerically integrating the system equations does not have to be equal to the data input interval. TRNSYS accounts for the difference by linearly interpolating the input data to coincide with the integration timestep. For example, the forcing function data can be input at hourly intervals, while the simulation increments through the simulation solving the system equations every five minutes (or whatever timestep desired). This makes it possible to observe the short term behavior of the system even though the driving data is only available at longer time intervals. If driving data is available at shorter time intervals, it should be used since less interpolation is needed.

III.2 DRIVING TRNSYS WITH EXPERIMENTAL DATA

As stated in the previous section TRNSYS is driven by environmental data which must be input at constant time intervals throughout the entire simulation. This presents a problem since there are many gaps in the NSDN data (see section II.2.2). This problem is solved in one of two ways depending on the type of components included in the simulation. If none of the simulation components include storage capabilities the data gaps can be filled in with zeros. This can be done since nonstorage components calculate the energy gains and transfers based only on the present timestep inputs; therefore, if zeros are input, no gains or transfers will be calculated. This is the same as if the data gap had been skipped. This approach is used when the collector model is used to determine the collector parameters, $F_R(\tau\alpha)_n$ and $F_R U_L$, from the experimental data (see section IV.2.1)).

This approach could also be used with decks containing storage components, but the results would not be comparable to the experimental data, if the data gaps occur when the storage component would normally gain or lose energy. This is shown in the

following example. Consider a solar system consisting of a collector, pump, and storage tank, and assume that the driving data contains a three hour gap from 11:00 am until 2:00 pm. Also assume that during this gap the experimental system actually collected energy, but due to a problem the data was not recorded. If the missing data is filled with zeros, the simulation will continue to run from 11:00 to 2:00, but no energy will be collected since the solar radiation has been set to zero. If both the simulation and experimental tank temperatures were originally 100° F at 11:00, at 2:00 the simulation tank temperature will be slightly less than 100° and the experimental tank temperature will be much larger than 100°. This occurs since even though the simulation tank is not gaining energy it is still loosing energy to the environment, the experimental tank also had losses to the environment but for this example it was also gaining energy, causing it to end up with a higher temperature. This can lead to significant errors in the system performance depending on the length of the data gaps and when they occur.

Due to the problems noted above a different method was needed. After looking at the data it was found that most of the gaps were either less than six hours or greater than seventeen hours in length, so it was decided to fill in the gaps less than six hours and restart the deck for gaps larger than that. This minimizes the number of starts and stops required to no more than three times per month.

A program was written to fill in the gaps by linearly interpolating the temperature and insolation values from the timesteps before and after the gap. Load flow rates are filled in differently depending on whether they were DHW or space heating loads. The houses for the two systems looked at in this study were not occupied; therefore, a simulated DHW load was mechanically induced with preset amounts of flow occurring at three specific times during the day. Knowing this, the DHW loads were manually corrected in the data file during any gaps that occurred. It is not possible to determine what the space heating load was during the gaps; therefore, the load was assumed to be

zero.

Linearly interpolating the data in the manner described above will cause errors if the data gap occurs at sunrise, sunset, or noon. However, even at these times a linear interpolation was done since it was not possible to determine exactly when the sun rose in the morning, went down at night, or how high the insolation value was at noon. Typically most of the data gaps were less than one hour in length; therefore, interpolating the data in this manner did not cause any problems.

IV. COLLECTOR THEORY

This chapter looks at how solar collector performance is predicted and two different methods that can be used to compare the predicted and experimental performance. The first two sections of the chapter introduce a reduced parameter model used to predict collector performance and the test procedure used to determine the model parameters. The last two sections describe the two comparison methods and the problems associated with each of them.

IV.1 THEORETICAL COLLECTOR PERFORMANCE AND TESTING

IV.1.1 Collector Model

The analysis of most flat plate collectors can be done using the Hottel-Whillier equation, which calculates the actual useful energy gain by the collector. It is written as:

$$Q_u = \underbrace{A_c F_R}_{(3)}\Big[\underbrace{I_T(\tau\alpha)_n K_{\tau\alpha}}_{(1)} - \underbrace{U_L(T_i - T_a)}_{(2)}\Big] \qquad (4.1.1)$$

where:

A_c = collector area

F_R = can be thought of as a collector effectiveness, the ratio between the actual useful energy gain and the maximum useful energy gain, if the

collector plate is at the fluid inlet temperature

I_T = solar radiation incident on the tilted surface of the collector

$(\tau\alpha)_n$ = the transmittance absorptance product incorporating the collectors optical properties at normal incidence

$K_{\tau\alpha}$ = the incidence angle modifier, which corrects $(\tau\alpha)_n$ to the actual incidence angle of the beam radiation

U_L = the heat loss coefficient of the collector

T_i = collector inlet fluid temperature

T_a = ambient temperature around the collector

Together parts (1) and (2) of this equation represent the maximum possible amount of useful energy gain by the collector per unit area, given the operating temperatures and a radiation intensity. Part (1) describes the energy gained by the collector from the solar radiation and part (2) describes the losses to the environment by the collector, assuming that the entire collector plate is at the inlet fluid temperature. This assumption causes the mean plate temperature to be higher than T_i resulting in the environmental losses being too small. To correct for this the multiplier F_R (part (3)) is included in the equation and works the same way as an effectiveness term in a heat exchanger.

In its general form the Hottel-Whillier equation is dependent on many different parameters as shown below:

$$F_R = f(F', U_L, \dot{m}, A_c)$$
$$(\tau\alpha)_n = f(n,KL)$$
$$K_{\tau\alpha} = f(b_o,\theta)$$
$$U_L = f(n,\beta,k,l,KL,w)$$

where:

F' = Collector efficiency factor, the ratio between the actual useful energy gain and the maximum useful energy gain, if the collector plate is at the local fluid temperature. In turn, F' is a function of the collector tube diameter, spacing, thickness, and material.

$\dot{m}$ = mass flow rate through the collector

n = number of collector covers

b_o = incidence angle modifier coefficient

θ = beam radiation incidence angle

β = collector tilt

k = collector insulation conductivity

l = collector insulation thickness

KL = product of the extinction coefficient (K) and the thickness (L) of a single collector cover

w = wind speed

Predicting collector performance on so many different parameters would entail a great deal of time and complexity, and that is assuming all of them are known. It turns out that the model can be simplified by combining F_R, $(\tau\alpha)_n$, and U_L into $F_R(\tau\alpha)_n$ and F_RU_L and approximating $K_{\tau\alpha}$ as:

$$K_{\tau\alpha} = 1 - b_o\left(\frac{1}{\cos\theta} - 1\right) \qquad (4.1.2)$$

where $F_R(\tau\alpha)_n$, F_RU_L, and b_o[1] are all constant values determined by the ASHRAE

93-77 test (see next section). The assumption that $F_R(\tau\alpha)_n$ and F_RU_L are constant implies the following:

1) the dependence of U_L on temperature and wind speed is ignored;

2) the dependence of F_R on U_L is ignored;

3) changes in the incidence angle, due to variations in the proportions of the beam, diffuse, and ground reflected components of the solar radiation, are ignored.

Approximating $K_{\tau\alpha}$ by equation (4.1.2) works well for the range $0° > \theta > 60°$. At larger angles equation (4.1.2) no longer holds and in this work $K_{\tau\alpha}$ is approximated by a straight line drawn from the $K_{\tau\alpha}$ value calculated at 60° to $K_{\tau\alpha}$ equals zero at 90°. As an example, figure (4.1) shows how $K_{\tau\alpha}$ varies as a function of the incidence angle for the Trident system, where b_o is 0.162.

The assumptions made to simplify the collector model equations have an effect on the short term collector performance when $\theta > 60°$, but this seldom occurs and when it does, the relative energy contribution to system output is very small. Thus the reduced parameter collector model is adequate for long term predictions.

IV.1.2 ASHRAE 93-77 Test

The ASHRAE 93-77 test [2] is a standardized method used to calculate the three collector parameters $F_R(\tau\alpha)_n$, F_RU_L, and b_o. The test is carried out in two parts, $F_R(\tau\alpha)_n$ and F_RU_L are calculated in the first, and b_o during the second.

The procedure used to calculate $F_R(\tau\alpha)_n$ and F_RU_L is developed in the following

[1]Everywhere in this thesis the sign on the value b_o is determined by equation (4.1.2). This is the form of the equation used in the TRNSYS collector model.

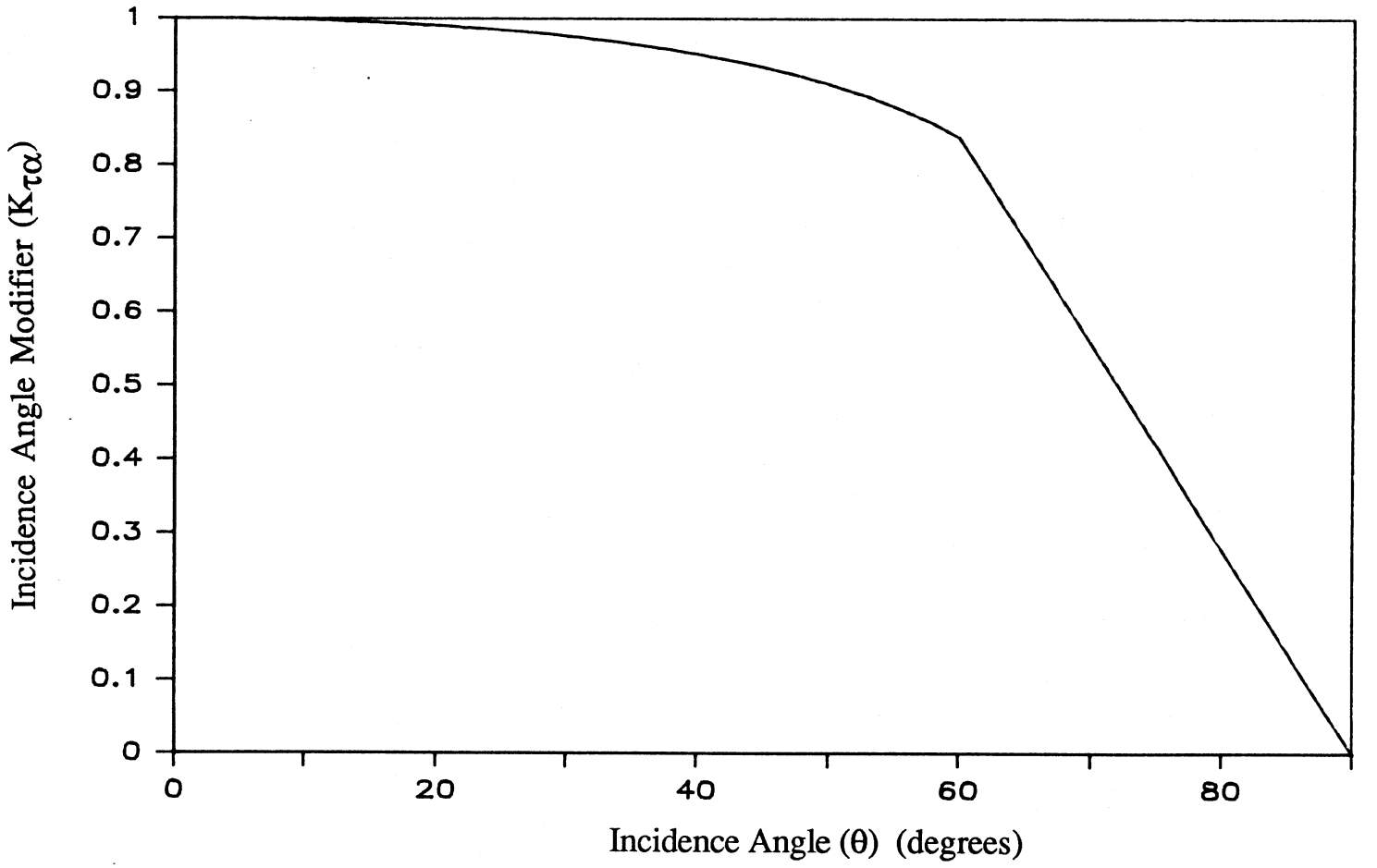

FIGURE 4.1 Example of the incidence angle modifier as a function of the beam radiation incidence angle.

manner. In general, collector performance can be experimentally determined by exposing an operating collector to solar radiation and measuring the inlet and outlet temperatures, and the fluid flow rate. The experimental useful energy gain can then be calculated as:

$$Q_{u,exp} = \dot{m}C_p(T_o - T_i) \qquad (4.1.3)$$

where:

$\dot{m}$ = collector fluid mass flow rate

C_p = collector fluid heat capacity

T_i = collector fluid inlet temperature

T_o = collector fluid outlet temperature

At the same time the solar radiation on the tilted collector (I_T) and the ambient temperature (T_a) are measured. These values are used to calculate the instantaneous efficiency (η_i) and operating point [$(T_i - T_a)/I_T$] of the collector which are defined by rearranging the Hottel-Whillier equation (4.1.1) into the form:

$$\eta_i = \frac{Q_u}{A_c I_T} = F_R(\tau\alpha)_n - F_R U_L \frac{(T_i - T_a)}{I_T} \qquad (4.1.4)$$

where $K_{\tau\alpha}$ is not shown since the radiation measurements are made when the beam radiation is approximately normal to the collector when $K_{\tau\alpha}$ is approximately equal to one. The tests are carried out at various inlet temperatures and the efficiencies plotted as a function of the operating point. By assuming that $F_R(\tau\alpha)_n$ and $F_R U_L$ are

constant, a linear curve fit of the data points will have an intercept of $F_R(\tau\alpha)_n$ and a slope of $-F_RU_L$.

The incidence angle modifier coefficient b_o (and ultimately the relationship between $K_{\tau\alpha}$ and the incidence angle) is found using the same test setup. The idea behind this part of the test can also be seen by starting with the Hottel-Whillier equation. The collector test is run with the collector inlet temperature set equal to the ambient temperature, causing the F_RU_L term to drop out of the equation. The equation can now be rearranged into the form:

$$K_{\tau\alpha} = \frac{\eta}{F_R(\tau\alpha)_n} \qquad (4.1.5)$$

The denominator $F_R(\tau\alpha)_n$ has already been found during the first part of the test; therefore, the efficiency, and then $K_{\tau\alpha}$, can be calculated from data at various incidence angles. Then plotting $K_{\tau\alpha}$ as a function of $[(1/\cos\theta) - 1]$ and linearly curve fitting the data will give b_o. The incidence angles used to determine b_o are 30, 45, and 60° for outdoor tests and 0, 30, 45, and 60° for indoor tests. (The difference between indoor and outdoor tests is explained later). As an example, figure (4.2) shows how $K_{\tau\alpha}$ varies as a function of $[(1/\cos\theta) - 1]$ for the Trident system collectors, where b_o is 0.162.

The actual test can be made either at an indoor or outdoor test facility. Although both the indoor and outdoor tests use the same test procedure the results are not always comparable. During indoor testing it is possible to hold the solar radiation (simulated by a source that produces radiant energy similar to solar radiation), wind speed (simulated by a fan), and incidence angle constant throughout the testing. Outdoors the radiation, wind speed, and incidence angle may be constantly changing during a test and/or from one test to the next. Also in the outdoor tests the "sky" temperature may be

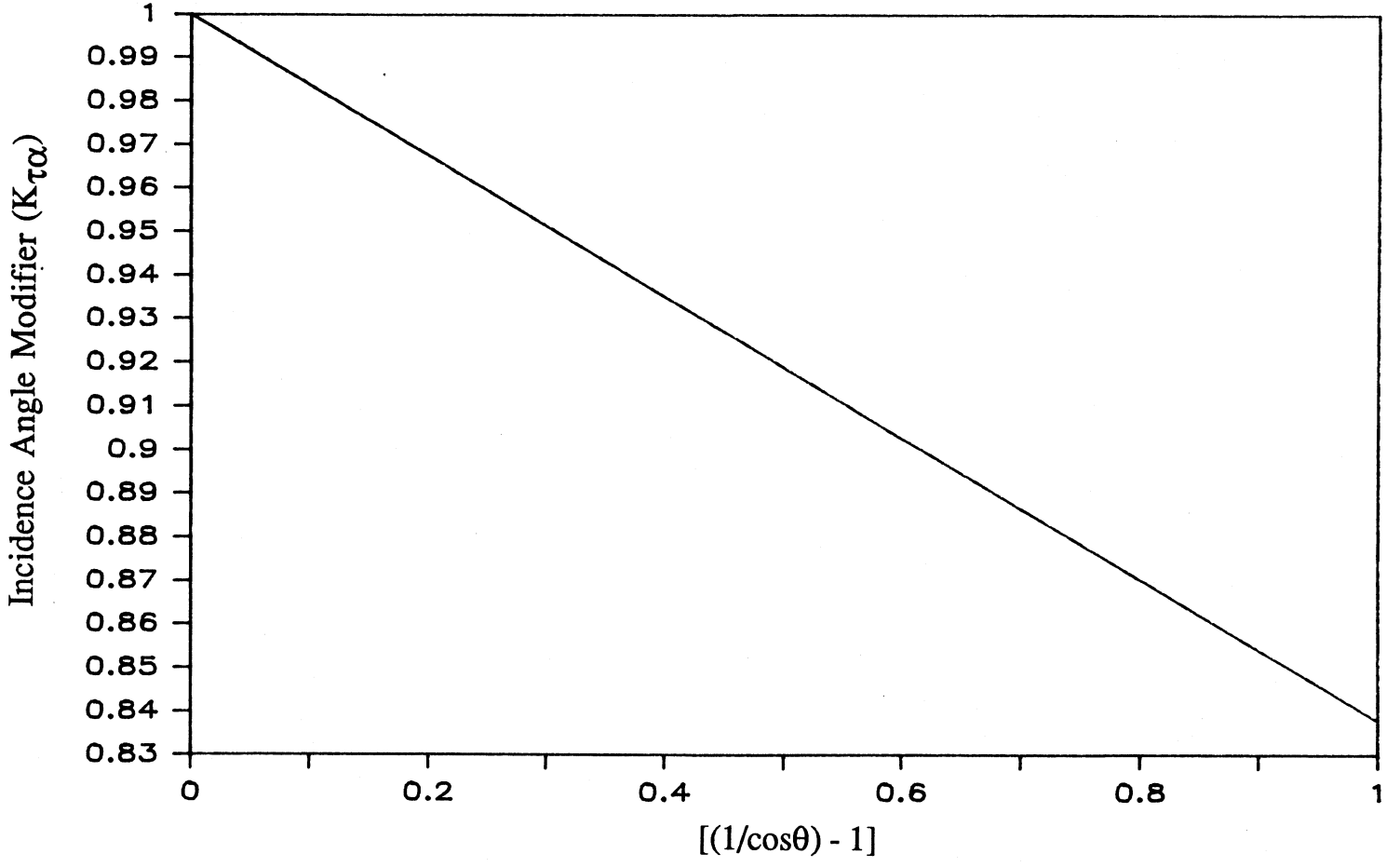

FIGURE 4.2 Example of the incidence angle modifier ($K_{\tau\alpha}$) as a function of [(1/cos θ) -1].

changing during the testing causing the radiation losses from the collector to vary (indoors the "sky" seen by the collector is the building walls which do not vary much during testing).

To try and overcome the variations stated above, the outdoor tests are usually conducted near mid-day with a clear sky and the beam radiation nearly normal to the test panel. By conducting the tests under these conditions the $F_R(\tau\alpha)$ value in equation (4.1.1) could be written with the subscript "n" (depicting normal incidence angle) which explains why $K_{\tau\alpha}$ was assumed equal to unity. When the collector has reached steady state conditions, the data (used to calculate the efficiency and operating point values) are recorded in nearly symmetrical pairs about solar noon. The resulting pairs are then averaged to minimize the heat capacity effects of the collector.

It should be noted that the area term (A_c) in equation (4.1.1) can either be the collector gross or aperture area, so long as the same area measurement is used consistently in all future calculations when the collector parameters are used. Gross area is defined as the total area occupied by the collector including the collector supports or housing. Aperture area is defined as the unobstructed cover area or the total cover area less the area of the cover supports. For the ASHRAE tests conducted on the two systems looked at in this work, the aperture area was used.

IV.2 COLLECTOR PERFORMANCE FROM EXPERIMENTAL DATA

When running simulations of a solar energy system, typically the ASHRAE test values ($F_R(\tau\alpha)_n$, F_RU_L, and b_o) are used in the collector model; however, it is not usually known if the test parameters actually represent the collector characteristics of the operating field collectors, which may have changed due to degradation of the collector material, dirt or snow on the collector, edge effects, etc. Therefore it was desired as

part of this thesis to calculate the collector parameters ($F_R(\tau\alpha)_n$ and F_RU_L) from the experimental data and compare them to the ASHRAE test results to determine how well the ASHRAE values represent the characteristics of the field collectors. (No attempt is made to calculate b_o from the experimental data; therefore, the ASHRAE test b_o value was used in all calculations).

Two different methods were used to calculate the collector parameters. The purpose of this subsection is to explain how $F_R(\tau\alpha)_n$ and F_RU_L were calculated from the experimental data. Also described is the manner in which the experimental data were "screened" by each method to account for data taken at times when the experimental collector was operating at conditions different (i.e. non steady state flow, varying incidence angle, wind, and sky conditions) from those under which the ASHRAE test were conducted.

IV.2.1 Efficiency Method

The efficiency method calculates $F_R(\tau\alpha)_n$ and F_RU_L using essentially the same procedure as used in the ASHRAE tests. The main difference is that the experimental data is first screened to try and remove all data recorded under conditions different from those encountered during the ASHRAE test.

Before calculating the $F_R(\tau\alpha)_n$ and F_RU_L values for all months the two main criteria and screening method #1 (explained later) were applied to the data to determine if averaging the efficiency values and operating point values calculated over a specified number of consecutive timesteps during which flow has occurred would produce better results. For example, if the data were averaged over 13 consecutive timesteps this means that the data records are checked one by one to determine if they meet the two main screening criteria (described below). When 13 consecutive records of data had

been found that met the screening criteria, the efficiency and operating point values were calculated for each record and then averaged to give a single efficiency - operating point pair. This was done for an entire month and the results linearly curvefit to determine the $F_R(\tau\alpha)_n$ - F_RU_L pair for the screening method and efficiency - operating point equations used. (These equations are also explained later.) The number of consecutive timesteps averaged ranged from 13 (1.15 hours) to a single timestep (0.0888888 hours). Once the best number of timesteps for averaging was determined, that number of timesteps was used to average the data for all the rest of the $F_R(\tau\alpha)_n$ - F_RU_L calculations.

The purpose for averaging the data was to try and smooth out any short term variations in the recorded data values. An example of a short term variation is when something happens to the system at the end of the timestep just before the data is recorded, in which case all values read instantaneously at the end of the timestep (i.e. temperatures) will change due to the variation. However values such as the solar radiation, which was averaged over the entire timestep, would not be affected as much. Therefore the radiation value would not reflect the sudden short term variance in the operating conditions causing the efficiency and operating point values to be in error.

Also averaging the data would smooth out the collector capacitance effects that would be reflected in the data measurements when the collector starts and stops running.

The two main criteria that the experimental data had to meet before before being used in the collector parameter calculation are listed below:

1) The collector flow was continuous during the entire timestep.

2) The solar insolation was greater that zero during the entire timestep.

In addition to the two main criteria (which were always applied to the data), four different screening methods were individually applied to the data to determine if the results from one of them compared better with the ASHRAE test results. The four screening methods are:

1) Apply the two main criteria and average the efficiency and operating point values over "X" number of consecutive timesteps (where "X" is determined as explained earlier in this section).

2) Average the data over "X" number of timesteps, as in #1, except exclude the first and last timestep in the averaging.

3) Average the data over "X" number of timesteps, as in #1, except exclude the first two and last two timesteps in the averaging.

4) Average the data over "X" number of timesteps, as in #1, except when applying the two main criteria also exclude data with a radiation incidence angle less than 40°.

The first criterion was used to remove data taken when the collector was not running, and to remove data recorded before the collector had reached steady state conditions (this should remove most of the times when capacitence effects would show in the data measurements). The second criterion was used since both the efficiency and operating point equations have I_T in the denominator. At first it may not seem possible that the collector would be running when the solar radiation was zero, but due to heat capacitance effects there are times when the collector had enough energy to continue delivering energy to the tank.

The first screening method only applied the two main criteria to the data. Both the second and third screening methods are the same as the first, only not all of the timesteps were averaged. For example, if the data was being averaged over 11 consecutive timesteps, instead of averaging all 11 timesteps to get the efficiency and operating point values, the first and last timestep were ignored and only timesteps 2 thru 10 were averaged. The same approach was used for screening method three except that, assuming 11 timesteps were used, only timesteps 3 thru 9 would be averaged. The reason for doing this was to try and make sure that the collector has reached steady state conditions. Full flow occuring before and after the data being averaged should guarantee that the averaged data was at steady state conditions, or at least as steady state as the collector will get.

The fourth screening method requires that in addition to the two main criteria, all the timesteps must have a beam radiation incidence angle less than 40°. The reason for choosing 40° as the cutoff incidence angle can be seen in figure (4.1) which shows how $K_{\tau\alpha}$ varies with the incidence angle. At $\theta < 40°$, $K_{\tau\alpha}$ is greater than 0.95; therefore, assuming that $K_{\tau\alpha}$ equals one at incidence angles less than 40° should not add much error.

One of the problems encountered when using experimental data in the efficiency method is that the sun does not shine continuously on the collector for two or three hours every day; therefore, depending on both the criteria used to eliminate undesired data and the number of timesteps averaged when calculating each efficiency-operating point value, the resulting total number of points for each month varies. (This can be seen for the Trident system by looking at the "#pts" column in table (5.3.13).) Also for many months the operating point does not vary, leaving a small cluster of points to be curvefit. This affects the fit and a few "bad" points can change the slope of the curve fit substantially. Thus, the collector parameters will be determined for each of the procedures listed above, on both a month by month and a yearly basis.

After the data was screened, two different sets of efficiency and operating point equations were used to calculate two different $F_R(\tau\alpha)_n$ - F_RU_L pairs. The first set (from here on referred to as set "a") are exactly the same as those used in the ASHRAE test. The second set (set "b") include the incidence angle modifier ($K_{\tau\alpha}$). Both sets of equations are shown below where (η) is the efficiency and (OP) is the operating point:

"a" equations:

$$\eta_a = \frac{Q_u}{A_c I_T}, \quad OP_a = \frac{(T_i - T_a)}{I_T} \tag{4.2.1}$$

"b" equations:

$$\eta_b = \frac{Q_u}{A_c I_T K_{\tau\alpha}}, \quad OP_b = \frac{(T_i - T_a)}{I_T K_{\tau\alpha}} \tag{4.2.2}$$

With four different screening methods and two sets of efficiency - operating point equations, a total of eight $F_R(\tau\alpha)_n$ - F_RU_L pairs were calculated for each month. However this does not necessarily mean that all eight pairs will be compared to the ASHRAE test values; the number compared depends on how different the four screening method results are from each other.

The following nomenclature is used throughout the rest of this thesis to identify which screening method and set of efficiency - operating point equations were used to calculate the $F_R(\tau\alpha)_n$ - F_RU_L results. If the results were calculated using screening method #1 and efficiency equations (4.2.1), then the results are said to have been calculated using "method (1a)". If screening method #3 was used with efficiency equations (4.2.2), then the results were calculated using "method (3b)", and so on.

IV.2.2 Collector Model Method

The $F_R(\tau\alpha)_n$ and F_RU_L values calculated from the experimental data using the efficiency method varied from month to month and did not use all of the available data. Therefore, an alternative method was developed that would use more of the experimental data giving a single $F_R(\tau\alpha)_n$ and F_RU_L pair that represented the collector characteristics over the entire year or other period for which data are available.

Development of this method started by determining how $F_R(\tau\alpha)_n$ and F_RU_L are used to calculate the useful energy gain of the collector. It was reasoned that if the collector parameters can be used to calculate the energy gain from the collector, then knowing the energy gain it would be possible to work backwards and find the $F_R(\tau\alpha)_n$ and F_RU_L values that describe the experimental field collector characteristics. These parameter values can then be compared to the ASHRAE test values to determine if the field collector is performing better or worse than the ASHRAE test indicated.

Rewriting the Hottel-Whillier equation (4.1.1):

$$Q_u = A_cF_R\left[I_T(\tau\alpha)_nK_{\tau\alpha} - U_L(T_i - T_a)\right] \qquad (4.1.1)$$

This is used to calculate the useful energy gain of the collector over a period of time when the solar radiation on the tilted collector surface (I_T), the collector inlet fluid temperature (T_i), and the ambient temperature (T_a) are known and are (or assumed to be) constant. Over this same period of time the actual energy gain can be calculated from the experimental data using equation (4.1.3) rewritten below:

$$Q_{u,exp} = \dot{m}C_p(T_o - T_i) \qquad (4.1.3)$$

Equating the experimental energy gain with equation (4.1.1) gives

$$Q_{exp} = A_c I_T K_{\tau\alpha} F_R(\tau\alpha)_n - A_c(T_i - T_a)F_R U_L \qquad (4.2.3)$$

where the coefficients can be grouped into the variables A and B, which are constant for a given timestep, giving

$$Q_{exp} = (A)\, F_R(\tau\alpha)_n - (B)\, F_R U_L \qquad (4.2.4)$$

There are an infinite number of $F_R(\tau\alpha)_n$ - $F_R U_L$ pairs that will satisfy this equation. This presents a problem since it is not possible to determine which pair represent the characteristics of the collector being used. However, by following the same procedure explained above for the next timestep, a different set of $F_R(\tau\alpha)_n$ - $F_R U_L$ pairs can be found and so on for all of the timesteps where an energy gain has occurred. The $F_R(\tau\alpha)_n$ - $F_R U_L$ pairs for each timestep form a line, and ideally the lines from all of the timesteps will intersect at a single point giving the two collector parameters that describe the collector. To illustrate this, an example is shown below, where the $F_R(\tau\alpha)_n$ - $F_R U_L$ lines are calculated for three separate timesteps, plotted, and the collector characteristics determined. (All of the values given in the example represent experimentally measured values.)

Example 4.1:

Timestep #1 (5 minutes 20 seconds)

Ac	=	309	ft^2	T_i	=	100	°F
I_T	=	200	Btu/ft^2	T_a	=	80	°F

$K_{\tau\alpha}$ = 1 $\qquad\qquad$ Q_{exp} = 32,754 Btu

timestep #2: -everything is the same as in #1 except:

T_i = 120 °F

Q_{exp} = 28,484 Btu

timestep #3: -everything is the same as in #1 except:

I_T = 150 Btu/ft^2

Q_{exp} = 23,484 Btu

Plugging the first timestep values into equation (4.1.1) yields

$$32{,}754 = \left[309(200)\right] F_R(\tau\alpha)_n - \left[309(100 - 80)\right] F_R U_L \quad (4.2.5a)$$

which can be rearranged into the form of a line as

$$F_R U_L = 10.0\, F_R(\tau\alpha)_n - 5.3 \quad (4.2.5b)$$

Doing the same thing for timesteps 2 and 3 yields

$$F_R U_L = 5.0\, F_R(\tau\alpha)_n - 2.3 \quad (4.2.6)$$

$$F_R U_L = 7.5\, F_R(\tau\alpha)_n - 3.8 \quad (4.2.7)$$

These three lines are plotted in figure (4.3) and when solved simultaneously yield $F_R(\tau\alpha)_n = 0.6$ and $F_RU_L = 0.7$ (Btu/hr-ft^2-°F). Since the experimental values used in this example where originally calculated using $F_R(\tau\alpha)_n = 0.6$ and $F_RU_L = 0.7$ (Btu/hr-ft^2-°F) these results were expected, thus showing that the lines do intersect at a single point for the ideal case. In reality, any of the measured parameters (I_T, T_i, T_a, Q_{exp}) may have errors in them (i.e. sensor drift, short term anomalies, etc.). (See section (II.2) for a more detailed discussion of sensor errors.) This will change the slope and/or y-intercept of the $F_R(\tau\alpha)_n$ - F_RU_L lines and they will not all meet at a single point; therefore, the equations are solved to find the $F_R(\tau\alpha)_n$ - F_RU_L pair that "best fits" all of the equations.

Two problems arise when calculating the collector parameters as explained above. First, doing this over a month would require that the procedure be done for between 500 and 1500 timesteps, and then an equal number of $F_R(\tau\alpha)_n$ - F_RU_L lines would all need to be solved simultaneously. It can be done but is not worth the effort as explained next. Second, the data would have to be screened as in the efficiency method to remove all timesteps that do not have continuous flow. If they were not removed (in the efficiency method) the collector capacitance would have a significant effect on the Q_{exp} term. This is not desired since part of the purpose of this method was to try and include all of the available data.

To overcome these problems the same approach described above was used except that it was done over an entire month instead of for each individual timestep. This gives twelve $F_R(\tau\alpha)_n$ - F_RU_L curves for the year which could be curve fit to find the collector characteristics for the entire year. This would be very useful when doing yearly system simulations because a single set of $F_R(\tau\alpha)_n$ - F_RU_L values are needed, and the values calculated in this manner would represent the field characteristics and performance of the collector which may be different from those obtained from the ASHRAE test.

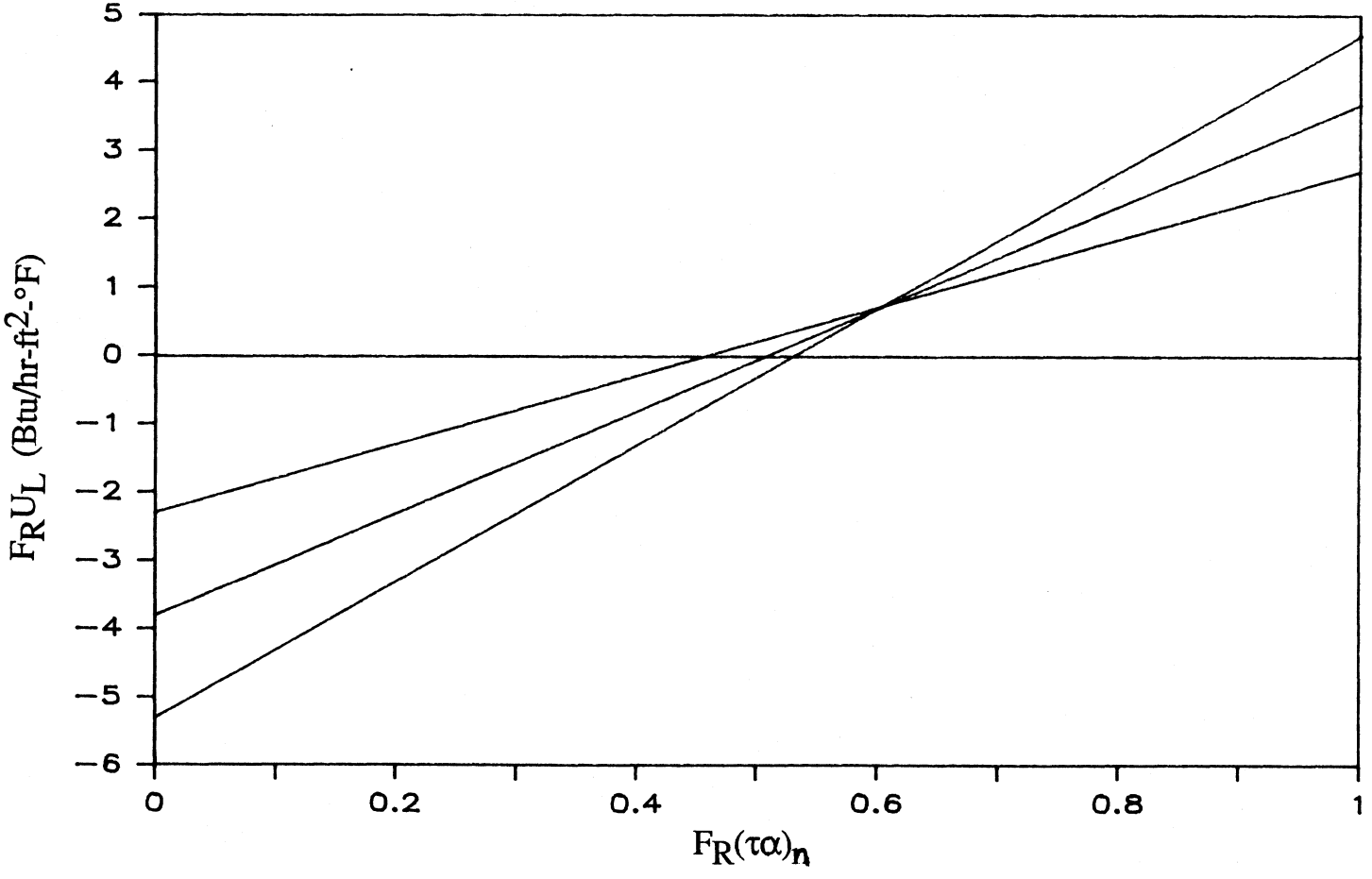

FIGURE 4.3 $F_R(\tau\alpha)_n$ - F_RU_L lines for the three sample months in example (4.1).

In the single timestep case it was possible to find the linear equation describing the $F_R(\tau\alpha)_n$ - F_RU_L relationship from the Hottel-Whillier equation, since all the values are known except $F_R(\tau\alpha)_n$ and F_RU_L. However the Hottel-Whillier equation can only be used to calculate the energy gain over a time period where I_T, T_i, T_a, and $K_{\tau\alpha}$ are constant. Therefore, the following method is used to find the $F_R(\tau\alpha)_n$ - F_RU_L relationship for each month:

1) Pick values of $F_R(\tau\alpha)_n$ and F_RU_L to be used in the TRNSYS collector model.

2) Run the collector model over the month.

3) Sum all of the energy gains (by the collector model) to give a total collector energy gain for the month.

4) Go back to #1 picking new values for $F_R(\tau\alpha)_n$ and F_RU_L, and repeat the process.

Once enough $F_R(\tau\alpha)_n$ - F_RU_L pairs have been found that give the experimental monthly energy gain, F_RU_L can be plotted as a function of $F_R(\tau\alpha)_n$, and a curvefit of the data done to determine their relationship.

As an alternative to this trial and error method, a more methodical approach is outlined below. It is explained using data from the Trident system during the month of March, since it is easier to follow if actual numbers are given.

The first step is to calculate the total monthly energy gain calculated by TRNSYS using the same F_RU_L value and several different $F_R(\tau\alpha)_n$ values. This was done, and the results are shown in table (4.2.1).

TABLE 4.2.1 Total energy gain using the F_RU_L and $F_R(\tau\alpha)_n$ values shown and March data in the TRNSYS collector model.

F_RU_L (Btu/hr-ft^2-°F)	$F_R(\tau\alpha)_n$	$(Q_{sim})_{mon}$ (million Btu)
0.6	0.1	-0.50
0.6	0.3	1.57
0.6	0.5	3.64
0.6	0.7	5.71
0.6	0.9	7.77

A plot of the $(Q_{sim})_{mon}$ value as a function of $F_R(\tau\alpha)_n$ from table (4.2.1) is shown in figure (4.4). Connecting the points gives a line of constant F_RU_L (in this case 0.6 (Btu/hr-ft^2-°F)), this means it is possible to find the collector model energy gain for any $F_R(\tau\alpha)_n$ value when F_RU_L = 0.6 (Btu/hr-ft^2-°F). Drawing a horizontal line on the plot (see figure (4.5)) representing the actual energy gain over the month, it is possible to graphically show the $F_R(\tau\alpha)_n$ - F_RU_L combination that is needed to have an amount of energy equal to $(Q_{exp})_{mon}$ calculated by the collector model. In this case $F_R(\tau\alpha)_n$ = 0.675.

If the above procedure is repeated for many different F_RU_L values, many different $F_R(\tau\alpha)_n$ - F_RU_L pairs will be found that when used in the collector model with the March data will gain over the month an amount of energy equal to $(Q_{exp})_{mon}$. This was done for F_RU_L = 0.2, 0.4, 0.6, 0.8, and 1.0 (Btu/hr-ft^2-°F) with the results plotted in figure (4.6). Lastly, the $F_R(\tau\alpha)_n$ - F_RU_L pairs can be curvefit to determine the equation of the line. This was done for the March $F_R(\tau\alpha)_n$ - F_RU_L pairs and the

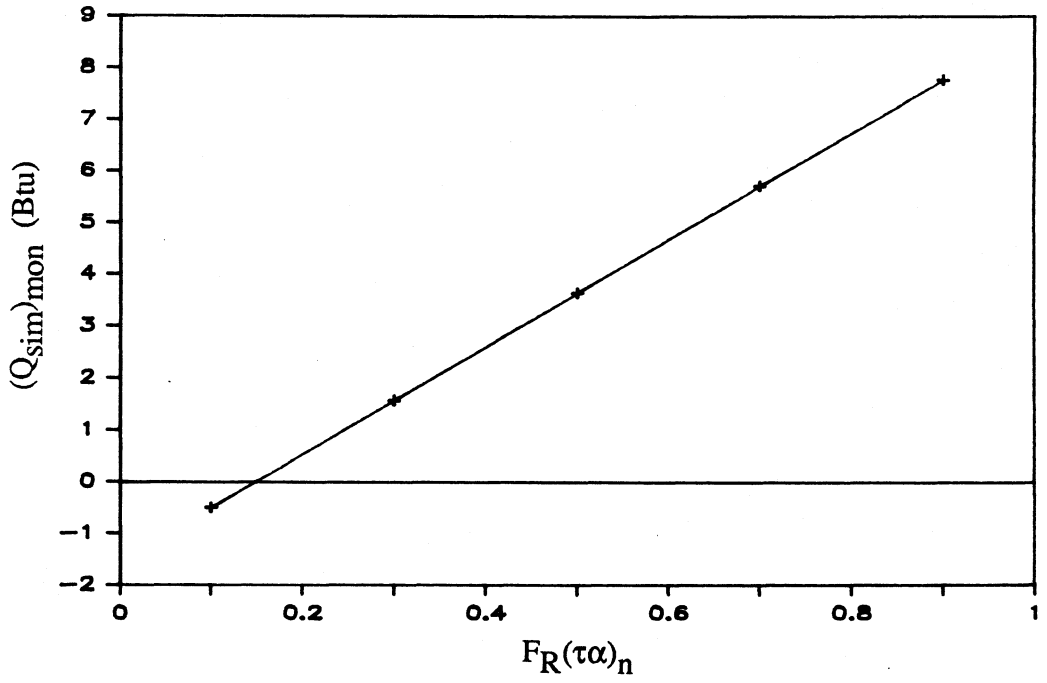

FIGURE 4.4 Monthly collector energy gain versus $F_R(\tau\alpha)_n$ for a constant F_RU_L value of 0.6 (Btu/hr-ft^2-°F). (March, Trident)

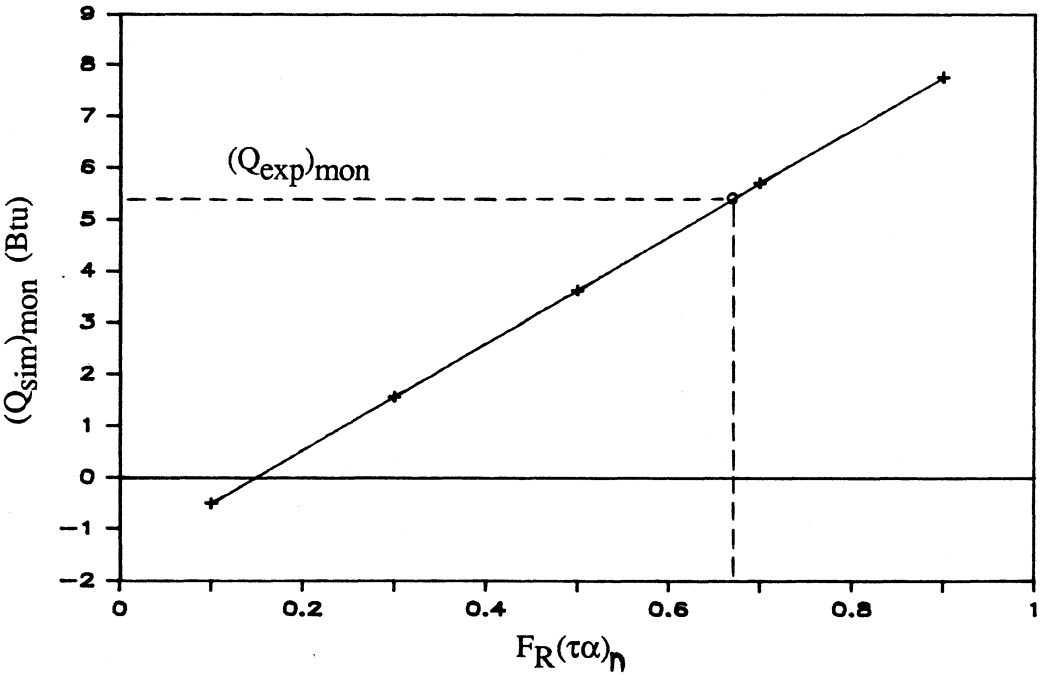

FIGURE 4.5 Determining $F_R(\tau\alpha)_n$ given the experimental monthly collector energy gain from figure (4.4).

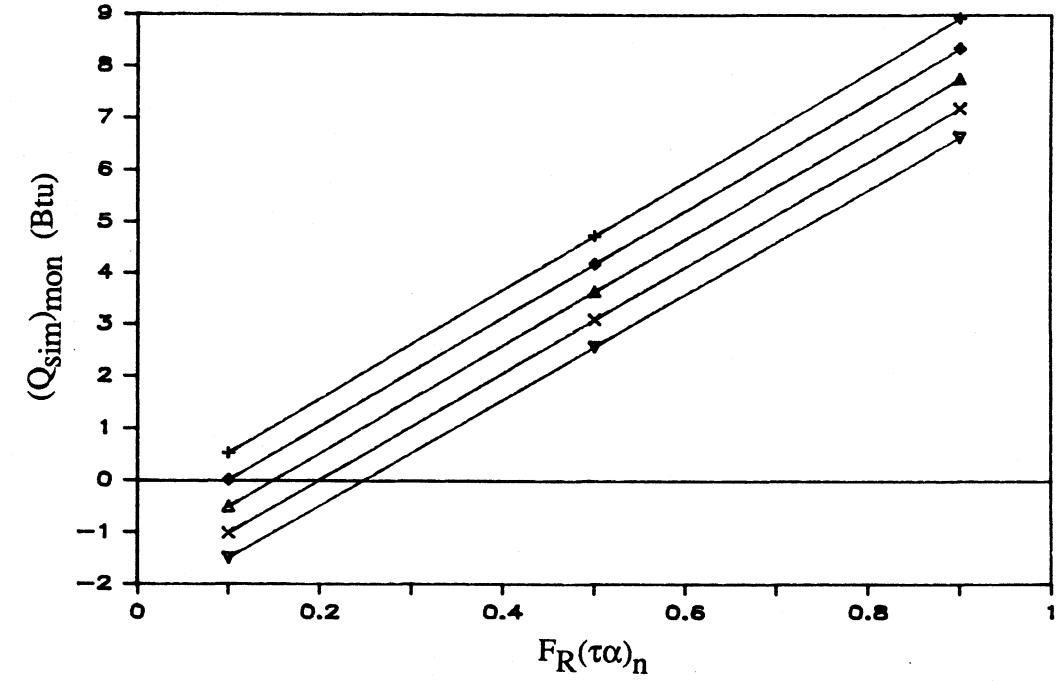

FIGURE 4.6 Monthly collector energy gain versus $F_R(\tau\alpha)_n$ with constant F_RU_L values (Btu/hr-ft^2-°F) connected by lines. (March, Trident)

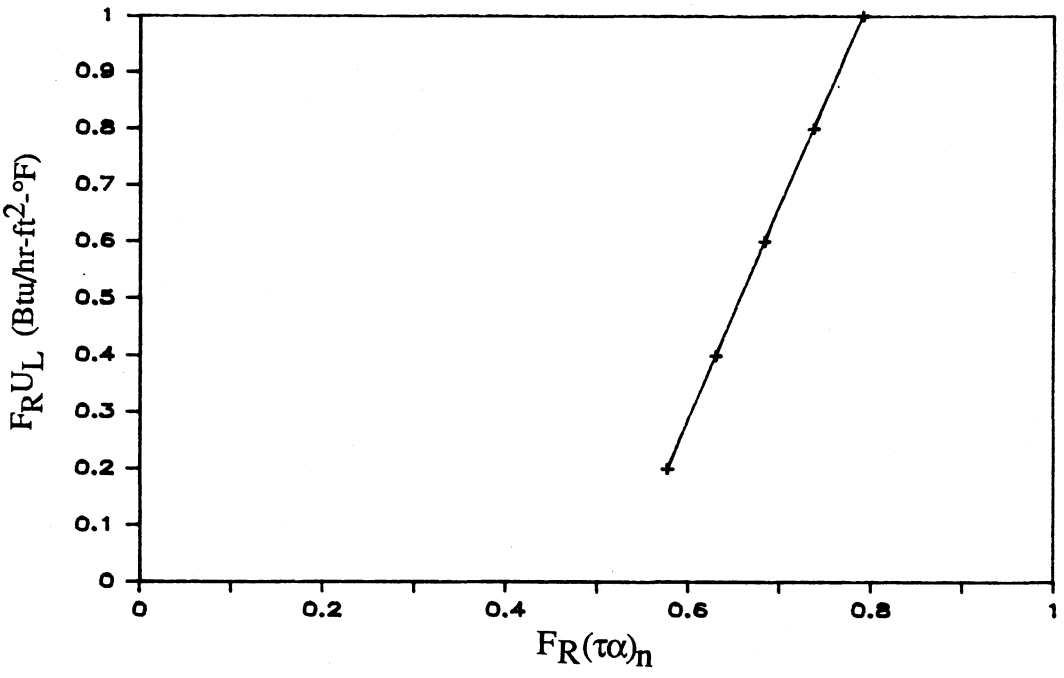

FIGURE 4.7 $F_R(\tau\alpha)_n$ - F_RU_L line for March. (Trident)

results plotted in figure (4.7).

This entire procedure can be done for all twelve months and all of the equations solved simultaneously to determine the $F_R(\tau\alpha)_n$ and F_RU_L values that "best fit" the equations. These values will represent the experimental collector characteristics for the entire year.

Two assumptions will further simplify the amount of work required. In figure (4.6) the lines of constant F_RU_L are almost linear therefore only two points on each line are needed to determine the equation of the line and ultimately the $F_R(\tau\alpha)_n$ value. Also the final $F_R(\tau\alpha)_n$ - F_RU_L relationship (figure (4.7)) is also nearly linear so again, only two points are needed. This means that the $F_R(\tau\alpha)_n$ - F_RU_L relationship can be found by running the TRNSYS collector model only four times each month. This greatly reduces the amount of work required for this method.

V. TRIDENT SYSTEM

This system was designed by Trident Energy Systems Inc. located in Davis, California. It was one of four systems designed and developed as part of the Packaged Space Heating Systems Development Program. The purpose of this program was to develop "packaged" solar space heating systems having performance characteristics and costs competitive with conventional heating systems.

V.1 SYSTEM DESCRIPTION

The Trident system is designed to provide space heating and preheated domestic hot water (DHW). The system used in this study is installed in a two story, single family home located in Westminster, CO. Figure (5.1.1), from [3], shows a schematic of the system. It shows the basic system configuration and includes the data sensor positions used by Vitro to record the system data. The nomenclature used to define the sensors are listed below:

Table 5.1.1 Nomenclature used to define the type of sensor.

T	-	temperature sensors
WT	-	liquid totalizing flow meters
ET	-	timers used to determine the length of time a pump or fan has run
P	-	pump
I	-	solar insolation
F	-	gas flow rate meters
DS	-	represents valve V2

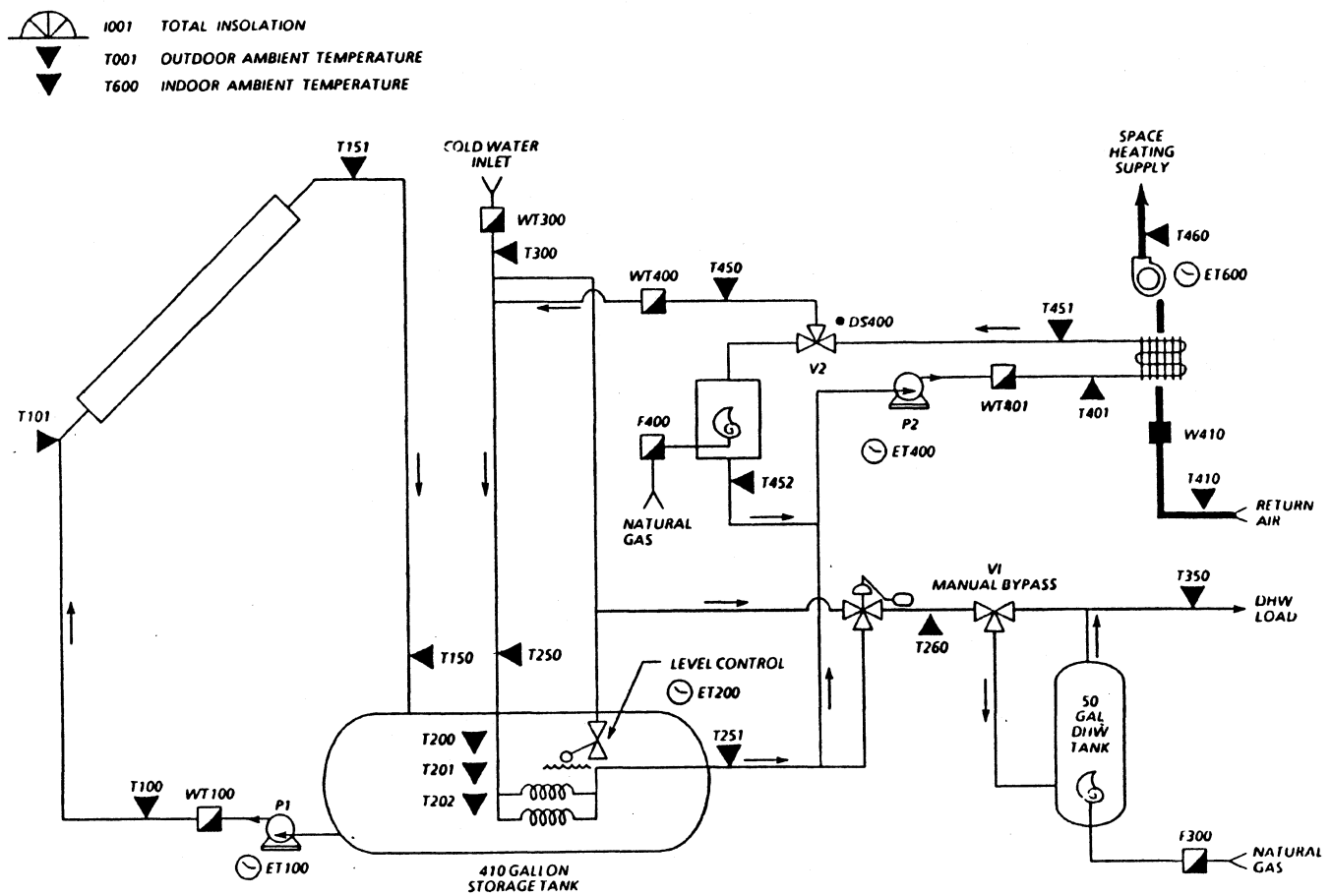

FIGURE 5.1.1 Schematic diagram of the Trident system (taken from ref. [3]).

The collector design incorporates characteristics of both flat plate and non-imaging concentrator collector characteristics. The design, shown in figure (5.1.2), consists of non-imaging reflectors located behind absorber fins, and a dual glazing consisting of a 4 mil outer film of Dupont Tedlar®, and a 1 mil inner film of Teflon®. Using the reflectors reduces the absorber plate area in half, this along with the lightweight glazing reduces the overall collector weight. The collector array consists of eight panels mounted on the roof. The gross and aperture areas are 309 and 280[1] ft^2 respectively. The array is tilted at a 22° angle from the horizontal, and oriented 10° west of due south. The collector panels are connected in parallel.

The storage tank is made from six molded foam parts that interlock when assembled to form the tank shell. Inside of this is a poly vinyl chloride (PVC) liner. The shell is made by laminating CADON®, a high temperature ABS derivative, on a 4 inch foam core of Dytherm®. The main advantage of this tank design is that it can be disassembled during shipment and will fit through a doorway. This is very useful when retrofitting a house with a solar system since the tank can easily be put in the basement. The tank holds approximately 410 gallons. There is also an extra cover that can be put over the collector pump, heat exchanger piping, and other plumbing fixtures which are mounted on top of the tank. The cover along with the other design features adds to the esthetics of the tank giving it a compact, attractive appearance.

The DHW subsystem provides solar preheated water to a standard natural-gas-fired hot water tank. When there is a demand for hot water the city mains cold water that would normally enter the hot water heater, replacing the hot water removed, first passes through two parallel, single-wall, fin-tube, 7/8 inch o.d. copper coiled heat exchangers located inside the storage tank. The tubing enters from the top of the tank, runs straight to the bottom and then spirals back up to the top in 14 inch loops. There

---

[1]This value was calculated from the aperture area for a single panel. None of the reports gave an aperture area for the mounted array.

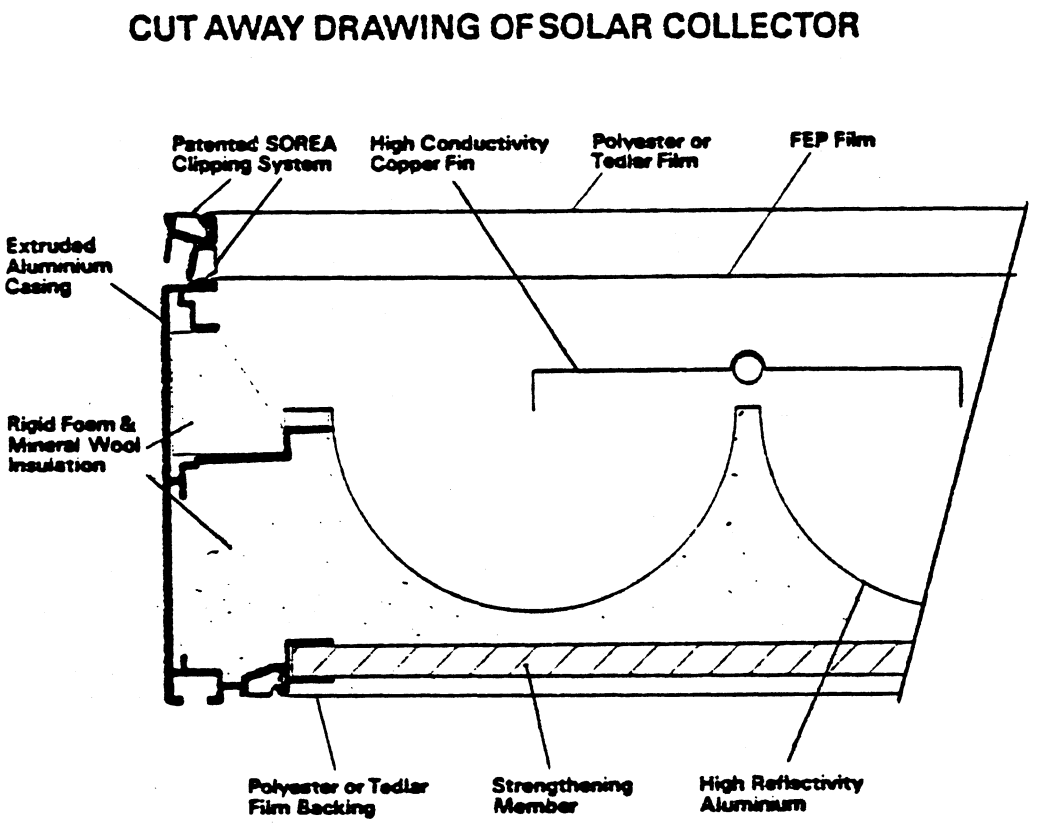

FIGURE 5.1.2 Cut away drawing of the Trident collector (taken from ref. [9]).

is a manual bypass valve that can be set to bypass the DHW tank, which can be used in summer if solar preheating supplies enough energy to satisfy the hot water demand. After the initial system startup the bypass value was never used.

The space heating subsystem consists of separate solar and auxiliary loops so that space heating is provided either by solar or by an auxiliary furnace, depending on the position of valve V2. In the solar mode, water is circulated through the dual coil heat exchanger (the same one described above) and heated before being delivered to the water-to-air heat exchanger to heat the house. If the solar mode cannot supply enough energy to meet the demand, the system switches to the auxiliary mode where the water is circulated through a tankless natural-gas-fired furnace which heats the water before it is circulated to the water-to-air heat exchanger. Note that only one of the space heating modes is operates at any given moment with all flow going through that loop.

The controller used in this system was designed by Trident and is based on an 8-bit microprocessor. In addition to implementing the basic system control functions (collection of solar energy, limiting the storage tank temperature, and delivery of energy to the space heating load), the controller also provided monitoring and diagnostic information, system status, and programmable thermostat setback features. The controller could be accessed by telephone for this information. It could even be set up to call a solar energy dealer for service when a problem occurs.

V.2 EXPERIMENTAL DATA

V.2.1 Data Availability

As it was noted in section (II.2.2), some of the experimental data are missing. Table (5.2.1) lists the amount of data available during each month for the Trident system.

TABLE 5.2.1 Amount of data available for the Trident solar energy system.

Month	Percent of Data Present
Jun '84	99 %
Jul	92
Aug	98
Sep	77
Oct	70
Nov	70
Dec	58
Jan '85	76
Feb	98
Mar	99
Apr	99
May	99

V.2.2 Storage Tank Energy Balances

Integrated monthly energy balances were done on the main storage tank with results shown in table (5.2.2). It is not reasonable to think that the tank energy balance calculated using experimental data will balance perfectly; therefore, the energy balance is written so as to define an error term.

$$Q_{err} = Q_{in} - Q_{load} - DE - Q_{env} \qquad (5.2.1)$$

where: (all values have units of Btu for the month)

Q_{err} = closure error in the energy balance

Q_{in} = energy supplied from the collector

Q_{load} = energy supplied to the load

DE = change in the internal energy of the tank

Q_{env} = energy lost to the environment from the tank

All of the energy flows except the error term are the summation, over the month, of the energy flows calculated for all time intervals, where the time difference between records is less than 10 minutes 40 seconds (two standard timesteps). (The equations used to calculate each term are given later.) There are two reasons for doing this. First, totalizing flow meters were used to measure the number of gallons of fluid flowing through the pipes. This means that if the flow rate is 6 gpm then during full flow conditions the flow meter will reset itself (done every 100 gallons for the Trident flow meters) in 16 minutes 40 seconds (3 timesteps). This would be the maximum time interval that could occur between data records in order for the correct flow over the time interval to be determined. Second, it was assumed that the temperature measurements recorded in each data record had been constant since the previous data record. As the time interval increases this approximation may be totally wrong if for example, a DHW draw occurred 30 seconds before the data record was recorded, the energy calculated over the entire time interval would be incorrect and the larger the time interval the larger the error. An error with the opposite sign would occur if a DHW draw had occurred during the entire time interval, then stopped 30 seconds before the data record was recorded. The two effects should tend to cancel each other out over the month, but to be on the safe side it is desirable to keep the time interval used as short as possible.

Table 5.2.2 Integrated monthly storage tank energy balances (for the available data during each month) on the Trident storage tank.

Month	Q_{in}	Q_{load}	DE (million Btu)	Q_{env}	Q_{err}	% Dif
Jun	2.93	2.82	0.11	0.57	-0.57	-19 %
Jul	4.27	2.91	0.06	0.74	0.56	13
Aug	5.8	4.54	0.05	0.63	0.58	10
Sep	3.43	2.77	0.09	0.48	0.09	3
Oct	2.37	2.06	-0.29	0.40	0.20	8
Nov	0.56	*	-0.16	0.09	*	*
Dec	1.37	0.40	0.33	0.18	0.46	34
Jan	1.46	0.61	0.44	0.53	-0.12	-8
Feb	2.81	2.77	-0.09	0.51	-0.38	-14
Mar	5.23	5.80	-0.08	0.44	-0.93	-18
Apr	3.96	3.97	0.10	0.61	-0.72	-18
May	3.7	3.24	0.17	0.80	-0.51	-14

* In November approximately 96,000 gallons of water went through the DHW subsystem, whereas the average monthly DHW draw was only 5,000 gallons; therefore, no energy to load value was calculated.

Calculating the energy balances using the time interval limit described above means that the energy quantities listed for each month in table (5.2.2) are only for the available data that meet the 10 minute 40 second maximum time length between records criteria. NO data is filled in for the missing records; therefore, the energy values listed in table (5.2.2) cannot be compared to the energy values listed in Vitro's report on the Trident system [3] unless almost all of the data is present (i.e. 98% or greater). When Vitro did their energy balances they filled in the missing data records using either the two records surrounding the gap, or the data recorded at the same time on the day

before and after the data gap, or sometimes on the monthly average values for that time period. The method used depended on the length of the data gap and what data values were present around it. Therefore, the monthly energy values listed in Vitro's report [3] are for the entire month even if less than 100% of the data is present.

The error term and percent error shows that the energy balances are not good. It is believed that the reason for the large errors is due to the energy to load (Q_{load}) calculation because during some of the months Qload is larger that the energy into the tank (Q_{in}) and this is not possible since the environmental losses (Q_{env}) and internal energy change (DE) values are at least a magnitude smaller than Q_{in} and Q_{load}. Further discussion of the Q_{load} term is given when the equation used to calculate it is defined.

The energy values in table (5.2.2) were calculated using the following equations where the position of the temperature sensors and flowmeters are shown on the system schematic (figure (5.1.1)). The working fluid was water, and the specific heat (C_p) was assumed constant and equal to 1 (Btu/lbm-°F) in all of the equations listed in this section.

Converting flow meter readings to mass flow (lbm)

$$M100 = (WT100 - WT100\_P)\, GTL \qquad (5.2.2)$$

where:

M100	=	total mass flow during the time interval (lbm/hr)
WT100	=	present totalizing flow reading (gal)
WT100_P	=	previous WT100 reading (gal)
GTL	=	8.3 converts gallons to lbm for water (lbm/gal)

M300 and M400 were calculated in the same manner.

Before multiplying equation (5.2.2) by GTL to convert the units from gallons to lbm the number of gallons was first checked to be sure that it was larger than 0.11. This was done because there is drift in the flow meter, and if no flow has occurred the first value of the flow meter might be at 80 gallons and then on the next reading be 79.99. Without the check, the number of gallons through the flow meter would be 99.99 which is incorrect.

Converting Timer Readings to Elapsed Time Between Records (hr)

$$ET600 = (ET600 - ET600\_P)\,MTH \qquad (5.2.3)$$

where:

ET600 = time air pump is on (hr)
ET600 = present totalizing flow reading (gal)
ET600_P = previous WT100 reading (gal)
MTH = 60.0 converts minutes to hours (hr/min)

All other timer readings are converted in the same manner.

Energy supplied from collector (Btu)

$$Q_{in} = \sum_{month} M100\, C_p (T150 - T100) \qquad (5.2.4)$$

From June 26th through September 10th temperature sensor T151 was substituted for sensor T150 due to problems with sensor T150.

Change in the internal energy of the tank (Btu)

$$DE = \sum_{month} STOCAP(TST - TST\_P)\,GTL \qquad (5.2.5)$$

where:

STOCAP = 410 (gallons) = amount of fluid in the storage tank

TST = average tank temperature - present record (°F)
TST_P = average tank temperature - previous record (°F)

Energy losses to the environment (Btu)

$$Q_{env} = \sum_{month} [\, U\,(SA_t)\ (T200 - T_b) + U\,(SA_m)\ (T201 - T_b) + U\,(SA_b)\ (T202 - T_b)\,]\,(\Delta t) \qquad (5.2.6)$$

where:

U = 0.1084 (Btu/h-°F-ft^2) = heat loss coefficient of the tank
SA_t = 50 (ft^2) = surface area of the top node of the tank
SA_m = 29 (ft^2) = surface area of the middle node of the tank
SA_b = 50 (ft^2) = surface area of the bottom node of the tank
T_b = 65 (°F) = basement temperature surrounding the tank
Δt = time interval since the last data record

The tank heat loss coefficient (U) was calculated from tests done by Farrington [5] on the Trident storage tank. In his report he lists a tank UA value of 14.0 (Btu/h-°F) based on a surface area of 129.2 ft^2. The surface areas were calculated based on the outside tank measurements which are 41.5 in. wide, 54.6 in. high, and 73 in. long. No temperature measurements were taken in the basement; therefore, T_b was assumed constant and equal to 65 °F during the entire year.

Energy supplied to the load (Btu)

$$Q_{load} = \sum_{month} [\, M300\, C_p (T260 - T300) + QSPC\,] \qquad (5.2.7)$$

where QSPC is the energy supplied to the space heating load in Btu and is calculated as

described below.

From June thru January equation (5.2.8) was used.

$$QSPC = M400\, C_p (T401 - T451) \qquad (5.2.8)$$

On January 6th temperature sensor T401 started reading high and was replaced in the energy calculations by T251. Also starting in January, problems with the controller caused the space heating system to run in the auxiliary mode when no space heating was needed. The effect of this was to circulate water through the space heating loop providing little if any energy to the house. When the loop was operating in this mode the temperature difference between T260 and T451 became as small as the temperature sensor resolution so that using equation (5.2.8) may be in error (for that timestep). Although the error is small over a single timestep it can add up and become significant over many time intervals. Therefore to ignore the times when the space heating loop was operating without providing any space heating, the following restrictions were applied when calculating Q_{load} for months January through May. (These restrictions were used by Vitro.)

If all of the following were true:

M401	>	0.0	
ET600	>	0.2	
T260	>	86.0	
DS400	=	1.0	(valve V2 is in space heating mode)

Then equation (5.2.8), with T260 substituted for T401, was used to calculate QSPC; otherwise, QSPC was set equal to zero.

An alternate method for calculation of the energy supplied to the load is represented by the following equation.

$$Q_{load} = \sum_{month} [\,(M300 + M400)\, C_p (T251 - T250)\,] \qquad (5.2.9)$$

This equation was not used in this thesis since sensors T251 and T250 were close enough to the storage tank that conduction up the inlet and outlet pipes affected the temperature read by them during stagnation times. Once flow resumed, a time lag would occur before the sensors correctly measured the fluid temperature. Table (5.2.3) shows the energy supplied to the load calculated using equations (5.2.8) and (5.2.9) and the percent error in the storage tank energy balances using each of them. (The percent errors calculated using equation (5.2.8) are also shown in table (5.2.2).) The table shows that using equation (5.2.9) generally gives worse energy balances. The reason this happens probably occurs during DHW draws because the city mains water temperature is very low (between 39 and 65 °F) compared to the storage tank temperature and the draws only occur over three timesteps. For this reason equation (5.2.8) was used during all months for the Trident system.

Vitro used equation (5.2.9) for June thru January and then they used equation (5.2.7) for the rest of the months. They switched equations since their energy balances worked better using equation (5.2.7) starting in February.

V.3 COLLECTOR RESULTS

This subsection presents the Trident collector results found when comparing the ASHRAE 93-77 collector parameters with those calculated from the experimental data.

Table 5.2.3 Integrated monthly energy delivered to the load calculated using equations (5.2.7) and (5.2.9), and the percent difference in the storage tank energy balances using the different energy to load values. The energy values are given in (million Btu).

Month	Q_{load}	% Dif	Q_{load}	% Dif
	eqn. (5.2.8)		eqn. (5.2.9)	
Jun	2.82	-19	2.82	-19
Jul	2.91	13	3.17	7
Aug	4.54	10	5.14	-0.3
Sep	2.77	3	3.32	-13
Oct	2.06	8	2.45	-8
Nov	*	*	*	*
Dec	0.40	34	1.45	-43
Jan	0.61	-8	0.70	-14
Feb	2.77	-14	2.73	-12
Mar	5.80	-18	5.78	-17
Apr	3.97	-18	4.14	-23
May	3.24	14	3.52	-21

* In November approximately 96,000 gallons of water went through the DHW subsystem, whereas the average monthly DHW draw was only 5,000 gallons; therefore, no energy to load value was calculated.

First the ASHRAE test results are presented. Second, the parameters used to screen the experimental data in the efficiency method and the parameters used to represent steady state flow in the collector are given. Third, the "collector model deck" is presented, which is used to calculate the monthly collector energy gain for the $F_R(\tau\alpha)_n$ - F_RU_L values calculated from the experimental data. After that the efficiency and collector model method results are presented. Lastly, comparisons are made between the "actual" total monthly collector energy gains (calculated directly from the

experimental data) and the total monthly energy gains calculated using the $F_R(\tau\alpha)_n$ and F_RU_L values calculated by the ASHRAE, efficiency, and collector model methods.

V.3.1 ASHRAE 93-77 Test Results

Two collectors from Trident were tested at DSET Laboratories, Inc., located in Phoenix, Arizona. The collector parameter values ($F_R(\tau\alpha)_n$, F_RU_L, and b_o), were determined using the ASHRAE 93-77 test. Both collectors were tested when initially received and again after a nine month stagnation period. The results from these tests are tabulated in table (5.3.1) and figure (5.3.1) shows the efficiency plots used to obtain the results for collector 1.

TABLE 5.3.1 ASHRAE 93-77 test parameters calculated based on the collector aperture area.

	$F_R(\tau\alpha)_n$		F_RU_L		b_o	
	Initial	Final	Initial	Final	Initial	Final
Collector 1	0.666	0.669	0.695	0.649	0.158	0.150
Collector 2	0.668	-*-	0.718	-*-	0.166	-*-

-*- during the initial testing the second collector developed a leak and was not retested after the stagnation period

A linear curve fit of the ASHRAE test data was performed as shown in figure (5.3.1). The figure indicates that the data might be better correlated by a curved line. This is

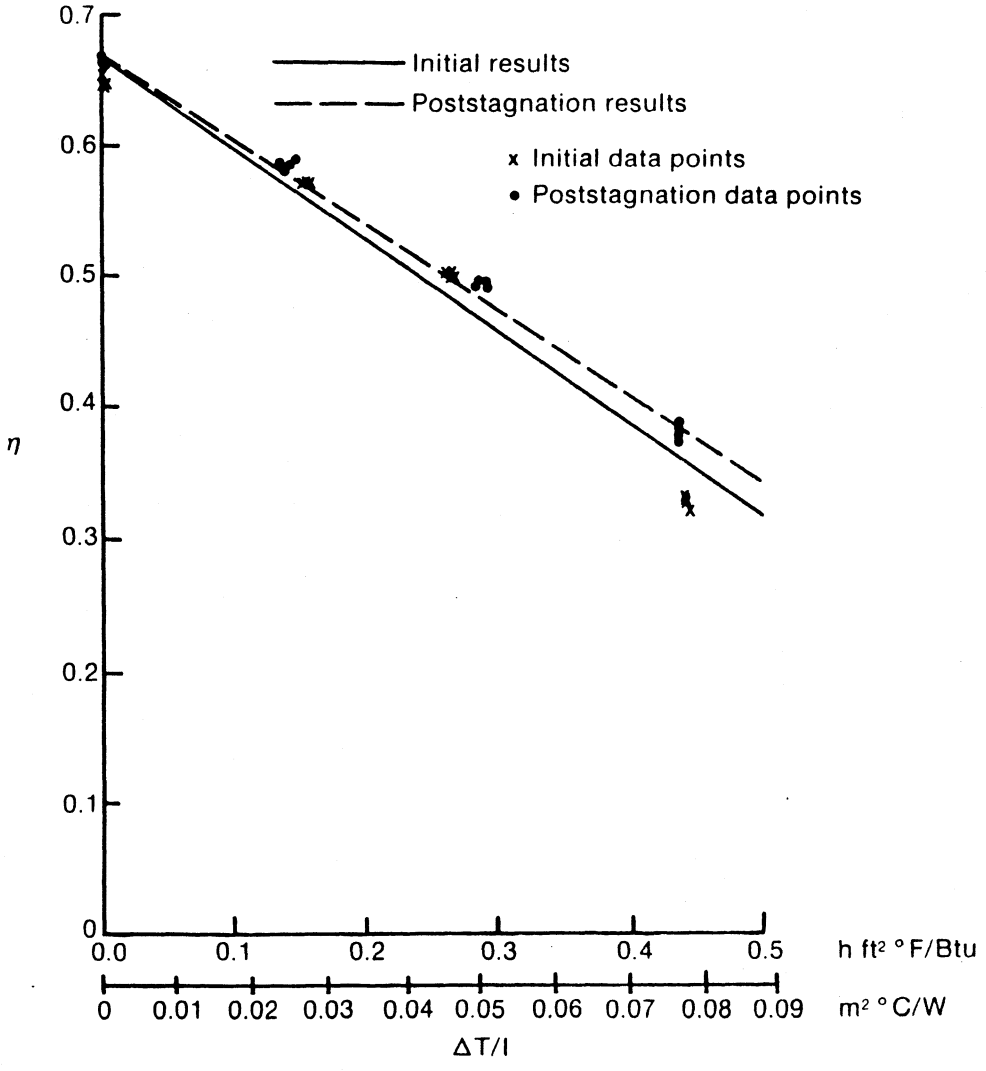

FIGURE 5.3.1 Efficiency test results for Trident collector 1 (taken from ref. [4]).

probably caused by the reflectors used in the collector design (shown in figure (5.1.2)) and suggests that a biaxial incidence angle modifier may be needed to correctly describe the collector performance. However, there is no way to determine what the biaxial incidence angle modifier is without performing tests on the collector; therefore, for this thesis it will be assumed that the collector characteristics are described by a linear correlation with a single incidence angle modifier.

Typically the three test parameters used to describe the characteristics of a collector are determined from a single collector put through the ASHRAE tests. Since three sets of collector parameters are available for the Trident collector, the effect of using the different collector test results (individually and averaged) would have on the total energy gain over a month was determined. The collector parameters are shown in table (5.3.2) with the total energy gain [$(Q_{col,sim})_{mon}$] calculated using them for the month of March (the collector model deck used to calculate the monthly energy gain is explained in the next section (V.3.3)).

The results show that the initial two collector test parameters give a 1.4 % difference in the energy collected over the month. This is small and is probably due to different ambient conditions (i.e wind speed, sky conditions) during the tests and/or to experimental error in the data measurements. The after-stagnation test results for collector 1 show that the collector performance theoretically improved. This occurs since F_RU_L and b_o are lower in value. The lower F_RU_L means less collector losses to the environment and the lower b_o means that a higher incidence angle modifier will be calculated at a given incidence angle, resulting in an increase in the energy gain. The energy gain calculated from the averaged collector parameters is the same as that calculated by averaging the individual energy gains. The difference in energy gain when averaging just the initial parameters and all three sets is 1.6%.

TABLE 5.3.2 Monthly energy gain using March data from the Trident system and the different collector parameters obtained during the ASHRAE tests, given in table (5.3.1).

Collector test	$F_R(\tau\alpha)_n$	F_RU_L (Btu/h-ft^2–°F)	b_o	$(Q_{col,sim})_{mon}$ (million Btu)
1-Initial	0.666	0.695	0.158	5.11
2-Initial	0.668	0.718	0.166	5.04
1-Final	0.669	0.649	0.150	5.29
Avg 1,2 Initial	0.667	0.707	0.162	5.07
Avg all three	0.668	0.687	0.158	5.15

Based on the results, the average of the initial test results for each parameter was selected to represent the ASHRAE test results. An average was used since there is no reason to expect that either one of the tested collectors should perform any different than the collectors actually used in the Trident solar energy system, and the results of the two modules are in good agreement. Only the initial tests were averaged on the grounds that the collectors in the system probably did not experience stagnation conditions very often.

These averaged parameter values are shown in table (5.3.3) along with the test flow rate and the test collector aperture and gross areas (note that the test parameters are based on the collector aperture area).

TABLE 5.3.3 Trident collector parameter values used to represent the collector characteristics determined by the ASHRAE 93-77 test.

$F_R(\tau\alpha)_n$	0.667	
$F_R U_L$	0.707	(Btu/h-ft^2-°F)
b_o	0.162	
test flow rate	511.14	(lbm/hr)
aperture area	34.96	(ft^2)
gross area	38.76	(ft^2)

V.3.2 Screening and Full Flow Parameters

Section (IV.2.1) explains the two main criteria and the screening methods used to determine which data records are used to calculate the efficiency and operating points; however, it did not explain in any detail what values were used to determine if constant flow had occurred during each timestep. For example, ideally if a 6 gallon per minute (gpm) pump was used to pump water through the collector and the time interval was 5 minutes, then 30 gallons of water would go through the collector if the pump had run continuously during the entire timestep. If this is what happened in the actual system then determining when the collector had run the entire timestep would be easy since the full flow value would be simply 6 gpm multiplied by the time interval (in minutes). Comparing the full flow value to the actual flow given by the totalizing flow meter then would indicate if full flow had occurred. Unfortunately, the actual system does not work that well. First, the totalizing flow meter is only accurate within $\pm$ 2.8%. Second, the actual flow rate will probably be less than 6 gpm due to pressure drop in the pipes.

To study these two problems, a program was written that calculated the "average" flow rate in between each record of data where the average flow rate is equal to the total

flow (gallons) through the collector during the time interval divided by the length of the time interval (minutes). Doing this for the entire month it was possible to determine the number of timesteps when the average flow rate was between a particular range of values, e.g., 5.9 and 6.0 gpm, or 5.2 and 5.3 gpm. This was done for the Trident system during the months July through October and March through May with the results shown in tables (5.3.4a) and (5.3.4b) respectively. The tables give the number of timesteps over the month that had an average flow rate in the range shown, where the average flow rate must be greater than or equal to the first number, and less than the second number. The last row of each table lists the total number of timesteps during the month when the average flow rate was greater than zero.

The collector pump was changed in February and it is believed that a 6 gpm collector pump was used from June through February 4th or 5th and a 4 gpm pump from February 4th or 5th through May. (Nowhere in the system reports prepared by Trident or Vitro is it stated specifically what size pump was installed.) The tables show that flow readings greater than 6 and 4 gpm occurred for each pump. This indicates that there are some inaccuracies in the data measurements. Also note that around 5.1 or 5.2 gpm (Jul-Oct) and 3.8 or 3.9 gpm (Mar-May) the number of timesteps flow occurred jumps. This implies that the actual steady state flow rate through the collector is in these ranges (5.1-5.2 gpm and 3.8-3.9 gpm). A more accurate way to determine the steady state flow rate is to list the average flow rates as a function of time for a time period when the average flow rate values stay approximately constant over an hour, indicating that the collector was running steadily over that time period. This will give the approximate steady state flow rate. Table (5.3.5) gives typical examples of the average flow rate over an hour for both flow rates. The left side was taken from August 2nd and the right side from March 6th. The values shown are typical for the two different pumps and show that full flow during a timestep can be indicated by making sure that average flow rate is greater than 5.1 and 3.8 gpm for the two different

pumps. These two values are used as the lower bounds when deciding if full flow occurred during a timestep for the efficiency method calculations.

TABLE 5.3.4a Number of timesteps when flow occurred in the ranges indicated for July-October. The last column is the total number of timesteps during the month when flow occurred. (Trident)

Flow (gallons)	Jul	Aug	Sep	Oct
> 6.2	1	1	1	3
6.1 - 6.2	3	1	1	1
6.0 - 6.1	3	0	0	1
5.9 - 6.0	6	3	1	1
5.8 - 5.9	6	3	3	1
5.7 - 5.8	11	3	6	3
5.6 - 5.7	20	3	4	135
5.5 - 5.6	3	3	2	35
5.4 - 5.5	8	14	6	5
5.3 - 5.4	11	5	9	5
5.2 - 5.3	105	672	1065	225
5.1 - 5.2	657	920	434	389
5.0 - 5.1	411	178	16	333
4.9 - 5.0	50	6	3	5
total #	1640	2059	1714	1274

TABLE 5.3.4b Number of timesteps when flow occurred in the ranges indicated for March-May. The last column is the total number of timesteps during the month when flow occurred. (Trident)

Flow (gallons)	Mar	Apr	May
> 4.2	12	18	40
4.1 - 4.2	43	66	56
4.0 - 4.1	187	170	404
3.9 - 4.0	772	447	459
3.8 - 3.9	506	405	145
3.7 - 3.8	209	81	23
3.6 - 3.7	17	12	9
3.5 - 3.6	19	16	21
total #	2245	1609	1641

In addition to the lower bound values described above, a second flow rate value is needed in the collector model deck (described in the next section (V.3.3)). Since the energy gain by the collector depends on the flow rate, the value chosen should be as close to the actual steady state flow rate as possible. The same values chosen as the full flow lower bounds could be used, but they are lower than the actual steady state flow rate. To show what the effect the chosen steady state flow rate has on the collector energy gains, three different flow rates (5.1, 5.2, and 6.0 gpm) were used in the collector model deck using August data. The only difference in the three, month long simulations is the collector flow rate used. The total monthly energy gain using the three flow rates is shown in table (5.3.6). There is a 1.8% difference in energy gain when using 5.1 and 5.2 gpm and a 14.6% energy difference when using 5.2 and 6.0 gpm. This indicates that if it were assumed that a 6 gpm pump had been used, and no experimentally measured data were available, the final results when making energy

TABLE 5.3.5 Examples of the collector flow rates during times of continuous operation. (Trident)

August 2nd		March 6th	
Time of day (hr)	flow rate (gpm)	Time of day (hr)	flow rate (gpm)
9.93	5.19	10.96	4.03
10.01	5.17	11.05	3.92
10.10	5.11	11.14	3.89
10.19	5.17	11.23	3.90
10.28	5.20	11.31	3.90
10.37	5.17	11.40	4.00
10.46	5.10	11.49	3.88
10.55	5.19	11.58	3.87
10.64	5.17	11.67	3.87
10.73	5.19	11.76	3.83
10.81	5.10	11.85	3.96
10.90	5.19	11.94	3.81
11.00	5.17	12.03	3.85

TABLE 5.3.6 Monthly total energy gain from the collector model where the only difference between the three cases is the value used as the "full flow" rate.

flow rate (gpm)	(Q_{sim}) mon (million Btu)
5.1	4.46
5.2	4.38
6.0	3.82

comparisons would vary significantly. The 1.8% difference between 5.1 and 5.2 gpm indicate that even a small difference in flow rate has an effect on the energy gain. (Note that the large difference in the energy gain when using 6.0 and 5.2 gpm occurs when doing the collector only simulations. This does not necessarily mean a 14 percent difference in collector energy gain would occur if 6.0 and 5.2 are used in a typical simulation that includes the rest of the solar energy system.) For this thesis, 5.2 gpm and 3.9 gpm for Jun-Jan and Feb-May respectively, are used in the collector model when calculating the total monthly energy gain for the different $F_R(\tau\alpha)_n$ - F_RU_L pairs found using the ASHRAE test, efficiency, and collector model methods.

Table (5.3.7) summarizes the values used for the Trident system to determine when full flow occurs in a timestep and the steady state flow values used in the collector model deck.

TABLE 5.3.7 Summary of the Trident system steady state flow rate and the lower bound used to determine when flow has occurred during an entire timestep.

	Steady state flow (lbm/hr)/(gpm)	Full flow (gpm)
Jun-Jan	2540 / 5.2	5.1
Feb-May	1943 / 3.9	3.8

V.3.3 Method For Calculating The Monthly Collector Energy Gain

The purpose of this subsection is to describe the "Collector Model Deck" which is a TRNSYS deck used to calculate the collector energy gain using different $F_R(\tau\alpha)_n$ -

F_RU_L pairs with the experimental as input. Also described is the method used to modify the TRNSYS radiation component so that it could be used since the solar radiation was measured on a tilted surface rather than on the horizontal.

Comparing the $F_R(\tau\alpha)_n$ - F_RU_L pairs calculated using the efficiency and collector model methods with the ASHRAE values cannot be done by comparing just the $F_R(\tau\alpha)_n$ values or just the F_RU_L values since it is not always possible to tell just by looking at them if one pair, when used in the collector model, will indicate more collected energy than the other for the same input values. Also the energy gain depends on the flow rate at which the $F_R(\tau\alpha)_n$ and F_RU_L values were calculated and the proper value must be used in the collector model in the form G_{test} which is the "test" flow rate per collector area. (The energy gain also depends on b_o, but it has been assumed that b_o is the same as that found during the ASHRAE test no matter which method is used). Therefore the collector model is used to calculate the total energy gain over a month using each of the $F_R(\tau\alpha)_n$ - F_RU_L pairs. Then the total energy gained by each pair can be compared. The energy gain can also be compared to the measured energy gain calculated directly from the experimental data to determine how close the calculated pair represent the measured collector characteristics for that month.

An example of the TRNSYS deck used to calculate the total energy gain over a month is given in Appendix (B.1) with the modified and special purpose components described next.

UNIT 1 Input (type 19 data reader):

Reads in the data values at 5 minute 20 second intervals. The values read in are the solar radiation measured on the tilted collector surface (Btu/hr-ft^2), ambient temperature (°F), collector inlet temperature (°F), and the "average" (i.e. total flow during a timestep divided by the timestep length) collector flow rate over the previous timestep (lbm/hr). (Note the units used.)

UNIT 2 Algebraic Operator (type 15):

This component is required since the radiation processor expects the solar radiation to have units of Btu/ft^2.

UNIT 3 Solar Radiation Processor:

This component is a modified version of the type 16 radiation processor. The TRNSYS collector model requires as input the total (I) and diffuse component (I_d) of the radiation incident on the horizontal and the total radiation (I_T) incident in the plane of the collector. Typically, total horizontal radiation data is available and the TRNSYS radiation processor is used to calculate the horizontal diffuse component and the total radiation incident on the tilted collector; however, both the Trident and Honeywell systems have radiation measurements in the plane of the collector (I_T). This allows the tilted radiation value to be directly input to the collector model, but the total and diffuse horizontal radiation are not known and the radiation processor is not written to calculate them from the tilted radiation. Therefore the radiation processor was modified to approximate the total and diffuse horizontal radiation. The relationship between the total horizontal and total tilted radiation is given by

$$I = \frac{I_T}{R} \qquad (5.3.4)$$

where R is by definition the ratio of the total radiation on a tilted surface to the beam radiation on a horizontal surface (I_T/I). As an approximation, the horizontal radiation can be treated as if it is all beam radiation, resulting in $R = R_b$, where Rb depends only on the collector position and time of day and year. This approximation is used in the modified radiation processor to calculate the total horizontal radiation, which is then

used to calculate the diffuse horizontal radiation.

UNIT 4 Collector (type 1):

Calculates the collector energy gain each timestep. The only parameter values that are changed are $F_R(\tau\alpha)_n$, F_RU_L, and G_{test} (the "test" flow rate per collector area used when calculating $F_R(\tau\alpha)_n$ and F_RU_L).

UNIT 5 Algebraic Operator:

The purpose of this unit is to calculate the energy gain by the collector model during a timestep when the field collector did not run continuously during the entire timestep. As stated earlier the flow rate through the collector affects its performance. This means that running the collector at 2 gpm for 4 minutes will not necessarily give the same energy gains as running the same collector with the same input values at 4 gpm for 2 minutes. Therefore the collector model input flow rate should always be equal to the steady state flow rate that occurs in the field collector. Also the collector model will run the collector at the input flow rate for the entire timestep. Therefore the energy gain will not be the same if the field collector had actually run only during half the timestep. To account for this discrepancy the energy gain calculated as if the collector had run during the entire timestep is multiplied by a ratio which give the amount of time the field collector ran to the total time interval. The ratio is calculated by dividing the "average" (input number 4 in the data reader) collector flow rate over the time interval by the steady state flow rate (CFLW) initialized in the Constants statement. The results of doing this is that over the month the collector model results are the same as if the model only ran when the field collector was operating.

To determine how much the collector flow rate affects the collector energy gain the deck was run inputting the "average" flow rate directly into the collector model. Doing this causes the same amount of fluid to flow through the collector over the month but the flow rate varies. The results using this method compared to the constant flow

method differed as much as five percent over a months time, showing that the flow rate does affect the energy gain by the collector.

V.3.4 Curvefitting Method

This subsection discusses the method used to linearly curvefit the efficiency and operating point values calculated from the experimental data using the efficiency method (for both the Trident and Honeywell systems). Once the efficiency and operating points have been calculated, the first step is to remove all points that lie outside of the following boundaries:

$$0 < \text{efficiency} < 1$$
$$0 < \text{operating point} < 1$$

This was done to remove points that are obviously in error (i.e. an efficiency value less than 0 or greater than 1 makes no sense by the definition of efficiency) and to remove points that will affect the curvefit if used, but lie outside of the typical operating range of the collector (i.e. operating points less than 0 and greater than 1).

The next step is to linearly curve fit the remaining data using the least squares method calculating the slope and y-intercept which are equal to $-F_R U_L$ and $F_R(\tau\alpha)_n$ respectively. Also calculated at this time is the standard deviation. The equations used to do this are listed below:

$$A = \frac{n\Sigma xy - \Sigma x \Sigma y}{n\Sigma x^2 - (\Sigma x)^2} \qquad (5.3.5a)$$

$$B = \frac{\Sigma y \Sigma x^2 - \Sigma x \Sigma y}{n\Sigma x^2 - (\Sigma x)^2} \qquad (5.3.5b)$$

$$SD = \sqrt{\frac{\Sigma(y_{pred} - y_{obs})^2}{n - 1}} \qquad (5.3.5c)$$

where:

A	=	slope
B	=	y-intercept
x	=	operating point values
y	=	efficiency values
n	=	total number of points being curvefit
SD	=	standard deviation from the mean
y_{pred}	=	Ax + B (using A & B values calculated in equations (5.3.5a) and (5.3.5b) and the x values)
y_{obs}	=	y values used in equations (5.3.5a) and (5.3.5b)

The final step is to remove any points that are over two standard deviations away from the curvefit line. Once this is done, the remaining points are curvefit again to obtain the final $F_R(\tau\alpha)_n$ and F_RU_L values for the data. The reason points greater than two standard deviations away from the line are deleted is that this was done by Vitro. Removing these points changes the slope and y-intercept for some months, however, it does not change the monthly energy gain to a significant degree as shown in table (5.3.8)). Screening method (1b) was used and the data were averaged when continuous flow had occurred over 11 timesteps.

TABLE 5.3.8 $F_R(\tau\alpha)_n$, F_RU_L values and the monthly energy gain (Q_{col}) from them calculated before and after removing any points greater than 2 standard deviations from the first curvefit. F_RU_L has units of (Btu/hr-ft^2-°F) and Q_{col} has units of (million Btu).

	before				after			
	$F_R(\tau\alpha)_n$	F_RU_L	#pts	Q_{col}	$F_R(\tau\alpha)_n$	F_RU_L	#pts	Q_{col}
Aug	.656	.121	67	5.64	.637	.048	62	5.63
Oct	.667	.331	47	2.61	.671	.334	44	2.62
Mar	.634	.441	85	5.56	.667	.573	81	5.56
May	.648	.471	56	4.35	.649	.471	53	4.35

V.3.5 Efficiency Method Results

Section (IV.2.1) describes the theory, approach, and different screening methods applied to the experimental data to determine the results presented in this subsection.

The initial step was to determine how $F_R(\tau\alpha)_n$ and F_RU_L varied when different numbers of consecutive data were averaged. To make these comparisons, screening method 1(a & b) were used. The results for August and March are shown in tables (5.3.9) and (5.3.10). The left side of each table contains the collector parameters calculated assuming $K_{\tau\alpha}$ equals 1 (method 1a) and on the right side $K_{\tau\alpha}$ is calculated using b_o from the ASHRAE test (method 1b). The column labeled "#pts" is the number of times during the month when there were "X" number of consecutive timesteps averaged when the collector was operating continuously. As explained in section (V.3.3)) it is not always possible to determine if one pair of $F_R(\tau\alpha)_n$ - F_RU_L values is better than another pair; therefore, the $F_R(\tau\alpha)_n$ - F_RU_L pairs are used in the collector model deck (described in section (V.3.3) to calculate the total monthly energy

gain, then by directly comparing the energy gains it is possible to indirectly compare the $F_R(\tau\alpha)_n$ - F_RU_L pairs. This was done for the $F_R(\tau\alpha)_n$ - F_RU_L pairs in tables (5.3.9) and (5.3.10) using G_{test} equals 9.25 and 6.94 for August and March, respectively. The resulting total monthly energy gains are listed in table (5.3.11) where the values are sorted in descending order (the "# timesteps" column lists the number of consecutive steps averaged and can be used to determine which energy gain value is calculated from which pair of $F_R(\tau\alpha)_n$ - F_RU_L values given in tables (5.3.9) and (5.3.10)).

TABLE 5.3.9 Collector parameters for August calculated from the Trident experimental data by averaging the efficiency and operating point values over time steps ranging from 1 to 13..

# time steps	August "a" $F_R(\tau\alpha)_n$	"a" F_RU_L (Btu/hr-ft^2-°F)	"a" #pts	August "b" $F_R(\tau\alpha)_n$	"b" F_RU_L (Btu/hr-ft^2-°F)	"b" #pts
13	.651	.195	63	.670	.169	60
12	.632	.139	65	.664	.161	63
11	.629	.112	67	.637	.048	62
10	.632	.120	84	.669	.179	80
9	.634	.144	94	.656	.126	89
8	.656	.216	106	.663	.149	101
7	.646	.176	126	.673	.202	121
6	.653	.213	166	.687	.259	158
5	.656	.226	203	.676	.215	195
4	.657	.231	255	.675	.214	243
3	.652	.201	412	.674	.201	396
2	.650	.224	636	.667	.206	614
1	.637	.188	1360	.659	.180	1316

TABLE 5.3.10 Collector parameters for March calculated from the Trident experimental data by averaging the efficiency and operating point values over time steps ranging from 1 to 13.

# time steps	March "a" $F_R(\tau\alpha)_n$	"a" F_RU_L (Btu/hr-ft^2-°F)	"a" #pts	"b" $F_R(\tau\alpha)_n$	"b" F_RU_L (Btu/hr-ft^2-°F)	"b" #pts
13	.661	.658	61	.664	.541	61
12	.656	.643	70	.664	.549	69
11	.664	.693	82	.667	.573	81
10	.677	.758	92	.682	.651	91
9	.676	.758	101	.680	.644	100
8	.665	.691	116	.674	.609	116
7	.660	.659	136	.663	.542	136
6	.662	.660	165	.665	.555	166
5	.658	.654	206	.666	.562	207
4	.659	.661	269	.666	.562	268
3	.642	.573	378	.644	.449	375
2	.627	.496	597	.633	.393	597
1	.597	.363	1390	.606	.285	1390

TABLE 5.3.11 Total monthly energy gain by the collector model using the corresponding $F_R(\tau\alpha)_n$ and F_RU_L values from tables (5.3.9) and (5.3.10). Energy gains are in million Btu.

August				March			
#	"1a"	#	"1b"	#	"1a"	#	"1b"
3	5.43	13	5.66	1	5.37	1	5.67
7	5.43	8	5.64	2	5.34	2	5.67
8	5.43	3	5.63	3	5.30	3	5.64
10	5.43	9	5.63	13	5.28	13	5.61
13	5.43	10	5.63	6	5.28	7	5.6
11	5.42	11	5.63	12	5.26	12	5.59
5	5.41	6	5.62	7	5.26	6	5.59
4	5.41	7	5.62	5	5.25	5	5.58
6	5.41	12	5.62	4	5.25	4	5.58
9	5.39	4	5.61	8	5.23	11	5.56
12	5.39	5	5.61	11	5.22	8	5.54
2	5.32	2	5.55	10	5.18	10	5.52
1	5.26	1	5.54	9	5.17	9	5.51

Table (5.3.12) shows the percent difference between the largest and smallest energy gain in each column of table (5.3.11). Three different percent differences were calculated by choosing the largest and smallest energy values in each column from (1) all 13 energy values, (2) energy values calculated by averaging three or more timesteps (i.e. neglect the energy values calculated when only 1 and 2 timesteps were averaged),

and (3) energy values calculated by averaging six or more timesteps. The results show that so long as three or more timesteps are averaged the final results are not very different; therefore, for the rest of the parameter calculations using the four screening methods, an arbitrary value of 11 timesteps (approximately one hour) was used.

TABLE 5.3.12 Largest percent differences between the total monthly energy gains in each column of table (5.3.11) for the method indicated in the first column of the table.

	% difference			
	August		March	
Method used	a	b	a	b
1	3.2%	2.2%	3.9%	2.9%
2	0.7	0.9	2.5	2.4
3	0.7	0.7	2.1	1.8

The results also show that including $K_{\tau\alpha}$ (method "b") in the efficiency and operating equations changes the collector parameters so that more energy (i.e. better collector characteristics) is collected over a month. In August four percent and in March six percent more energy is collected using the collector parameters calculated when including $K_{\tau\alpha}$. The same size energy increase is not seen in both months due to the sun's position in the sky (the collector slope is 22 degrees from the horizontal). In summer the sun is higher in the sky; therefore, the beam radiation will be closer to normal with the collector. Since $K_{\tau\alpha}$ corrects for the deviation of the beam radiation from a normal position, less correction is needed during the summer months.

Applying each of the four different screening methods to each month gives the $F_R(\tau\alpha)_n$ and F_RU_L values shown in table (5.3.13). Also included in the table are the total monthly energy gains by the collector model using the $F_R(\tau\alpha)_n$ and F_RU_L pairs and the experimental data from the month. For June through January G_{test} is 9.25 and

TABLE 5.3.13 Collector parameters calculated using the four different screening methods in the efficiency method along with the corresponding energy gain calculated using the parameters in the TRNSYS collector model. F_RU_L has units of (Btu/hr-ft^2-°F) and Q_{col} has units of (million Btu).

Month	Meth	$F_R(\tau\alpha)_n$	F_RU_L	Q_{col}	Meth	$F_R(\tau\alpha)_n$	F_RU_L	Q_{col}
Jun	1a	.712	.383	2.44	1b	.730	.361	2.55
	2a	.674	.246	2.46	2b	.702	.288	2.52
	3a	.666	.233	2.44	3b	.699	.292	2.50
	4a	.702	.379	2.41	4b	.712	.359	2.47
Jul	1a	.642	.113	4.19	1b	.657	.124	4.27
	2a	.638	.075	4.22	2b	.653	.087	4.31
	3a	.637	.043	4.27	3b	.652	.055	4.35
	4a	.655	.117	4.27	4b	.660	.122	4.29
Aug	1a	.629	.112	5.42	1b	.637	.048	5.63
	2a	.634	.135	5.41	2b	.669	.180	5.63
	3a	.631	.121	5.42	3b	.644	.074	5.64
	4a	.666	.187	5.59	4b	.678	.193	5.68
Sep	1a	.647	.333	3.35	1b	.666	.273	3.61
	2a	.643	.330	3.34	2b	.667	.289	3.58
	3a	.650	.349	3.34	3b	.671	.306	3.56
	4a	.664	.323	3.48	4b	.676	.318	3.57
Oct	1a	.646	.387	2.41	1b	.671	.335	2.62
	2a	.639	.377	2.39	2b	.664	.314	2.62
	3a	.639	.370	2.40	3b	.663	.337	2.58
	4a	.664	.382	2.50	4b	.680	.377	2.59

Nov	1a	.635	.598	0.49	1b	.782	.706	0.61
	2a	.632	.579	0.49	2b	.738	.638	0.59
	3a	.663	.615	0.51	3b	.726	.626	0.58
	4a	*	*	*	4b	.677	.371	0.62
Dec	1a	.605	.357	1.46	1b	.640	.282	1.64
	2a	.597	.325	1.47	2b	.632	.255	1.64
	3a	.594	.314	1.47	3b	.613	.209	1.63
	4a	*	*	*	4b	*	*	*
Jan	1a	.658	.462	1.66	1b	.693	.454	1.81
	2a	.655	.455	1.66	2b	.689	.444	1.82
	3a	.653	.453	1.66	3b	.686	.440	1.81
	4a	.688	.514	1.68	4b	.719	.511	1.81
Feb	1a	.742	.958	2.59	1b	.778	.950	2.85
	2a	.725	.884	2.66	2b	.760	.880	2.91
	3a	.722	.872	2.67	3b	.758	.871	2.92
	4a	*	*	*	4b	*	*	*
Mar	1a	.664	.693	5.22	1b	.667	.573	5.56
	2a	.661	.679	5.22	2b	.670	.596	5.53
	3a	.664	.695	5.21	3b	.675	.627	5.50
	4a	.658	.612	5.36	4b	.664	.557	5.57
Apr	1a	.629	.425	4.33	1b	.636	.403	4.44
	2a	.638	.462	4.33	2b	.645	.439	4.44
	3a	.637	.458	4.53	3b	.638	.411	4.44
	4a	.658	.558	4.31	4b	.663	.540	4.38

May	1a	.650	.535	4.21	1b	.649	.471	4.34
	2a	.658	.595	4.15	2b	.657	.525	4.29
	3a	.650	.573	4.13	3b	.656	.525	4.29
	4a	.665	.616	4.16	4b	.665	.554	4.30

* Times when no points were left after screening the data or when the curvefit resulted in negative $F_R U_L$ values.

for February through May G_{test} is 6.94. In November no values are shown for the fourth method since only two points were left after screening the data, with only two points the resulting collector parameters would not necessarily reflect the collector characteristics. In December no points were left after screening so no values are given for the fourth method. In February seven points were available using the fourth method but the resulting curvefit had a positive slope which does not conform to theory so the values are not shown. Comparing the monthly energy gain found using the four pairs of $F_R(\tau\alpha)_n$ and $F_R U_L$ values in each month shows some variation, but when used in the collector model the resulting monthly energy gains show that there is not much difference between the four methods. For the months when $K_{\tau\alpha}$ was ignored the largest percent difference between methods (within a month) is five percent occuring in April. When $K_{\tau\alpha}$ is included, the largest difference is three percent occuring in June. Also the method giving the highest and lowest monthly energy gain varies from month to month; therefore, since there is not much difference between methods and all of the methods vary, it was decided to use only the values calculated by the first method (both "a" and "b") when making comparisons with the experimental monthly energy gain calculated directly from the experimental data and the monthly energy gain calculated using the ASHRAE test parameters.

In addition to calculating the two collector parameters on a monthly basis from the experimental data, a single linear curve fit was also done on all of the efficiency and operating points for all of the months using each of the four methods. The results of

this are shown in table (5.3.14), with the values calculated excluding $K_{\tau\alpha}$ on the left and including $K_{\tau\alpha}$ on the right. When calculating the monthly total energy gain using these $F_R(\tau\alpha)_n$ and F_RU_L values G_{test} was set equal to 8.1 which is the average between the G_{test} value for June-January (9.25) and February-May (6.94). The average was used to account for the change in collector flow rate that occurs in February, however if 9.25 or 6.94 had been used for all of the months, the difference in the monthly energy gain is usually less than one percent, so it does not really make any difference in the results for the Trident system.

TABLE 5.3.14 $F_R(\tau\alpha)_n$ and F_RU_L values calculated by curvefitting all of the efficiency and operating points for the entire year.

	"a"			"b"		
Method	$F_R(\tau\alpha)_n$	F_RU_L (Btu/hr-ft^2-°F)	#pts	$F_R(\tau\alpha)_n$	F_RU_L (Btu/hr-ft^2-°F)	#pts
1	.612	.264	505	.633	.238	497
2	.621	.237	310	.631	.232	310
3	.610	.261	502	.634	.252	496
4	.614	.287	498	.631	.248	495

Based on the monthly collector results, the energy gains calculated using the "year" $F_R(\tau\alpha)_n$ - F_RU_L pairs were only done using method "b" (i.e. including $K_{\tau\alpha}$). The resulting monthly energy gains are listed in table (5.3.15). The results show that, again, the data screening method used does not make a large difference in the final results; however, in this case the fourth method always gives the lowest monthly energy gain and either the first or second method give the highest. This is expected since the same pair of $F_R(\tau\alpha)_n$ and F_RU_L values were used for each month.

Therefore, as with the monthly calculated values, only the values calculated using the first method will be included when making comparisons with the experimental monthly energy gain calculated directly from the experimental data and the monthly energy gain calculated using the ASHRAE test parameters.

TABLE 5.3.15 Monthly total energy gain by the collection model for each month using the "year" $F_R(\tau\alpha)_n$ and F_RU_L values from the "b" side of the table (5.3.14).

Total Monthly Energy Gain using "year" values (million Btu)

Month	Method			
	1b	2b	3b	4b
Jun	2.30	2.30	2.29	2.28
Jul	3.95	3.95	3.94	3.92
Aug	5.18	5.18	5.16	5.14
Sep	3.48	3.48	3.46	3.45
Oct	2.62	2.62	2.60	2.59
Nov	0.63	0.63	0.62	0.62
Dec	1.67	1.67	1.65	1.65
Jan	1.99	1.99	1.97	1.96
Feb	3.68	3.68	3.65	3.64
Mar	6.06	6.06	6.04	6.02
Apr	4.73	4.73	4.71	4.69
May	4.70	4.70	4.68	4.66

Summarizing the results presented for the efficiency method, it has been shown that all four data screening methods give approximately the same monthly total energy gains. This is true when $F_R(\tau\alpha)_n$ and F_RU_L are calculated on both the monthly and

yearly basis. It has also been determined that including $K_{\tau\alpha}$ when calculating the efficiency and operating point values changes the $F_R(\tau\alpha)_n$ and F_RU_L values so that the collector performance improves (i.e. energy gain over the month increases).

V.3.6 Collector Model Method

Section (IV.2.2) describes the theory and approach used to obtain the results given in this section. This method differs from the efficiency method since the $F_R(\tau\alpha)_n$ and F_RU_L values were not calculated for each individual month. Instead an equation was found that gives all of the $F_R(\tau\alpha)_n$ - F_RU_L pairs that cause the collector model to gain the same monthly total energy that was actually gained by the Trident system.

The twelve lines calculated from the experimental data (one per month) are plotted in figure (5.3.2) and have the form:

$$F_RU_L = A\,(F_R(\tau\alpha)_n) + B \qquad (5.3.6)$$

where (A) and (B) for each month are given in table (5.3.16). As stated in section (IV.2.2) theoretically all of the lines should cross at a single point if the collector characteristics are the same for every month. However figure (5.3.2) shows that two distinct groupings are formed from the twelve lines. One group consists of the months June through October and the other group from November through May. In November water in the collector froze damaging three of the absorber plates. It is believed that when the panels were replaced the characteristics of the entire collector array were changed, causing the two separate groupings. This seems to be the only explanation since no other significant events happened between October and November.

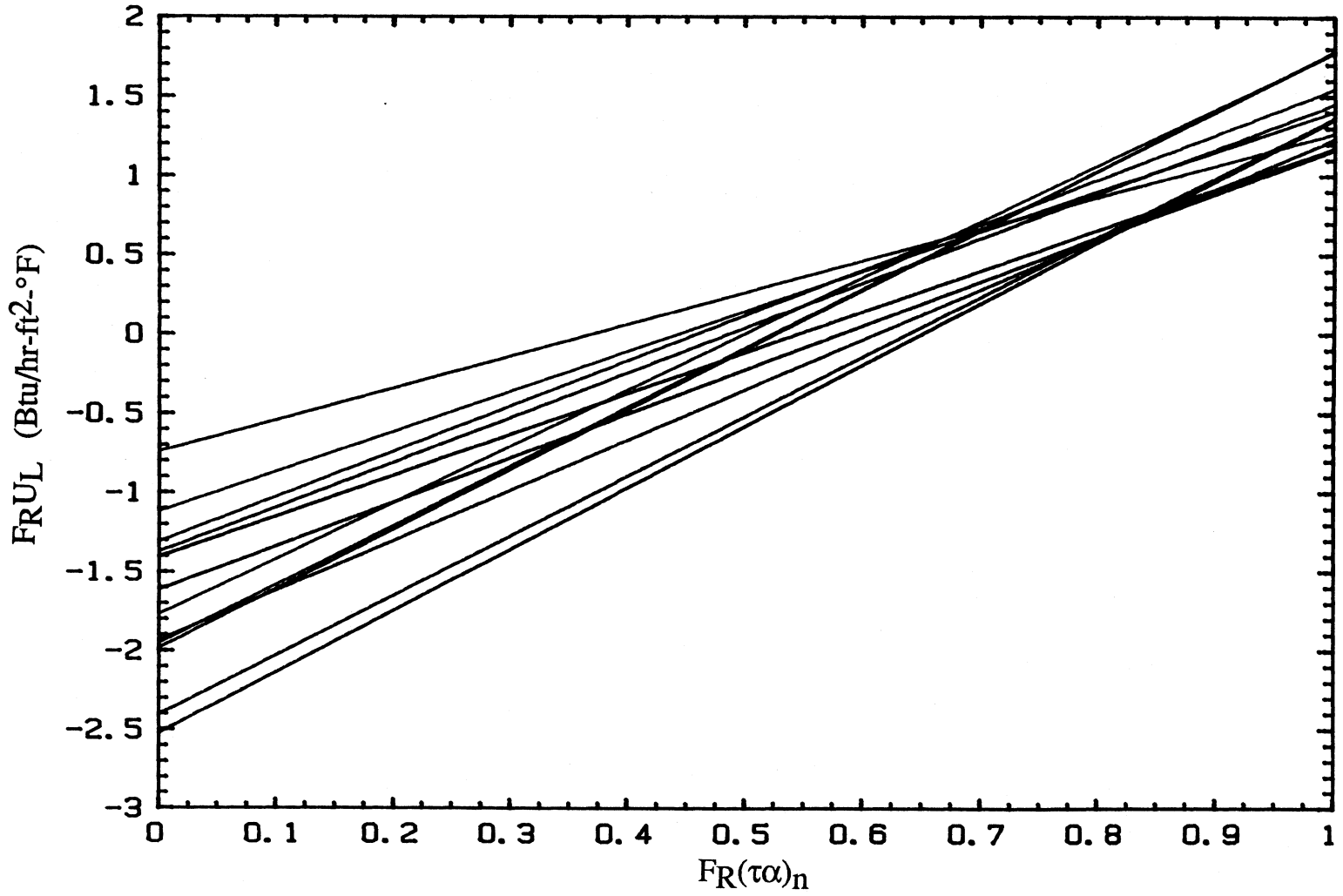

FIGURE 5.3.2 Monthly $F_R(\tau\alpha)_n$ - F_RU_L relationship lines calculated using the collector model method. (Trident)

TABLE 5.3.16 $F_R(\tau\alpha)_n$ - F_RU_L relationship equations calculated for each month.

Month	Equation Values A	B
Jun	3.167	-1.938
Jul	3.770	-2.408
Aug	3.880	-2.526
Sep	2.782	-1.617
Oct	2.581	-1.408
Nov	2.831	-1.375
Dec	2.863	-1.312
Jan	2.014	-0.743
Feb	2.532	-1.121
Mar	3.738	-1.957
Apr	3.774	-1.988
May	3.552	-1.775

Upon closer inspection (look ahead to figure (5.3.3)) it can be seen that within each grouping the lines do not all intersect at a single point. This is to be expected since experimental measurements were being used to calculate the $F_R(\tau\alpha)_n$ and F_RU_L lines. Also the collector characteristics can vary just by having dirt or snow on the cover; therefore, some variance is expected.

Since there are two distinct groupings, two $F_R(\tau\alpha)_n$ - F_RU_L pairs were determined, one that best "fits" each grouping and one that best fits all twelve of the values. The resulting pairs are given in table (5.3.17), and also plotted in figure (5.3.3) which is an expanded view of figure (5.3.2).

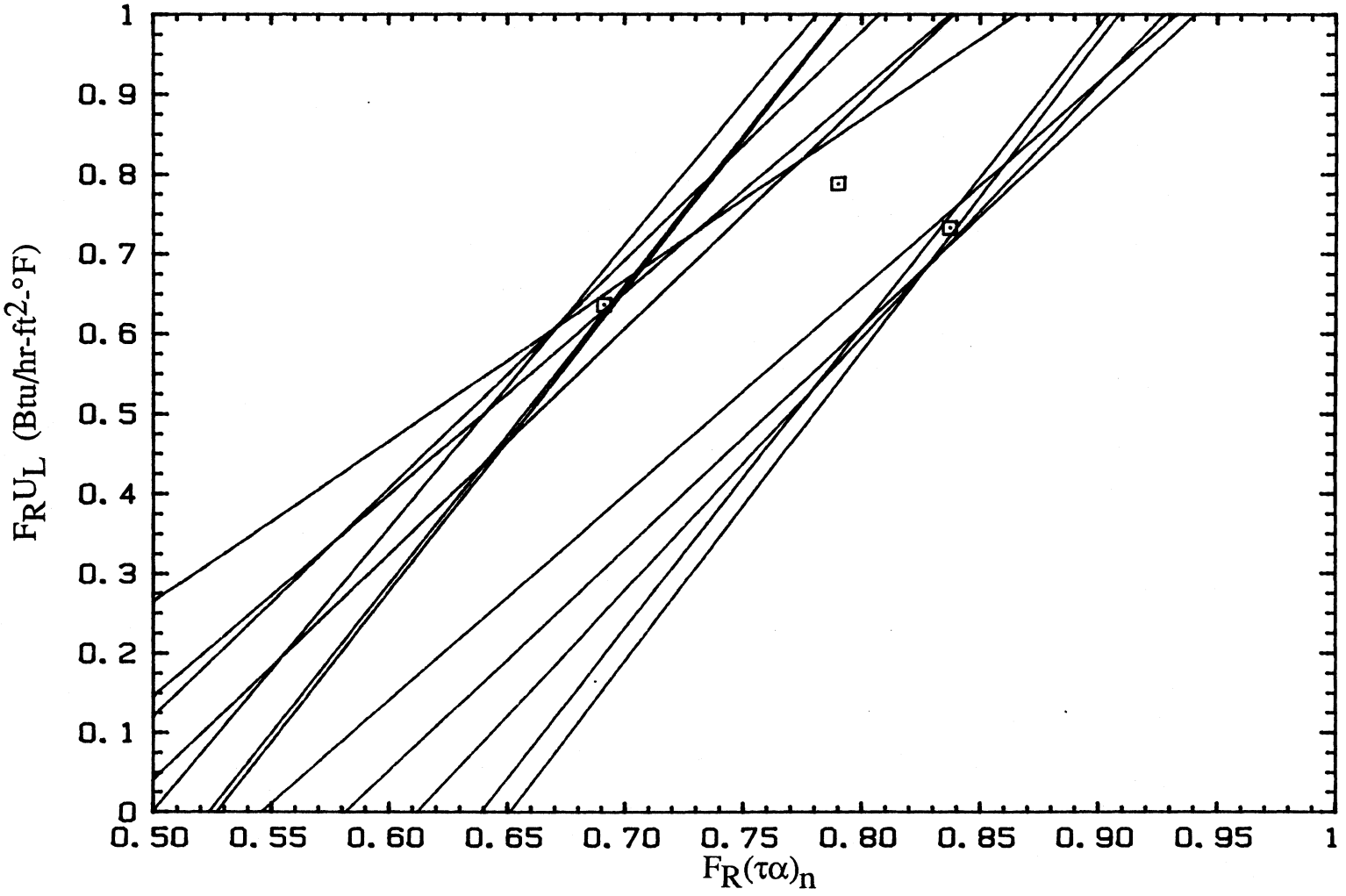

FIGURE 5.3.3 Expanded view of figure (5.3.1) showing the "best fit" $F_R(\tau\alpha)_n$ - F_RU_L values for all twelve lines and for each group.

TABLE 5.3.17 $F_R(\tau\alpha)_n$ and F_RU_L values that "best fit" the $F_R(\tau\alpha)_n$ - F_RU_L lines calculated using the collector model method. (Trident)

	$F_R(\tau\alpha)_n$	F_RU_L (Btu/hr-ft^2-°F)
Jun-Oct	0.838	0.732
Nov-May	0.691	0.636
Jun-May	0.790	0.788

These values can now be used in the collector model to calculate the total monthly energy gain for each month. The results of this are shown in the next section in table (5.3.18) in columns 6 and 7.

V.3.7 Final Comparison Results

So far, results have been presented comparing the different ways of calculating $F_R(\tau\alpha)_n$ and F_RU_L from the experimental data using the efficiency and collector model methods. The next step is to compare the total monthly collector energy gains (calculated from the $F_R(\tau\alpha)_n$ and F_RU_L values by using them in the collector model deck (described in section (V.3.3)) from each method with those found using the ASHRAE test values and with the experimental monthly energy gain calculated from the experimental data. Table (5.3.18) contains a summary of the total monthly collector gain values that will be compared. Column (1) contains the energy gains calculated from the experimental data. Column (2) contains the energy gains calculated using the $F_R(\tau\alpha)_n$ - F_RU_L pair from the ASHRAE tests. Column (3) and (4) (from table (5.3.13) were calculated using the efficiency method with screening methods (1a) and

(1b) respectively, on a month by month basis. Column (5) (from table (5.3.15)) was also calculated using the efficiency method with screening method (1b) on a yearly basis. Columns (6) and (7) were calculated using the collector model method by calculating the "best fit" for all twelve months for column (6) and for each of the two groups (Jun-Oct and Nov-May) for column (7).

TABLE 5.3.18 Monthly total collector energy gain (in million Btu) calculated using the methods as described in the text.

Month	Experi-mental	ASHRAE	Efficiency Method			Collector Model Method	
			(month)		(year)		
			1a	1b	1b	12 Mon	groups
	(1)	(2)	(3)	(4)	(5)	(6)	(7)
Jun	2.51	1.83	2.44	2.55	2.30	2.22	2.49
Jul	4.36	3.29	4.19	4.27	3.95	3.97	4.40
Aug	5.86	4.38	5.42	5.63	5.18	5.29	5.84
Sep	3.67	2.62	3.35	3.61	3.48	3.20	3.63
Oct	2.62	1.90	2.41	2.62	2.62	2.33	2.66
Nov	0.55	0.47	0.49	0.61	0.63	0.58	0.53
Dec	1.38	1.27	1.46	1.64	1.67	1.55	1.41
Jan	1.42	1.22	1.66	1.81	1.99	1.54	1.44
Feb	3.01	2.65	2.59	2.85	3.68	3.26	2.99
Mar	5.54	5.07	5.22	5.56	6.06	6.13	5.51
Apr	4.35	3.97	4.33	4.44	4.73	4.80	4.31
May	4.13	3.88	4.21	4.34	4.70	4.70	4.23

Comparing the experimental and ASHRAE values (columns (1) and (2) respectively) it can be seen that the experimental monthly energy gains are larger than the "predicted" (ASHRAE) energy gains during every month. This was not expected since typically the experimental system performance is worse than the predicted performance. There are two possible reasons that this would occur.

1) One or more of the measured sensor values (i.e. solar radiation, fluid flow, and/or temperatures) are in error.

2) The field collector actually operated better than the ASHRAE test parameters predicted it would.

First the solar radiation measurement was checked. Two days of experimental data with smooth radiation (i.e. clear sky conditions) were chosen and compared to the solar radiation incident on the collector calculated by Hottel's clear sky equation using the 23 km visibility standard atmosphere [10]. Figures (5.3.4) and (5.3.5) show the experimental and calculated solar radiation incident on the tilted collector surface for August 29th and December 16th, respectively. The results show close agreement indicating that the measurements are probably not the cause of the large difference between the experimental and predicted monthly energy gains.

It is not possible to determine if the collector flow rate, or the collector inlet and outlet temperatures are accurate, since there is no way to verify them. This means that it is also not possible to determine if the experimental monthly energy gain or the predicted energy gains are accurate since each calculation uses the experimental data. (The experimental energy gain uses the collector flow rate, and the collector inlet and outlet temperature data. The predicted energy gain uses the collector flow rate, collector inlet temperature, ambient temperature, and solar radiation data.) Therefore, it is not

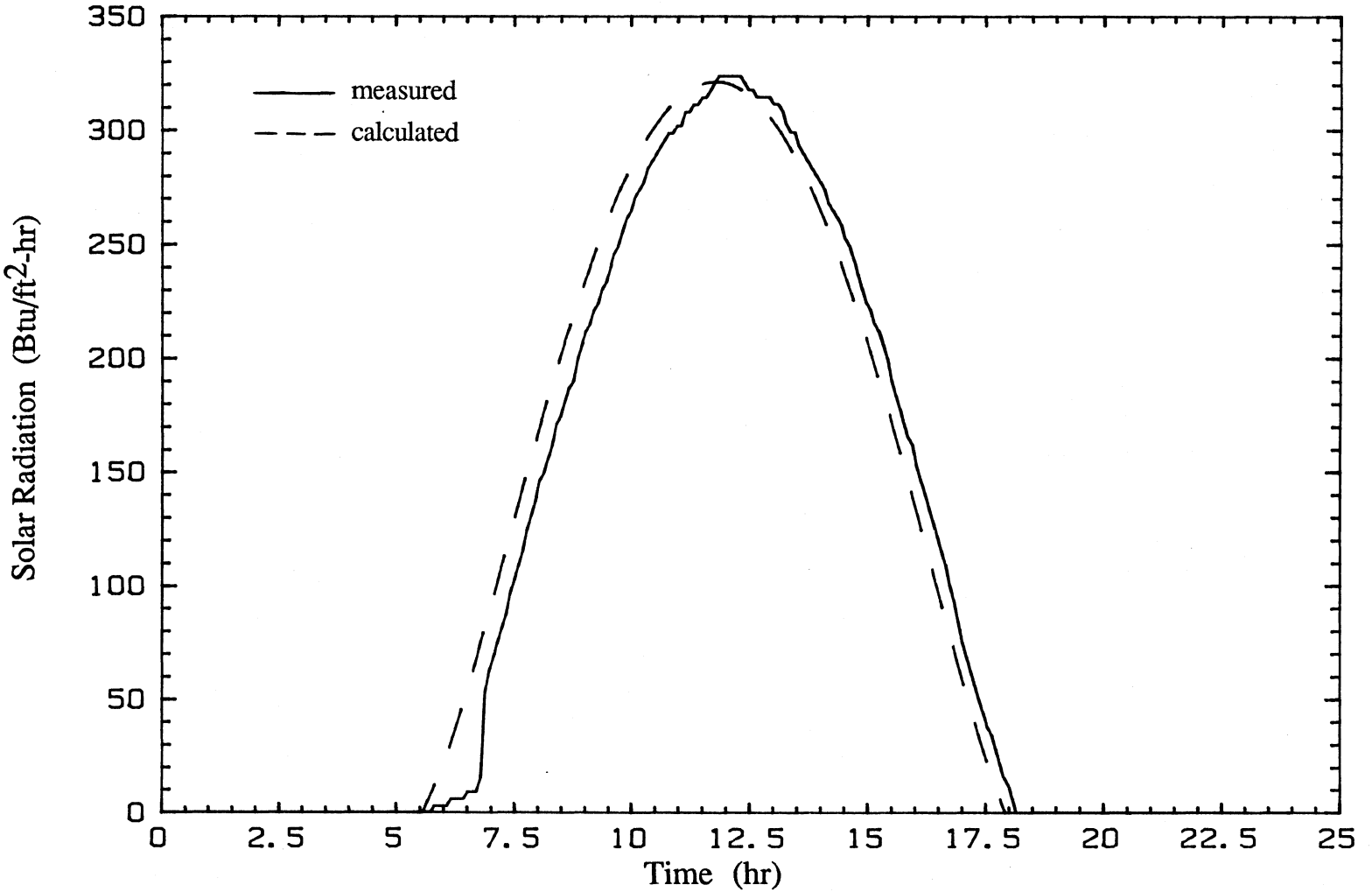

FIGURE 5.3.4 Measured and calculated (by Hottel's clear sky equation using a 23 km visibility standard atmosphere) solar radiation on the tilted collector surface for August 29. (Trident)

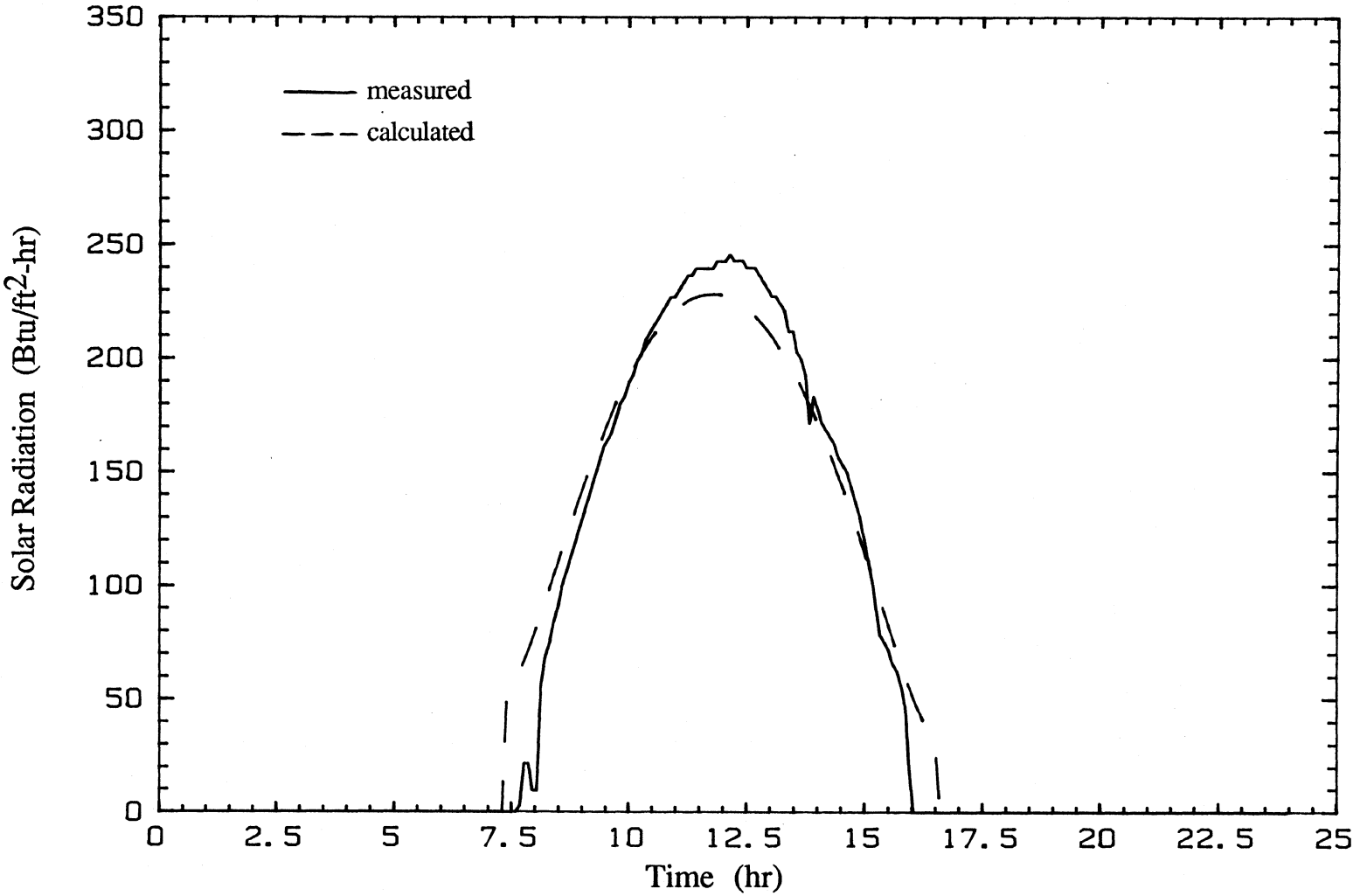

FIGURE 5.3.5 Measured and calculated (by Hottel's clear sky equation using a 23 km visibility standard atmosphere) solar radiation on the tilted collector surface for December 16. (Trident)

possible to determine if the field collector performed better than was predicted by the ASHRAE test values or if the experimental data are inaccurate. Therefore, reasons for the difference between the experimental and predicted values cannot be determined. The only way to find out why they are different would have been to check the sensors on the solar system when the data was collected.

Although reasons for the differences between the experimental and ASHRAE values cannot be determined the rest of the methods used to calculate the collector energy gain were still compared to the experimental data. This was done to determine how well the ASHRAE test values ($F_R(\tau\alpha)_n$ and F_RU_L) represent the measured operating collector characteristics. Each method is compared to the experimental energy gain values by subtracting the energy gain of each method (by months) from the measured energy gain. The differences are presented in table (5.3.19), where column (A) is column (1) minus column (2) from table (5.3.18), column (B) is column (1) minus column (3), etc. (The columns in table (5.3.18) will be referred to as columns (1) thru (7) and the columns in table (5.3.19) as columns (A) thru (F).)

The energy differences from table (5.3.19) are plotted in figures (5.3.6), (5.3.7), and (5.3.8). Figure (5.3.6) shows the ASHRAE (A) and efficiency method (on a yearly basis) (D) differences. The ASHRAE values always overpredicts gains. The efficiency method first overpredicts and then underpredicts the energy gains. Figure (5.3.7) shows the month by month efficiency method values setting $K_{\tau\alpha}$ equal to one (B) and by calculating $K_{\tau\alpha}$ (C). Both methods overpredict in the summer but then vary during the rest of the year. The plot shows that when including the $K_{\tau\alpha}$ (C) calculation (C) the resulting collector parameters do a better job predicting the actual energy gains. This indicates that the beam radiation incidence angle affects the collector results. Figure (5.3.8) shows the collector model method results (E and F). The collector parameters calculated by solving all 12 equations at once first overpredicts and then underpredicts the monthly total energy balances. On the other hand using the

TABLE 5.3.19 Monthly energy difference values between methods 2-7 and the experimental monthly energy values (1) in million Btu.

	A (1-2)	B (1-3)	C (1-4)	D (1-5)	E (1-6)	F (1-7)
Jun	.68	.07	-.04	.21	.29	.02
Jul	1.07	.17	.09	.41	.39	-.04
Aug	1.48	.44	.23	.68	.57	.02
Sep	1.05	.32	.06	.19	.47	.04
Oct	.72	.21	0	0	.29	-.04
Nov	.08	.06	-.06	-.08	-.03	.02
Dec	.11	-.08	-.26	-.29	-.17	-.03
Jan	.20	-.24	-.39	-.57	-.12	-.02
Feb	.36	.42	.16	-.67	-.25	.02
Mar	.47	.32	-.02	-.55	-.59	.03
Apr	.38	.02	-.09	-.38	-.45	.04
May	.25	-.08	-.21	-.57	-.57	-.10

collector parameters calculated by solving the two groups separately does the best job of all the methods.

While figures (5.3.6), (5.3.7), and (5.3.8) give a graphical representation of the energy differences, table (5.3.20) shows the mean and standard deviation for each method over the year. The mean indicates how well the method does over the entire year. The closer the mean is to zero the closer the long term results will be to the actual results. The standard deviation indicates how the individual months vary. Table (5.3.20) shows that column (F) (method (7)) does the best job over the entire year and over the individual months. All of the methods, ranked from best to worst, are as follows: (F), (C), (B), (E), (D), and (A). This indicates that predicting the $F_R(\tau\alpha)_n$,

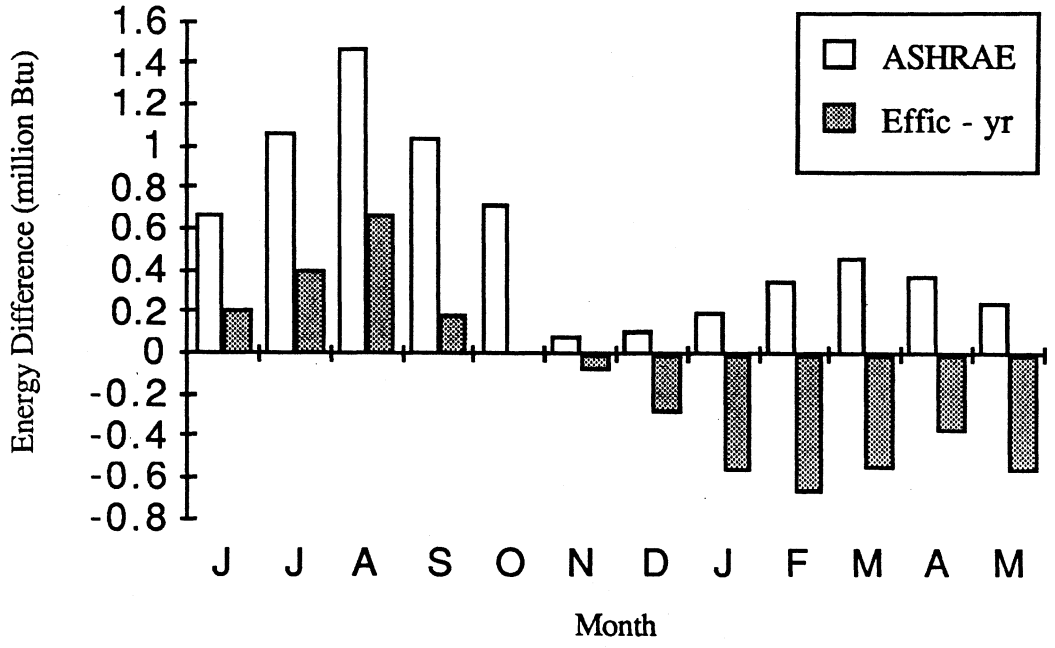

FIGURE 5.3.6 Energy differences from columns (A) and (D) in table (5.3.19).

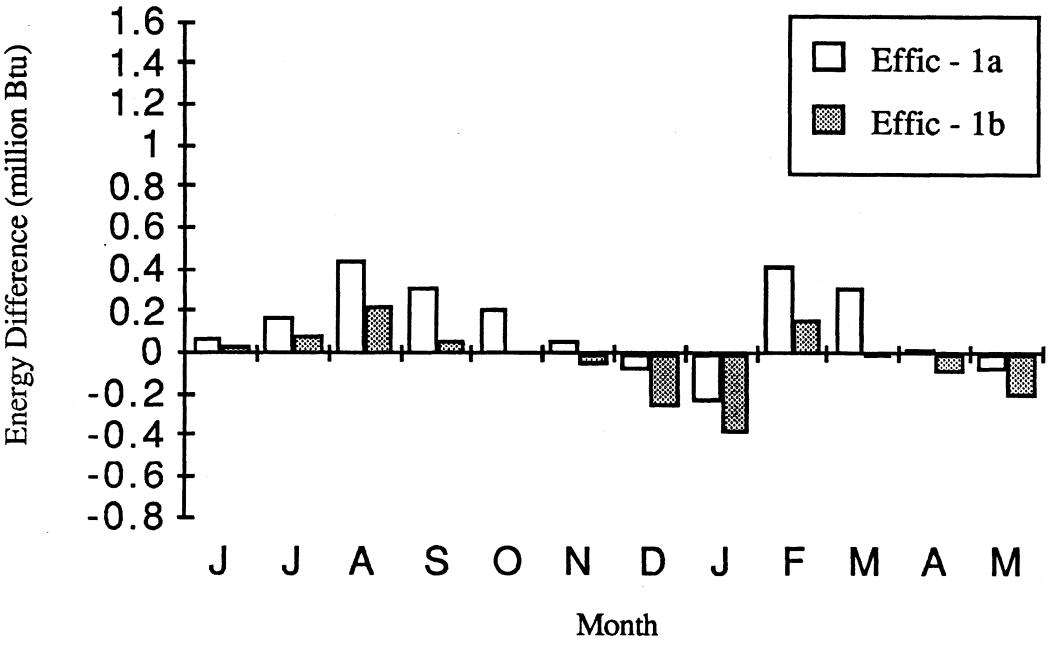

FIGURE 5.3.7 Energy differences from columns (B) and (C) in table (5.3.19).

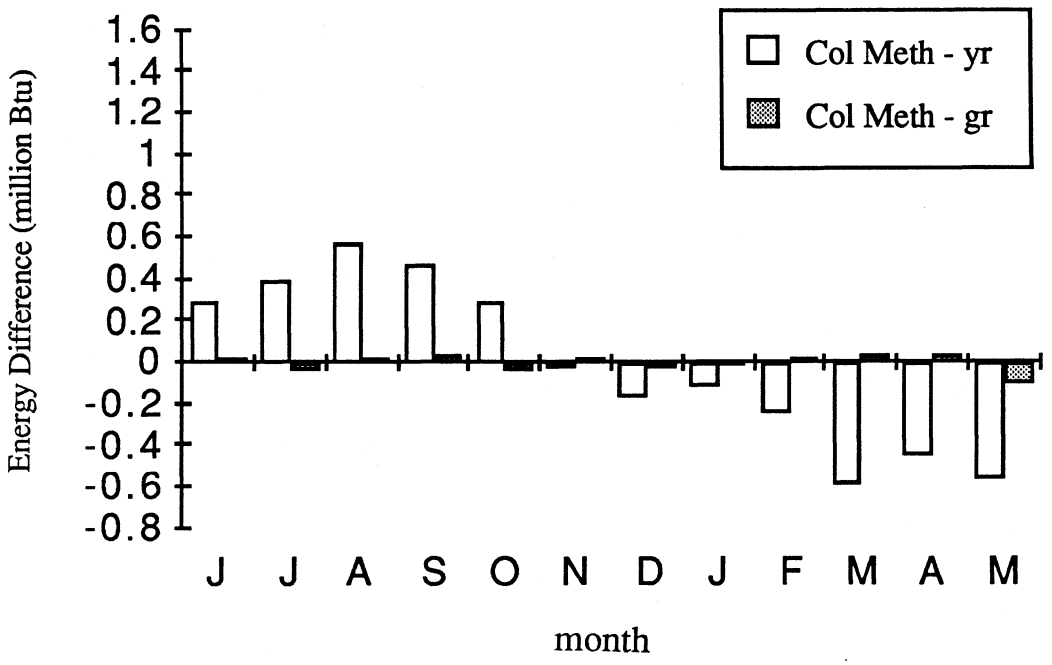

FIGURE 5.3.8 Energy differences from columns (E) and (F) in table (5.3.19).

TABLE 5.3.20 Mean and standard deviation (in million Btu) of the energy differences listed in table (5.3.19).

Column	mean	standard deviation
A	0.570	0.44
B	0.136	0.21
C	-0.044	0.18
D	-0.135	0.44
E	-0.014	0.41
F	-0.003	0.04

F_RU_L values on a monthly basis (for the efficiency method (C and B)) is better than finding a single value over the entire year; however, the collector model method has shown that the collector characteristics changed in November. This indicates that any method calculated using a single pair of $F_R(\tau\alpha)_n$, F_RU_L values over the entire year will, at best, determine an averaged value and therefore will be in error for both groups. If the collector characteristics had not changed drastically in November the year methods would have done a better job than they did for the Trident system. The worst method uses the ASHRAE $F_R(\tau\alpha)_n$, F_RU_L values.

The methods could also have been compared by looking at the total energy supplied over the year; however, this does not take into account the variations during the individual months. Table (5.3.21) shows the total collected energy over the year for each method (obtained by summing the twelve monthly values) and the percent difference it is from the actual value.

The table shows that method (7) does the best job over the entire year, which was expected since it had the smallest mean and standard deviation. The table also shows that every method except (2), (which used the ASHRAE $F_R(\tau\alpha)_n$ - F_RU_L values) are

TABLE 5.3.21 Total collector energy gain over the entire year calculated by summing the monthly values given in table (5.3.18).

Method	Total energy gain (million Btu)	% difference from (1)
1	39.4	-
2	32.6	-17
3	37.8	-4
4	39.9	1
5	41.0	4
6	39.6	-0.5
7	39.4	0

within 5 percent of the experimental values. This indicates that all of the methods (except (2)) do a good job over the year; however, since the collector model is only one part of the solar energy system its performance over the months will affect the other parts which will then affect the collector. This means that the overall system results (i.e. energy collected, energy to load, solar fraction, etc) would probably be different by using, for example, the efficiency year method (5) and the collector model method (using the values from curvefitting the two groups (7)). Therefore it is recommended that the monthly totals be looked at to determine which method does the best job.

V.4 IMMERSED HEAT EXCHANGER

V.4.1 External Heat Exchanger Model

Modeling the immersed heat exchanger as a constant effectiveness, external heat exchanger is done, as shown in figure (5.4.1), by moving the heat exchanger outside

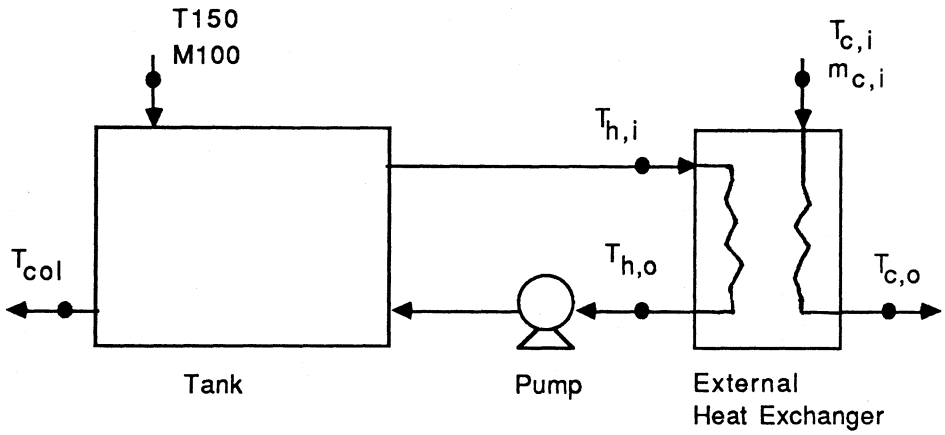

FIGURE 5.4.1 Modeling the immersed heat exchanger as an external heat exchanger.

of the tank and adding a pump to circulate the tank water through the heat exchanger. The model consists of the multi-node, stratified fluid storage tank model (type 4), connected to the heat exchanger model (type 5) in the constant effectiveness mode, via a pump (type 3). The model is driven using the experimental temperature value T150 and the collector flow rate M100 as the tank inlet variables, and using the experimental heat exchanger coil inlet temperature and flow rate for the load variables. The experimental temperature ($T_{c,i}$) and flow rate ($\dot{m}_{c,i}$) are calculated as:

$$T_{c,i} = \left[\frac{(T300)(M300) + (T400)(M400)}{M300 + M400} \right] \qquad (5.4.1)$$

$$\dot{m}_{c,i} = M300 + M400 \qquad (5.4.2)$$

The time interval used for the external heat exchanger model simulation tests was 5 minutes 20 seconds. The data was "fixed" as explained in section (III.2) for TRNSYS decks containing storage components (i.e. tank) with missing data records being filled by linearly interpolating the data before and after the gap. All model testing was done for the months February through May since at least 98 percent of the data was available for them. A sample TRNSYS deck of the external heat exchanger model is given in Appendix (B.2).

The tank is modeled as a three node tank since three experimental tank temperatures were measured.

V.4.1.1 Problems associated with the external model

There are two major problems encountered when using the external heat exchanger model.

1) The model does not adequately model tank stratification since adding a pump mixes the tank, destroying stratification.

2) There is no adequate way of determining what effectiveness should be used in the model.

The first problem occurs since the heat exchanger is no longer inside the tank and a pump must be added to circulate the tank water through the external heat exchanger. This causes forced mixing in the tank destroying any existing stratification. If the tank is not stratified this is not a problem. Feiereisen et al. [6] showed that for supply-side heat exchangers, stratification is negligible and can be ignored. However, experimental temperature data from the Trident storage tank show that the load-side heat exchanger actually induces stratification in the tank as shown in figure (5.4.2). Stratification mainly is established when DHW draws occur, which can be attributed to the large temperature difference between the city mains water and the tank temperature.

The second problem occurs because an overall effectiveness value is affected by the degree of stratification found in the tank. For tests done on the Trident heat exchanger, Farrington [5] concluded:

"The effectiveness is not a strong function of the temperature difference between the heat exchanger inlet and storage tank, but is a strong function of the stratification as it changes with time"

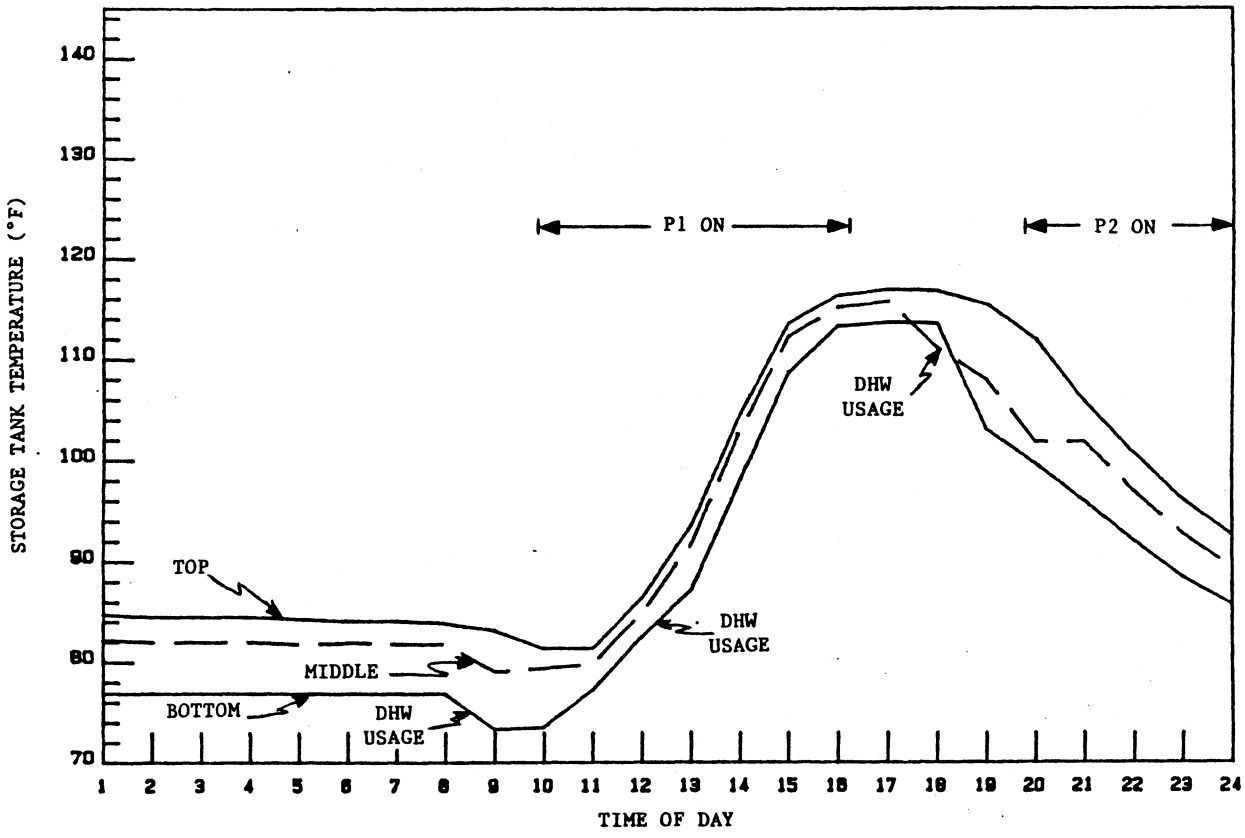

FIGURE 5.4.2 Trident system storage tank stratification for March 30, 1985 (taken from ref. [3]).

This indicates that the more stratification there is in a tank the more difficult it is to calculate an average effectiveness that will be accurate.

V.4.1.2 Pump flow rate control

The pump causes mixing in the tank, which does not occur with the actual immersed heat exchanger since it does not require a pump. Therefore to minimize tank mixing the pump flow rate must be made as small as possible; however, the pump flow rate must not become smaller than the heat exchanger coil flow rate (i.e. load flow rate). The reason for this is that the minimum flow rate affects the amount of energy transfer across the heat exchanger (see equation (5.4.3)). (Actually the minimum thermal capacitance rate ($(mC_p)_{min}$) is used, but the flow rate will be used for discussion purposes since both fluids are water with $C_p \approx 1$ Btu/lbm-°R.)

$$Q_T = \varepsilon (\dot{m}C_p)_{min}(T_{h,i} - T_{c,i}) \qquad (5.4.3)$$

Therefore the pump flow rate should always be set equal to the coil flow rate during each timestep. This will cause the coil flow rate to control the heat transfer rate and minimize tank mixing since the pump will operate at the lowest possible flow rate without controlling the heat transfer and run only when heat transfer is occurring (i.e. when the coil flow is greater than zero).

V.4.1.3 Comparisons of different pump flow rate patterns

To show how the heat exchanger pump flow rate affects tank mixing, comparisons were done using the following three pump patterns:

1) The heat exchanger pump is run continuously at a constant flow rate during the entire simulation.

2) The heat exchanger pump is run only when there is flow in the coil at a constant flow rate.

3) The heat exchanger pump is run only when there is flow in the coil and at the coil flow rate.

The first comparison was made using the first two pump flow patterns in the external heat exchanger model. March data was used to drive the model with an effectiveness of 0.4. Figure (5.4.3) shows the total energy transfer over the month plotted as a function of the pump flow rate used during the month for each of the patterns. The plot shows that less heat transfer occurs when the pump runs continuously. This occurs due to mixing of the three tank nodes by the pump flow. The effects of the mixing can be seen in figures (5.4.4) and (5.4.5) where the daily average node temperatures are plotted for a flow rate equal to 2000 lbm/hr and an effectiveness equal to 0.8. For the constant flow model (figure (5.4.4)) the two bottom nodes tend to be closer together in temperature which shows the effect of mixing caused by removing water from the top node and returning it to the bottom node. For the variable flow case (figure (5.4.5)) the temperatures are more spread out with the middle temperature slightly closer to the top temperature. To compare the two methods (1 and 2), the difference between each of the node temperatures has been calculated (variable flow model (2) temperatures minus the constant flow model (1) temperatures) and plotted in figure (5.4.6). The plot shows that the top and middle node temperatures from the variable model are always higher than in the constant model and that the bottom temperature is always lower. Again this shows that the continuously running pump transfers energy from the top node to the middle and bottom nodes through mixing.

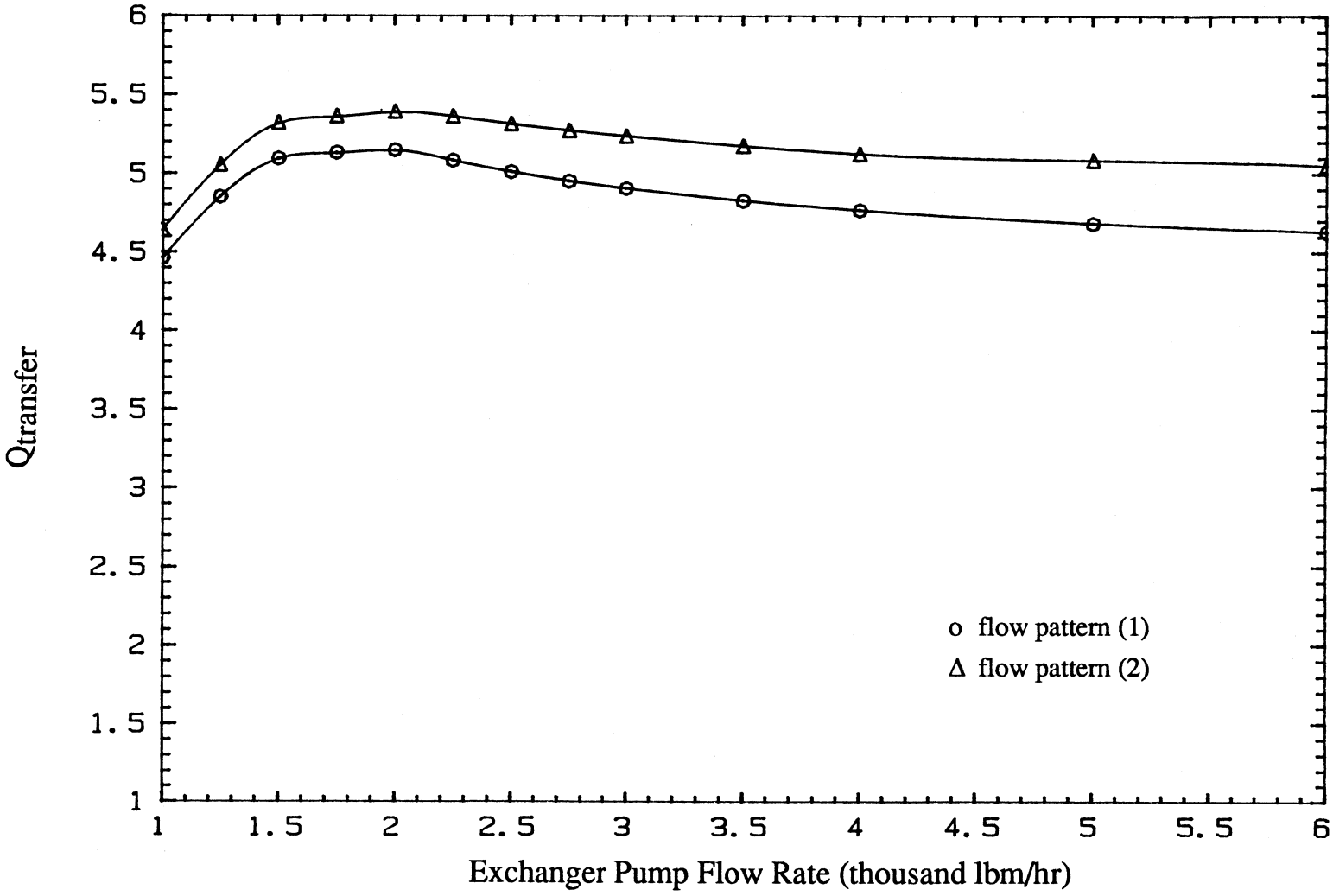

FIGURE 5.4.3 Total monthly energy transferred across the external heat exchanger model using flow patterns (1) and (2).

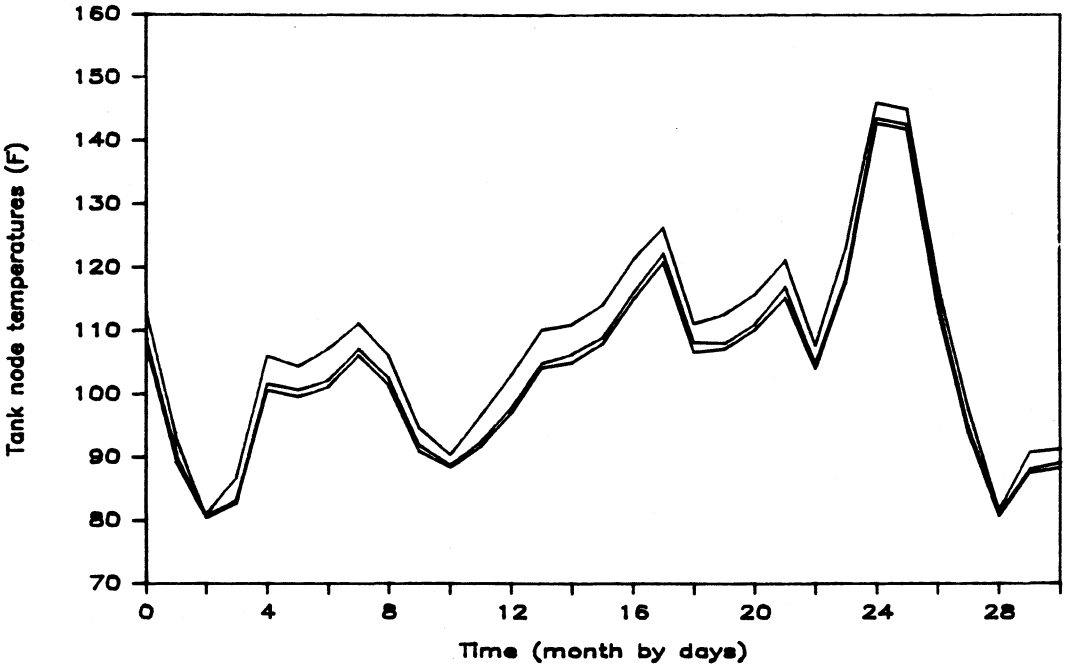

FIGURE 5.4.4 March tank node temperatures calculated using flow pattern (1) in the immersed heat exchanger model. ($\varepsilon = 0.8$, $\dot{m} = 2000$ lbm/hr).

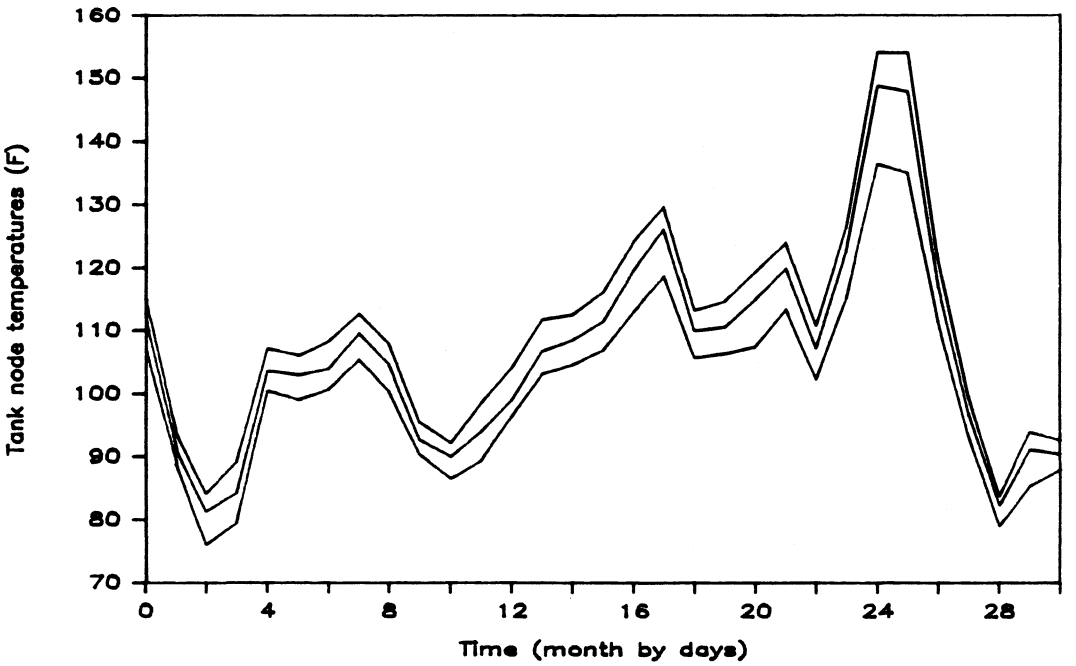

FIGURE 5.4.5 March tank node temperatures calculated using flow pattern (2) in the immersed heat exchanger model. ($\varepsilon = 0.8$, $\dot{m} = 2000$ lbm/hr).

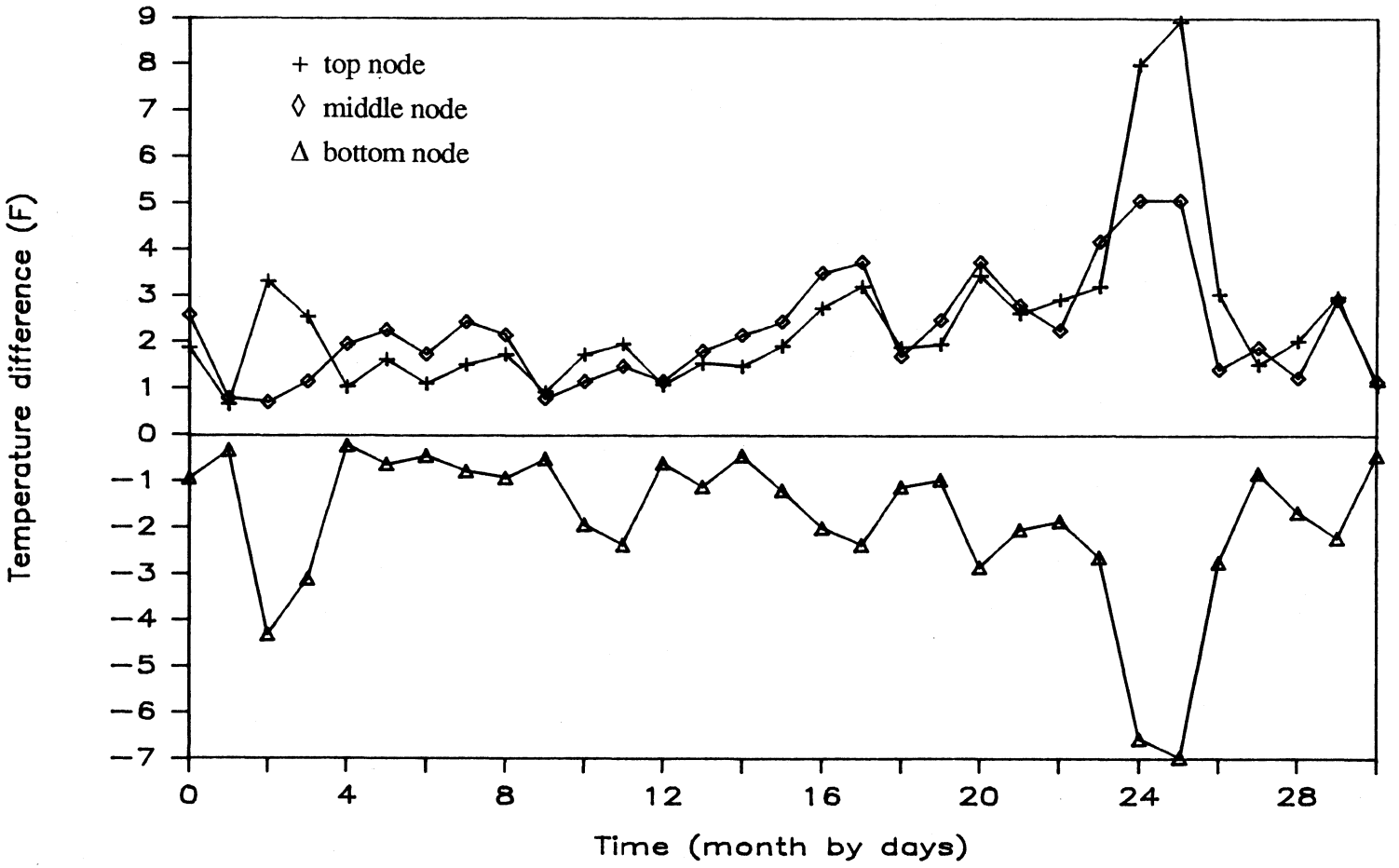

FIGURE 5.4.6 Difference between the tank node temperatures found using flow patterns (2) and (1), where ΔT = T(flow pattern (2)) - T(flow pattern (1)).

V.4.1.4 Model results

As noted earlier, the storage tank energy balances are off by as much as 20 % over a single month, and it is believed that the reason for the large error is in the energy to load (Q_{load}) calculation. This presents a problem since the way to determine how well the heat exchanger model works is to compare the energy to load calculated by the model to the actual energy to load calculated from the experimental data. Therefore, comparisons were made between the experimental total collector energy delivered to the tank (Q_{in} in section (V.2.2)) and the total energy entering the tank model calculated using the equation:

$$Q_{in} = \sum_{month} \dot{m} C_p (T_{col} - T150) \qquad (5.4.4)$$

where:

$\dot{m}$ = (M100) mass flow rate to the collector calculated from the experimental data

T_{col} = calculated temperature of the water leaving the tank to go to the collector (i.e. the bottom node temperature)

T150 = experimental temperature input to the tank model

If the model works correctly, then at the "correct" effectiveness it should provide the same energy to load as the actual tank did and provide water to the collector at the same temperature as the actual tank. Then the return water (to collector) temperature in equation (5.4.4) will give the same energy Q_{in} as that calculated directly from the experimental data. Therefore, to determine how well the model works, the

effectiveness is found for each month that, when used in the external heat exchanger model, gives the same inlet energy as that calculated directly from the experimental data. If the effectiveness values are the same for each month then the model should do a good job modeling the tank and heat exchanger, that is at least on a monthly basis.

An example plot of the total monthly collector inlet energy as a function of the effectiveness used in the model is shown for March in figure (5.4.7), assuming 1, 3, and 10 nodes of stratification in the tank. The experimental energy into the tank is 5.23 $* 10^6$ (Btu) which from the figure gives the effectiveness values shown in table (5.4.1) along with values calculated for the rest of the months.

Table 5.4.1 Effectiveness values calculated using the external heat exchanger model, that give the same energy into the tank as that calculated directly from the experimental data.

	# nodes		
Months	1	3	10
Feb	0.94	0.67	0.62
Mar	> 1.0	0.61	0.54
Apr	0.88	0.59	0.53
May	0.82	0.63	0.60

For a fully mixed tank (i.e. 1 node) the effectiveness values vary significantly with the March value greater than one. The high effectiveness values indicate that ignoring tank stratification is not a good way to model the tank.

The effectiveness values decrease as a higher degree of stratification is assumed, but the difference between assuming 3 and 10 nodes indicates that the effectiveness values will level off at some point as more nodes are assumed.

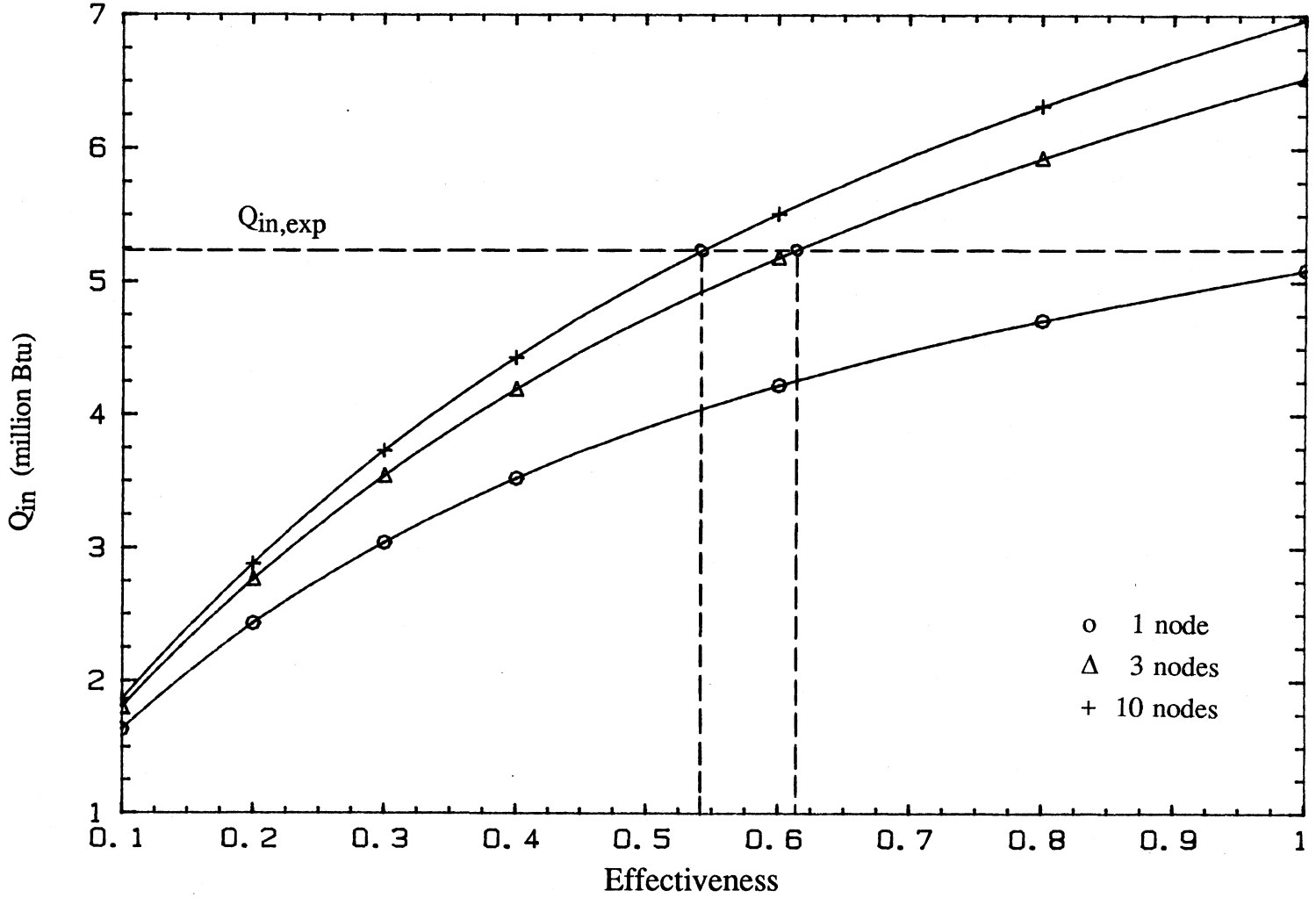

FIGURE 5.4.7 Energy into the external heat exchanger model as a function of the effectiveness used, where $Q_{in,exp}$ is the experimental energy into the tank. Done for March data. (Trident)

The table suggests that an effectiveness of 0.6 might work using the external heat exchanger model even with the mixing caused by the pump. Further discussion of the model results are given in section (V.4.3) where the results can be compared to the effectiveness values calculated using the immersed heat exchanger model.

V.4.2 Immersed Heat Exchanger Model

The immersed heat exchanger model works for 1 to 10 nodes (which can be easily increased by increasing the size of the data arrays in the model) and incorporates the heat exchanger equations into the tank node equations already present in the multi-node, stratified tank model (type 4). The changes that need to be done to the type 4 tank model to convert it to the immersed heat exchanger model are given in Appendix (B.3), and an example of the TRNSYS deck used to test the model is given in Appendix (B.4).

V.4.2.1 Model development

The development of the immersed heat exchanger model starts with the effectiveness equation for an external heat exchanger.

$$\varepsilon = \frac{(\dot{m}C_p)_c \quad (T_{c,o} - T_{c,i})}{(\dot{m}C_p)_{min}(T_{h,i} - T_{c,i})} \tag{5.4.5}$$

where:

$(\dot{m}C_p)_c$ = C_c = thermal capacitance rate of the cold fluid

$(\dot{m}C_p)_h$ = C_h = thermal capacitance rate of the hot fluid

$(\dot{m}C_p)_{min}$ = C_{min} = the smaller of $(\dot{m}Cp)_c$ and $(\dot{m}Cp)_h$

$T_{c,o}$ = Outlet temperature of the cold fluid

$T_{c,i}$ = Inlet temperature of the cold fluid

$T_{h,o}$ = Outlet temperature of the hot fluid

$T_{h,i}$ = Inlet temperature of the hot fluid

This equation is inappropriate for immersed heat exchangers since $(\dot{m}C_p)$ for the tank is unknown. To overcome this problem, Feiereisen *et al.* [6] redefined this equation for a supply-side immersed heat exchanger (where energy is transferred from the fluid in the coil to the fluid in the tank) in the following manner:

$$\varepsilon = \frac{(\dot{m}C_p)_{coil}(T_{c,i} - T_{c,o})}{(\dot{m}C_p)_{coil}(T_{c,i} - T_T)} = \frac{T_{coil,i} - T_{coil,o}}{T_{coil,i} - T_T} \qquad (5.4.6)$$

where:

$(\dot{m}C_p)_{coil}$ = thermal capacitance rate of the coil fluid

$T_{coil,i}$ = inlet temperature of the cold fluid

$T_{coil,o}$ = outlet temperature of the cold fluid

T_T = average tank temperature

Redefining the equation in this manner can be done since the mass of the tank fluid is much larger than the coil fluid and therefore the tank has a larger heat capacitance. C_{min} is equal to the coil fluid heat capacitance rate and drops out of the equation. Also the temperature $T_{c,i}$ is replaced with the average tank temperature T_T and equation (5.4.5) reduces to equation (5.4.6).

For a load-side immersed heat exchanger, the temperatures in equation (5.4.6) must be reversed as follows:

$$\varepsilon = \frac{T_{coil,i} - T_{coil,o}}{T_T - T_{coil,i}} \qquad (5.4.7)$$

This equation assumes negligible stratification in the tank which is not true for the Trident storage tank as explained earlier. The problem with using this equation for stratified tanks is determining what value should be used for the tank temperature (T_T). Farrington [5], in testing the Trident immersed heat exchanger tank, tried the following four methods for calculating a tank temperature.

(1) Tank center temperature. Using only the center temperature does not make any allowances for the top or bottom temperatures. Also if the center temperature equals the heat exchanger inlet temperature the effectiveness will be zero, but energy may still be removed from warmer water in the top of the tank.

(2) Average tank temperature calculated from five vertically mounted temperature sensors in the tank. The problem with this method is that the calculated effectiveness will be greater than one if the top is much hotter than the average temperature since the heat exchanger outlet temperature can be greater than the average tank temperature.

(3) Tank top temperature. As when using the tank center temperature using only the top temperature ignores the temperature of the rest of the tank which has an effect on the energy transfer to the heat exchanger fluid.

(4) Bulk tank temperature calculated from an energy balance. This approach used the following equation to calculate the new tank temperature for time t:

$$T_s(t) = \frac{1}{1 + \left\{\frac{(\dot{m}C_p)_s}{UA\,\Delta t}\right\}} \times \left[\frac{(\dot{m}C_p)_s}{UA\,\Delta t} \times T_s(t - \Delta t) + T_a - \frac{(\dot{m}C_p)_{hx}(T_{hx,o} - T_{hx,i})}{UA}\right] \quad (5.4.8)$$

where the previous tank temperature ($T_s(t-\Delta t)$) is from the previous timestep and all of the other measurements are measured at time t. The main problem with this approach is that any error made in the calculated tank temperature are continually propagated through the rest of the simulation since each new temperature is based on the old one.

Farrington showed that none of the four methods provided an accurate basis for calculating the effectiveness of the exchanger in a stratified tank. Therefore an approach was needed that accounts for stratification in the tank.

The approach used is based on the method TRNSYS uses to account for stratification in the tank model. TRNSYS breaks the tank into N fully mixed segments or nodes, were N specifies the degree to which the tank is stratified. Setting N equal to one indicates a fully mixed tank. By thinking of each node as a separate fully mixed tank, equation (5.4.7) can be applied and the original tank can be thought of as N tanks connected in series. The heat exchanger fluid flow enters through the bottom node and passes up through each node until it exits from the top node (for explanation purposes three nodes will be used when presenting the heat exchanger equations since the tank temperatures are measured at three levels). For example if the tank is assumed to have three nodes then the tank would be broken up as shown in figure (5.4.8). Another way to visualize the tank and heat exchanger coil temperatures is shown in figure (5.4.9).

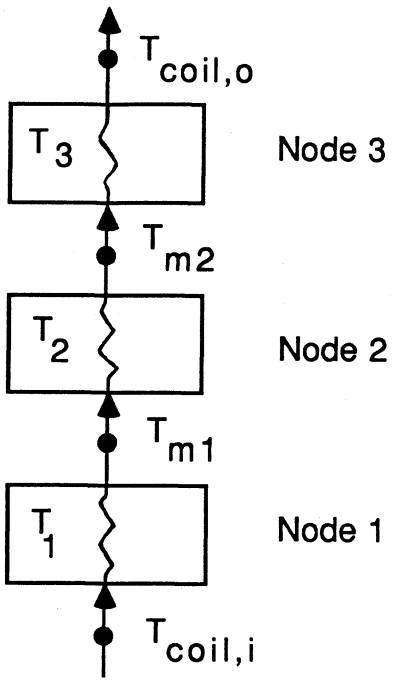

FIGURE 5.4.8 Breaking a stratified tank up into N separate constant temperature tanks in series.

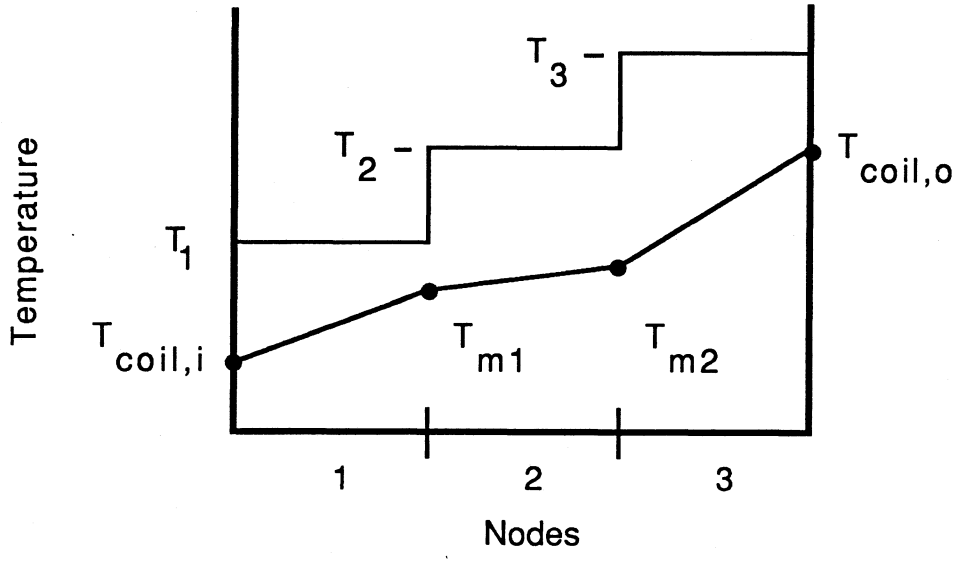

FIGURE 5.4.9 Visualization of the tank node temperature and coil temperature relationships.

The effectiveness values for each of the three nodes (using the variables shown in figures 5.4.8 and 5.4.9) would be written as:

$$\varepsilon_1 = \frac{T_{m1} - T_{coil,i}}{T_1 - T_{in}} \qquad (5.4.9a)$$

$$\varepsilon_2 = \frac{T_{m2} - T_{m1}}{T_2 - T_{m1}} \qquad (5.4.9b)$$

$$\varepsilon_3 = \frac{T_{coil,o} - T_{m2}}{T_3 - T_{m2}} \qquad (5.4.9c)$$

where:

$\varepsilon_1, \varepsilon_2, \varepsilon_3$ = the effectiveness values for nodes 1, 2, and 3 respectively

T_1, T_2, T_3 = the temperatures of nodes 1, 2, and 3 respectively

T_{M1}, T_{M2} = the intermediate coil temperatures between nodes 1 and 2, and 2 and 3 respectively

The TRNSYS multi-node stratified tank model considers the tank to be N fully mixed nodes. At each timestep of the simulation, TRNSYS calculates the new node temperatures based on the fluid flows in and out of the tank and the environmental losses. The node equations are solved one at a time. For any given node TRNSYS calculates the net flow either into or out of the node. For example, for the two flows shown in figure (5.4.10), $\dot{m}_1$ and $\dot{m}_2$ are added, and the resultant flow, either up or down, is determined. Neglecting losses, an energy balance on the ith node will be:

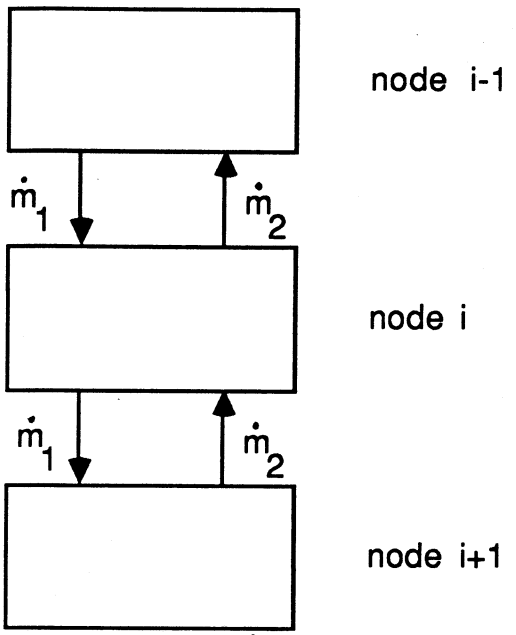

FIGURE 5.4.10 Flow between nodes.

$$M_i C_{pf} \frac{dT_i}{dt} = \begin{cases} (\dot{m}_1 - \dot{m}_2) C_{pf} (T_{i-1} - T_i) & \text{if } \dot{m}_1 \geq \dot{m}_2 \\ (\dot{m}_2 - \dot{m}_1) C_{pf} (T_{i+1} - T_i) & \text{if } \dot{m}_1 < \dot{m}_2 \end{cases} \qquad (5.4.10)$$

where:

M_i = the mass of the tank fluid

C_{pf} = the specific heat of the tank fluid

T_i = the new temperature for node i

T_{i-1} = the temperature for node i at the beginning of the timestep

Equation (5.4.10) is a first order linear differential equation that can be solved analytically.

To include the immersed heat exchanger in the tank model the energy transferred to the coil fluid from each node must be calculated. Using the form of equation (5.4.7) the coil energy gain will be (for the ith node):

$$\varepsilon = \frac{Q_{act}}{Q_{max}} = \frac{T_{m_i} - T_{m_{i-1}}}{T_i - T_{m_{i-1}}} \qquad (5.4.11)$$

Therefore the energy gain is:

$$Q_{act} = \varepsilon_i (\dot{m} C_p)_{coil} (T_i - T_{m_{i-1}}) \qquad (5.4.12)$$

Adding this equation and the environmental loss term to equation (5.4.10) gives:

$$M_i C_{pf} \frac{dT_i}{dt} = \dot{m}_{io} C_{pf} (\Delta T) + UA_{env} (T_{env} - T_i) + \varepsilon_i (\dot{m}C_p)_{coil} (T_{coil,in,i} - T_i) \quad (5.4.13)$$

where:

$\dot{m}_{io}$ = resultant mass flow rate into or out of node i

UA_{env} = overall environmental heat loss coefficient of node i

T_{env} = environmental temperature

$(\dot{m}C_p)_{coil}$ = thermal capacitance rate of the coil fluid

$T_{coil,in,i}$ = coil inlet temperature for node i

To use equation (5.4.12) the node equations must be solved starting with the bottom node and working up to the top. This is required since the coil inlet temperature for each node ($T_{coil,in,i}$) cannot be calculated until the equation for node i+1 (the next lower node) has been solved. Once the new node temperature for a node has been calculated, the coil outlet temperature can be calculated as follows:

$$Q_{act} = (\dot{m}C_p)_{coil}(T_{coil,out,i} - T_{coil,in,i}) \quad (5.4.14)$$

Thus

$$T_{coil,in,i-1} = T_{coil,out,i} = T_{coil,in,i} + \frac{Q_{act}}{(\dot{m}C_p)_{coil}} \quad (5.4.15)$$

Since the coil fluid energy gain (Q_{act}) was already calculated using equation (5.4.12),

equation (5.4.14) can be rearranged as shown to solve for the present nodes coil outlet temperature which is the coil inlet temperature to the next higher node (node i-1).

V.4.2.2 Effectiveness value used in the model

The effectiveness value used in the immersed heat exchanger model for the results shown in section (V.4.2.3) was a single constant value used during the entire simulation for all of the nodes. This is similar to what is done in the external model except the heat exchanger has been moved back inside the tank eliminating the mixing caused by the extra pump.

A second method was also tried which attempted to use the experimental data to find a relationship for the effectiveness values (during each timestep) as a function of the difference between the tank and coil water temperatures and capacitance rates. Unfortunately this method did not work. It is outlined in Appendix (C) since it could be useful as a basis for future work regarding the immersed heat exchanger model.

V.4.2.3 Tank model comparison results

The immersed heat exchanger model using a single constant effectiveness value was run for the months of February through May in the same manner as that used for the external heat exchanger model (see section V.4.2.2). The results are shown in table (5.4.2).

The effectiveness values calculated assuming a fully mixed tank are the same when using either the immersed or external heat exchanger. When more than one node is used the effectiveness will be lower due to the way the effectiveness is defined in equation (5.4.7). As the number of nodes is increased, the coil inlet and outlet temperature difference will be lower; therefore, the effectiveness will be lower. Note

that this does not mean that the overall heat exchanger effectiveness decreases.

Table 5.4.2 Effectiveness values calculated using the immersed heat exchanger model, that give the same energy into the tank as that calculated directly from the experimental data.

Months	# nodes 1	3	10
Feb	0.94	0.38	0.12
Mar	> 1.0	0.36	0.11
Apr	0.88	0.32	0.09
May	0.82	0.32	0.11

Although the results show that the effectiveness values vary from month to month for a given number of nodes, it is possible that if the models were compared to the energy supplied to the load that the resulting effectiveness values might be closer from month to month for the immersed method. Since the Trident load values are uncertain, it is not possible to do further checking.

VI. HONEYWELL SYSTEM

This system was designed by Honeywell's Technology Strategy Center. It was also one of four systems designed and developed as part of the Packaged Space Heating Systems Development Program.

VI.1 SYSTEM DESCRIPTION

The Honeywell system is designed to provide both space heating and domestic hot water (DHW). The system used in this study is installed in a split-entry, single family home located in Bismarck, North Dakota. Figure (6.1.1), from [3], is a schematic of the system showing the basic system configuration and the data sensor positions used by Vitro to record the system data. The same nomenclature is used as in the Trident system and is defined in table (5.1.1).

The collectors used in this system are modified Ramada Energy Systems TES 6000 modules. The array is composed of 22 modules arranged in two vertical rows each containing 11 collectors. The two sets are mounted on the side of the house with one set of panels mounted directly above the other. The collector is comprised of a top layer of Tedlar® laminated to a double-layer polycarbonate glazing. The absorber is made from a polysulfone material with a black absorbtivity enhancer. The backing consists of aluminum-foil clad, 3/4 inch thick polyisocyanuarate foam. The collector fluid is water that drains from the collectors when the pump is shut off, providing freeze protection during freezing weather. The gross and aperture areas are

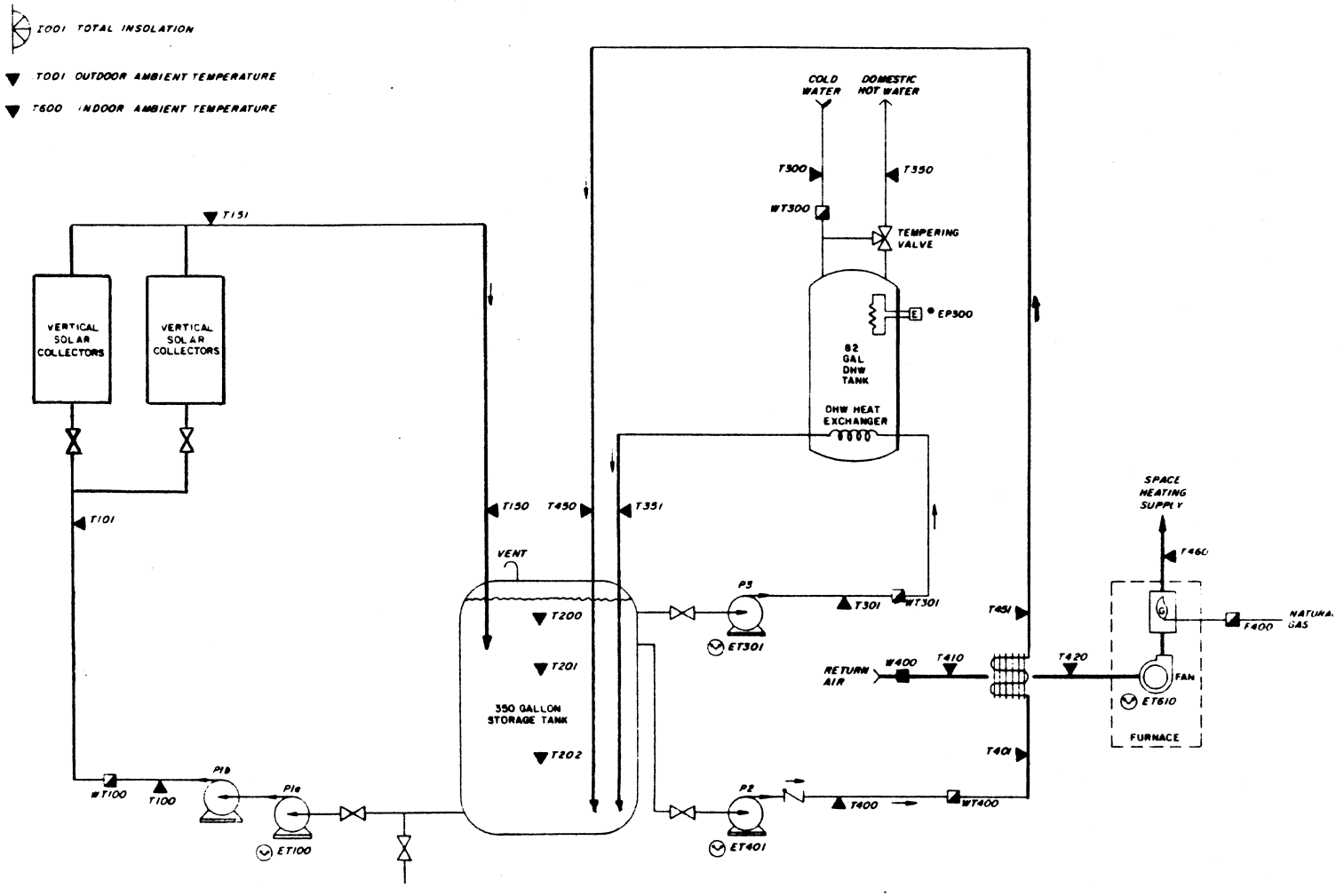

FIGURE 6.1.1 Schematic diagram of the Honeywell system (taken from ref. [3]).

302[1] and 286[2] ft^2. The array panels are mounted vertically and oriented due south.

The storage tank (shown in figure (6.1.2)) is a polyethylene tank insulated with 3 inches of R-19 urethane foam, and protected by a steel shell. The space, domestic hot water (DHW) and two collector pumps are mounted on the side of the tank. The top of the tank has holes for the return lines from the collector, space heating, and the DHW loops. It also contains a 20 inch manhole to provide access to the interior of the tank. The tank holds 350 gallons of water.

The DHW subsystem uses a stone-lined 80 gallon hot water tank with a finned copper heat exchanger in the bottom and an electric auxiliary coil located approximately one-third of the way down from the top of the tank. The heat exchanger is used to heat the domestic hot water supply from the main storage tank when it is available, otherwise the auxiliary coil is used. Figure (6.1.3) shows the DHW tank.

The space heating subsystem consists primarily of a Lennox CW3-45 water-to-air heat coil mounted adjacent to the forced -air, gas-fired furnace. When solar energy is available the solar loop operates heating the return air. With this design it is possible to have both the solar coil loop and the auxiliary furnace operating at the same time.

The system controller is a Honeywell T8300A microelectronic thermostat designed to maintain the house temperature while maximizing the solar energy usage. The thermostat can be programmed to set back the night temperature and then extend this setting (if solar energy is available) for up to two hours past the reset time (time when the thermostat resets back to the normal daytime temperature). This increases the usage of available solar energy. Also integral action (shortening or lengthening the duty cycle (percent on-time)) is used to respond to load changes. This control strategy

---

[1] Quoted from Vitro.

[2] The Honeywell report gave conflicting sizes for the aperture area; therefore, the value given is calculated from the aperture area given for a single panel from the ASHRAE 93-77 tests.

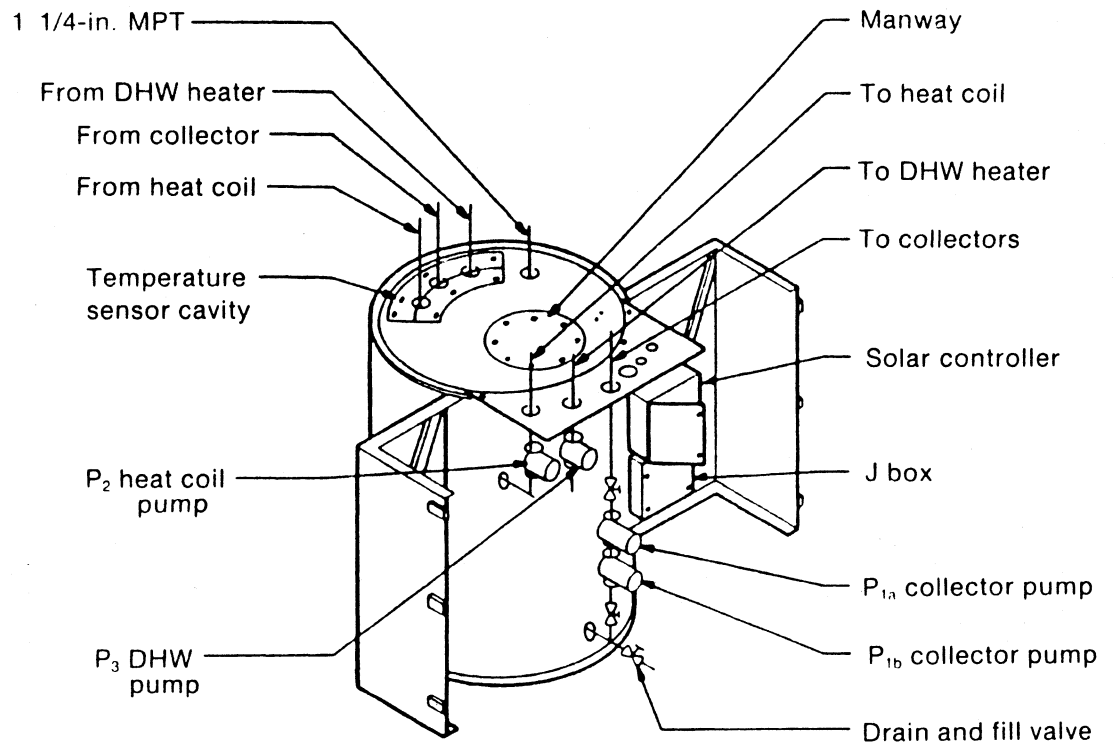

FIGURE 6.1.2 Honeywell storage tank (taken from ref. [7]).

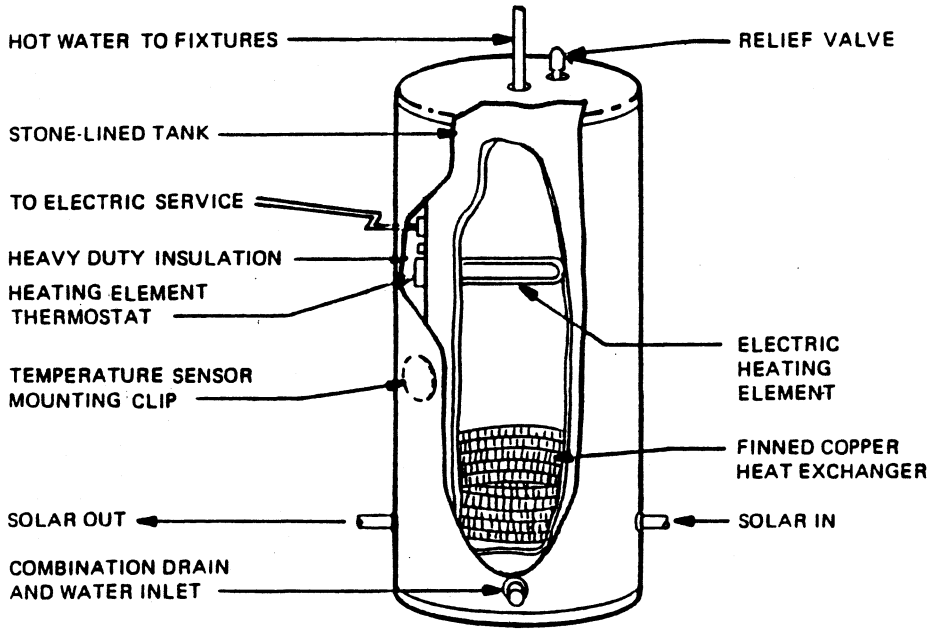

FIGURE 6.1.3 Honeywell DHW tank (taken from ref. [7]).

keeps the deviation of the house air temperature from the set point at less than 1° F rather than the typical 5° F.

VI.2 EXPERIMENTAL DATA

The Honeywell data had many of the same problems as the Trident system data.

VI.2.1 Data Availability

As was noted in section (II.2.2) some of the experimental data are missing. Table (6.2.1) lists the amount of data available during each month for the Honeywell system.

TABLE 6.2.1 Amount of data available for the Honeywell solar energy system.

Month	Percent of Data Present
Oct '83	70 %
Nov	91
Dec	70
Jan '84	46
Feb	89
Mar	99
Apr	99
May	92
Jun	99
Jul	62
Aug	99
Sep	28

VI.2.2 Storage Tank Energy Balances

As with the Trident system, integrated monthly energy balances were were done on the main storage tank. The energy balances were done in the same manner as in the Trident system. Each term (except Q_{err}) was calculated for each interval between records with the time difference between records less than 10 minutes 40 seconds. Again, the energy balances are only calculated for the available data, meaning that no data is filled in for the missing records. Also the energy balance is set equal to an error term. (See equation (5.2.1)). The energy balance results for the Honeywell system are shown in table (6.2.2).

Table 6.2.2 Integrated monthly storage tank energy balances on the Honeywell storage tank.

Month	Qin	Qload	DE (million Btu)	Qenv	Qerr	% Dif
Oct	1.38	1.61	-0.04	0.28	-0.47	-34
Nov	0.82	0.97	-0.09	0.14	-0.20	-24
Dec	1.71	1.90	-0.01	0.13	-0.32	-19
Jan	1.20	1.28	0.03	0.10	-0.22	-18
Feb	2.12	2.15	-0.08	0.21	-0.16	-8
Mar	1.73	1.50	-0.007	0.23	0.01	0.01
Apr	2.15	1.77	0.03	0.28	0.06	3
May	1.55	1.22	0.05	0.28	-0.003	~0
Jun	0.72	0.82	-0.07	0.32	-0.35	-49
Jul	0.58	0.60	0.12	0.29	-0.42	-72
Aug	1.32	1.57	-0.02	0.59	-0.82	-62
Sep	0.30	0.42	-0.06	0.16	-0.22	-73

The energy balances are worse than those for the Trident system; however, in this case the energy from the collector (Q_{in}) is probably causing the energy balances to be off. The reason for this is explained in the next section (VI.3.1).

The monthly energy values given in the table were calculated using the following equations where the position of the temperature sensors and flowmeters are shown on the system schematic (figure (6.1.1)). The working fluid is water, and the specific heat (C_p) is assumed constant and equal to 1.0 (Btu/lbm-°F) in all of the equations listed in this section.

Converting flowmeter readings to mass flow (lbm)

$$M100 = (WT100 - WT100\_P)\, GTL / \Delta T \qquad (6.2.1)$$

where:

M100	=	mass flow rate during the time interval (lbm/hr)
WT100	=	present totalizing flow reading (gal)
WT100_P	=	previous WT100 reading (gal)
GTL	=	8.3 converts gallons to lbm for water (lbm/gal)
ΔT	=	time interval since the last flow reading (hr)

M301 and M400 were calculated in the same manner.

Two sizes of totalizing flowmeters were used in the Honeywell system. One type counted up to 1000 gallons before resetting and the other up to 100 gallons. Therefore, due to sensor drift, the number of gallons that had to pass through the flowmeter had to be larger than 1.1 gallons and 0.11 gallons for the two sizes, respectively. If the flow reading was less than 1.1 gallons the mass flow rate for the time interval was set to zero.

Energy supplied from collector (Btu)

$$Q_{in} = \sum_{month} M100\, C_p (T150 - T100) \qquad (6.2.3)$$

Vitro reported that starting in January T100 (and T101) appeared to be reading low and a reason for the low readings could not be determined. They made the following sensor substitutions for T100 and T101 starting in January.

1/1/84 - 1/26/84 - T202
2/1/84 - 2/7/84 - T200
2/7/84 - 9/30/84 - T202

The same substitutions were made when doing the energy balances in this thesis.

Change in the internal energy of the tank (Btu)

$$DE = STOCAP\ (TST - TST\_P)\ GTL \qquad (6.2.4)$$

where:

STOCAP = number of gallons of fluid in the storage tank
TST = average tank temperature - present record (°F)
TST_P = average tank temperature - previous record (°F)

Energy losses to the environment (Btu)

$$Q_{env} = \sum_{month} [\ UA\ (TST - T_b]\ (\Delta t) \qquad (6.2.5)$$

where:

UA = 11.4 (Btu/hr-°F) = heat loss coefficient of the tank

TST	=	average tank temperature (°F)
T_b	=	65 (°F) = basement temperature surrounding the tank
Δt	=	time interval since the last data record

The tank heat loss coefficient (UA) was calculated from tests done by Farrington [5] on the Honeywell storage tank. This values is based on a surface area of 104 ft^2. The average tank temperature was used to calculate the environmental losses since the storage tank did not maintain very much stratification. No temperature measurements were taken in the basement; therefore, T_b was assumed constant and equal to 65 °F during the entire year.

Energy supplied to the load (Btu)

$$Q_{load} = \sum_{month} [\, M301\, C_p (T351 - T301) + M400\, C_p\, (T450 - T400)\,] \qquad (6.2.6)$$

The experimental data indicated that the sensors at the inlet and outlet pipes were far enough away from the tank so that conduction up the pipes was not a problem as it had been in the Trident system

VI.3 COLLECTOR RESULTS

This subsection presents the Honeywell collector results found when comparing the ASHRAE 93-77 collector parameters with those calculated from the experimental data. This section is presented in the same format as used for the Trident system collector results given in section V.3. First the ASHRAE test results are presented.

Then $F_R(\tau\alpha)_n$ and F_RU_L values are given, calculated from the experimental data using the two different method (efficiency and collector model methods). Also presented are the total monthly collector energy gains calculated using the $F_R(\tau\alpha)_n$ and F_RU_L values. Lastly, comparisons are made between the experimental total monthly collector energy gains and the ASHRAE, efficiency, and collector model methods.

The comparisons are done for October thru December in one section, since starting in January temperature sensor T101 started giving faulty readings. In a separate section, results are presented for January through August, where even though the results cannot be compared to the experimental values, conclusions can be drawn about the collector.

No results are given for April and September. April is excluded since the collector pumping scheme changed during the month. September was excluded since only 8 days of data were available during the month.

VI.3.1 ASHRAE 93-77 Test Results

Two collectors from Honeywell were tested at DSET Laboratories, Inc. The collector parameter values ($F_R(\tau\alpha)_n$, F_RU_L, and b_o), were determined using the ASHRAE 93-77 test. Both collectors were tested when initially received and again after a nine month stagnation period. The results from these tests are tabulated in table (6.3.1) and figure (6.3.1) shows the efficiency plots used to obtain the results for both collectors.

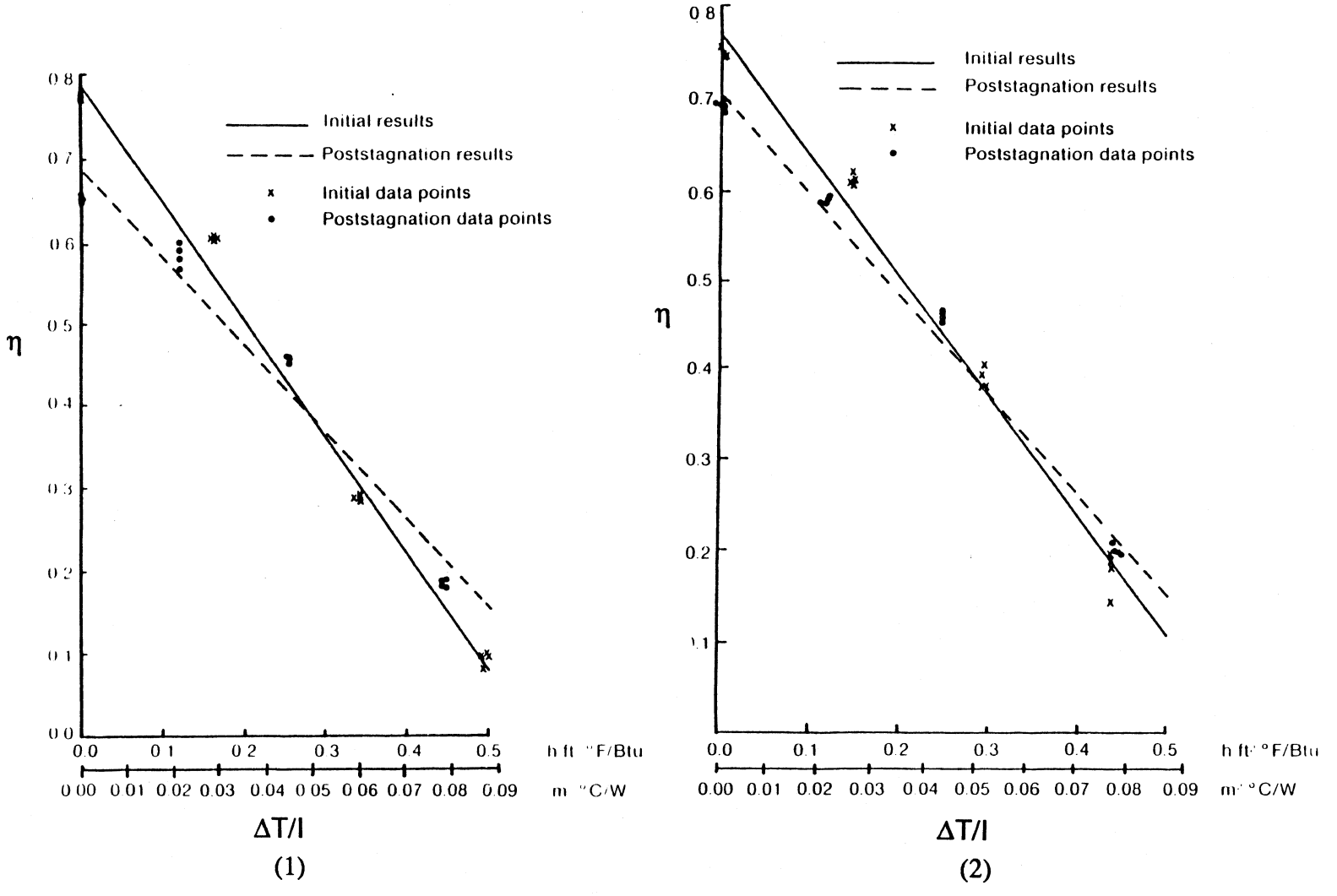

FIGURE 6.3.1 Efficiency test results for Honeywell collectors (taken from ref. [8]).

TABLE 6.3.1 ASHRAE 93-77 test parameters calculated based on the collector aperture area.

	$F_R(\tau\alpha)_n$		F_RU_L		b_o	
	Initial	Final	Initial	Final	Initial	Final
Collector 1	0.793	0.692	1.429	1.078	0.198	0.188
Collector 2	0.781	0.717	1.345	1.129	0.274	0.146

The final values used to represent the ASHRAE test values for all comparisons were determined by averaging the collector parameters determined on the initial tests only. This was done because the collectors in the system probably did not experience stagnation conditions very often. These values are listed in table (6.3.2) along with the test flow rate and the test collector aperture and gross areas (note that the test parameters are based on the collector aperture area).

TABLE 6.3.2 Honeywell collector module parameter values used to represent the collector characteristics determined by the ASHRAE 93-77 test.

$F_R(\tau\alpha)_n$	0.787	
F_RU_L	1.25	(Btu/hr-ft^2–°F)
b_o	0.236	
test flow rate	190.65	(lbm/hr)
aperture area	12.98	(ft^2)
gross area	27.99	(ft^2)

VI.3.2 Screening and Full Flow Parameters

The screening and full flow parameters were calculated in the same manner as for the Trident system as described in section (V.3.3). However, on April 16th the collector pump control strategy was changed for the Honeywell system. The original control strategy ran both collector pumps (connected in series) continuously whenever the collector was operating. In the new scheme both pumps were run for only the first 10 minutes in order to fill the collector array with fluid, then one pump would shut off and the other one would continue operating until the collector shut off.

For October through March (when both pumps ran continuously during collector operation) the full flow lower bound (used in the efficiency method to determine if continuous flow had occurred during the previous timestep) was set equal to 15.7 gpm. For the same period of time the steady state flow value (used as the collector flow rate in the collector model deck) was set equal to 16.1 gpm (8018 lbm/hr). For May through August the full flow lower bound was set equal to 12.7 gpm. The steady state flow value changed depending on the experimental flow rate. If the experimental flow rate was greater than 13.2 gpm during the timestep, the steady state flow rate was set equal to 15.7 gpm (7818 lbm/hr). If the experimental flow rate was less than 13.2 gpm then the steady state flow rate was set equal to 12.9 gpm (6424 lbm/hr). Table (6.3.3) summarizes the values used to determine when full flow occurs in a timestep and the steady state flow values used in the collector model deck.

TABLE 6.3.3 Summary of the Honeywell system steady state flow rate and the lower bound used to determine when flow has occurred during an entire timestep.

	Steady state flow (lbm/hr)/(gpm)	Full flow (gpm)
Oct-Mar	8018/15.7	16.1
May-Aug	*	12.7

* If the experimental flow rate was > 14.5 gpm then use 7818 lbm/hr (15.7 gpm), otherwise use 6424 lbm/hr (12.9 gpm).

VI.3.3 Data problems

There were two problems encountered when the experimental data was used in the efficiency and collector model methods to calculate $F_R(\tau\alpha)_n$ and F_RU_L.

(1) Beginning in January the collector pipe inlet temperature sensors T101 and T100 started to read low. They were not fixed, and therefore the tank bottom node temperature T202, was substituted for T101.

(2) The collector control strategy was changed beginning on April 16th.

The first problem makes all of the collector results presented beginning in January only approximations since the collector inlet fluid temperature must be approximated.

Normally the collector energy gain from each timestep is calculated using the following equation:

$$Q_{col} = \dot{m}C_p(T151 - T101) \qquad (6.3.1)$$

However, when sensors T101 and T100 started giving faulty readings in January temperature T202 was substituted. This would not be a problem if T202 were close to T101 in temperature. This was not the case for the Honeywell system as shown in table (6.3.4). In the table the total monthly energy gain was calculated from the experimental data (summing equation (6.3.1)) using T101, T100, and T202.

TABLE 6.3.4 Total monthly energy gain calculated from the experimental data using T101, T100, and T202.

	Energy Gain (million Btu)			% difference	
Month	T101	T100	T202	T100	T202
Oct	1.32	1.61	1.77	22%	34%
Nov	0.77	0.88	0.94	14%	22%
Dec	1.64	1.87	2.04	14%	24%

The results show that the calculated energy gain increases when sensors T100 and T202 are used. This indicates that the fluid got warmer as it flowed from the tank to the collector. This should not happen since the sensor T101 is located in the pipe exposed to the environment. During times when the pump is not running (the water had drained back to the tank so it is not in the pipes) the sensor reads the ambient temperature. Also the tank water was almost always warmer than the house temperature; therefore, between sensors T100 and T101 the pipe fluid should not have increased in temperature. These results cast a doubt on sensors T100 and T101 during October

through December when it was reported that they were working correctly.

Based on the results given above and the fact that sensors T100 and T101 were not working during the rest of the year, comparisons cannot be made between the "actual" collector gains and the rest of the ASHRAE, efficiency, and collector model methods. However the results are presented since comparisons can be made between the individual methods and conclusions can be drawn about the collector.

Also, as noted for the Trident system, all of the total monthly energy gains calculated using the collector model deck (explained in section (V.3.3)) were done using the data records only when the time interval between records was less than 10 minutes 40 seconds (two standard timesteps) and greater than 3 minutes. The lower bound was used since occasionally data was recorded at 32 second intervals when checks were done on the data reader. Since this only occurred a maximum of 2 hours during any given month these readings were excluded with the time they occurred considered as a data gap.

VI.3.4 Efficiency Method Results

As noted in the previous subsection the results presented do not necessarily represent the actual characteristics of the collector since sensor T202 had to be used as the inlet temperature to the collector; however, they are presented since conclusions can be drawn from the results. Section (IV.2.1) describes the theory, approach, and different screening methods applied to the experimental data to determine the results presented in this subsection.

As with the Trident system, the initial step was to determine how $F_R(\tau\alpha)_n$ and F_RU_L varied when different numbers of consecutive data points were averaged. The results for November (using screening methods 1(a & b)) are shown in table (6.3.5). The corresponding total monthly energy gain calculated for each of the $F_R(\tau\alpha)_n$ -

F_RU_L pairs are given in table (6.3.7), where the energy values are sorted in descending order (the "#" column lists the number of consecutive steps averaged and can be used to determine which energy gain value is calculated from which $F_R(\tau\alpha)_n$ - F_RU_L pair given in tables (6.3.5)).

The results from table (6.3.7) show that it does not matter how many timesteps are averaged since for example, the lowest energy gain does not always occur when using only 1 timestep or two timesteps as was the case in the Trident system (see table (5.3.11)). This was also done for other months with the same results. Therefore an arbitrary value of 11 timesteps (same number used for the Trident system results) was chosen to be used for the rest of the parameter calculations done with the four screening methods.

Applying each of the four screening methods to each month (using the lower bounds given in table (6.3.4)) gives the $F_R(\tau\alpha)_n$ - F_RU_L values shown in table (6.3.8). Also included in the table are the total monthly energy gains by the collector model using the $F_R(\tau\alpha)_n$ - F_RU_L pairs and the experimental data from the month. No values are shown for the fourth method in May through August since no efficiency - operating point values were left after the screening method was applied to the experimental data. Also total monthly energy values depicted by a "*" sign were not calculated since the F_RU_L value is negative.

Comparing the total monthly energy gain found using the four pairs of $F_R(\tau\alpha)_n$ - F_RU_L values in each month show very little difference. (The Trident system also showed very little difference.) For May through August most of the F_RU_L values for method "b" are negative. This means that the linear curvefit has a positive slope which does not conform to theory. Since the negative values only occur when method "b" is used (i.e. including $K_{\tau\alpha}$ in the efficiency and operating point equations) the error cannot be due to using sensor T202 instead of T101. The reason for the negative

values is due to the collector slope (vertical orientation) and the sun's position in the sky during the summer months.

TABLE 6.3.7 Total monthly energy gain by the collector model using the corresponding $F_R(\tau\alpha)_n$ and F_RU_L values from tables (6.3.5).

November			
(million) Btu		(million) Btu	
#	"1a"	#	"1b"
9	.70	9	.70
8	.70	8	.74
13	.69	7	.74
7	.69	4	.73
5	.69	2	.73
2	.69	13	.72
1	.69	12	.72
12	.68	11	.72
11	.68	10	.72
10	.68	6	.72
4	.68	3	.72
6	.67	1	.72
3	.67	5	.71

TABLE 6.3.8 Collector parameters calculated using the four different screening methods in the efficiency method along with the corresponding energy gain calculated using the parameters in the TRNSYS collector model. F_RU_L has units (Btu/hr-ft^2-°F) and Q_{col} has units of (million Btu).

Month	Meth	$F_R(\tau\alpha)_n$	F_RU_L	Q_{col}	Meth	$F_R(\tau\alpha)_n$	F_RU_L	Q_{col}
Oct	1a	.600	.769	1.18	1b	.647	.773	1.34
	2a	.605	.748	1.18	2b	.655	.794	1.34
	3a	.600	.766	1.18	3b	.650	.777	1.34
	4a	.631	.805	1.24	4b	.676	.888	1.31
Nov	1a	.609	.622	0.68	1b	.627	.586	0.72
	2a	.626	.691	0.68	2b	.648	.664	0.72
	3a	.622	.670	0.67	3b	.629	.605	0.71
	4a	.652	.786	0.67	4b	.680	.818	0.70
Dec	1a	.649	.769	1.44	1b	.669	.772	1.52
	2a	.648	.764	1.45	2b	.670	.773	1.52
	3a	.637	.728	1.45	3b	.658	.738	1.52
	4a	.648	.763	1.45	4b	.668	.765	1.52
Jan	1a	.652	.612	1.22	1b	.657	.566	1.28
	2a	.668	.669	1.21	2b	.686	.652	1.28
	3a	.671	.683	1.20	3b	.689	.665	1.27
	4a	.657	.629	1.22	4b	.669	.607	1.27
Feb	1a	.645	.519	2.13	1b	.646	.383	2.34
	2a	.645	.521	2.13	2b	.645	.382	2.34
	3a	.646	.524	2.13	3b	.634	.339	2.35
	4a	.672	.611	2.12	4b	.705	.616	2.26

Mar	1a	.673	.701	1.43	1b	.680	.478	1.74
	2a	.667	.676	1.44	2b	.649	.381	1.75
	3a	.655	.649	1.43	3b	.634	.339	1.75
	4a	.751	.895	1.45	4b	.798	.883	1.63
May	1a	.480	.556	0.95	1b	.669	.296	1.84
	2a	.481	.566	0.92	2b	.670	.304	1.84
	3a	.468	.498	0.98	3b	.670	.303	1.84
	4a	*	*	*	4b	*	*	*
Jun	1a	.369	.211	0.51	1b	.603	.049	1.15
	2a	.383	.264	0.48	2b	.547	-.118	*
	3a	.379	.288	0.44	3b	.547	-.139	*
	4a	*	*	*	4b	*	*	*
Jul	1a	.412	.378	0.37	1b	.630	.074	1.02
	2a	.419	.396	0.36	2b	.593	-.054	*
	3a	.421	.410	0.35	3b	.597	-.043	*
	4a	*	*	*	4b	*	*	*
Aug	1a	.441	.246	1.19	1b	.381	-.251	*
	2a	.440	.231	1.21	2b	.386	-.247	*
	3a	.450	.262	1.20	3b	.373	-.293	*
	4a	*	*	*	4b	*	*	*

* Times when no points were left after screening the data or when the curvefit resulted in negative $F_R U_L$ values.

During the summer the beam radiation incidence angle is usually greater than 60 degrees, which means that equation (4.1.2):

$$K_{\tau\alpha} = 1 - b_o\left(\frac{1}{\cos\theta} - 1\right) \qquad (4.1.2)$$

does not hold and $K_{\tau\alpha}$ is calculated by the linear approximation from the $K_{\tau\alpha}$ value evaluated at 60 degrees to a value of zero at 90 degrees (see figure (4.1) for the general shape). Table (6.3.9) shows the average beam radiation incidence angle, the number of timesteps when the beam radiation is over 60 degrees, and the total number of timesteps used in the efficiency method calculations (i.e. the number of timesteps left after screening method 1 has been used) for both the Honeywell and Trident systems. The table shows that starting in February the number of times that the incidence angle is greater than 60 degrees increases until in June and July it is always greater than 60 degrees. (Also note that the same trend occurs in for the Trident system. However, since the Trident collector is mounted at a slope of 22 degrees from the horizontal, the beam incidence angle is greater than 60 degrees very few times compared to the total number of timesteps used in the calculation.) These results indicate that the linear approximation may not be very good and should not be used when most of the timesteps have a beam radiation incidence angle greater than 60 degrees. Figures (6.3.2a) and (6.3.2b) show how $K_{\tau\alpha}$ affects the efficiency - operating point values for August in the Honeywell system. The figures show that the data has been scattered enough so that the slope is positive.

Another possible explanation is that the beam radiation measurements may be substantially in error during the summer months due to the high beam radiation incidence angle on the pyranometer which was mounted in the plane of the collector (i.e. at 90 degrees to the horizontal).

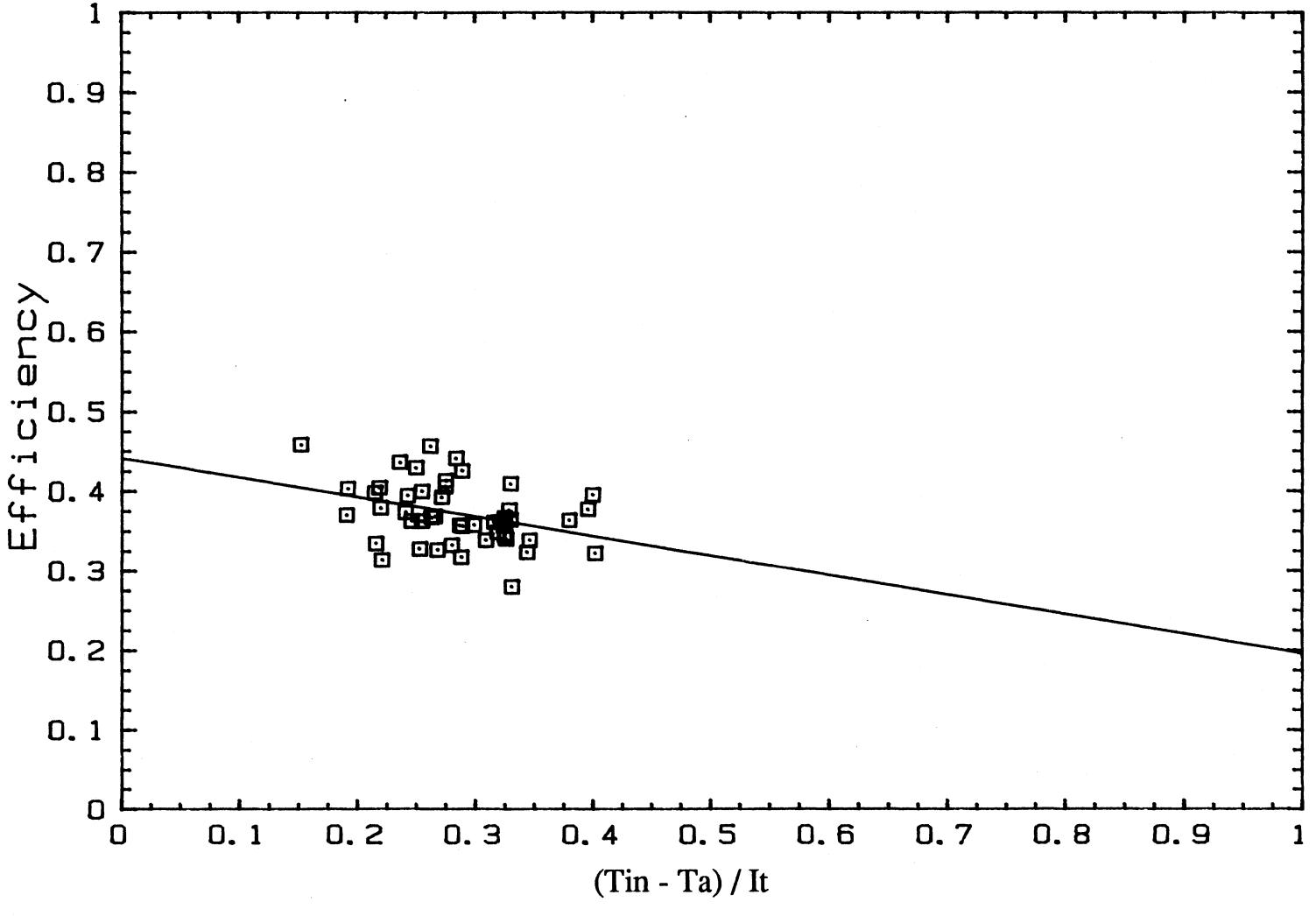

FIGURE 6.3.2a Curvefit of the efficiency - operating point values calculated for August using screening method (1a) in the efficiency method. (Honeywell)

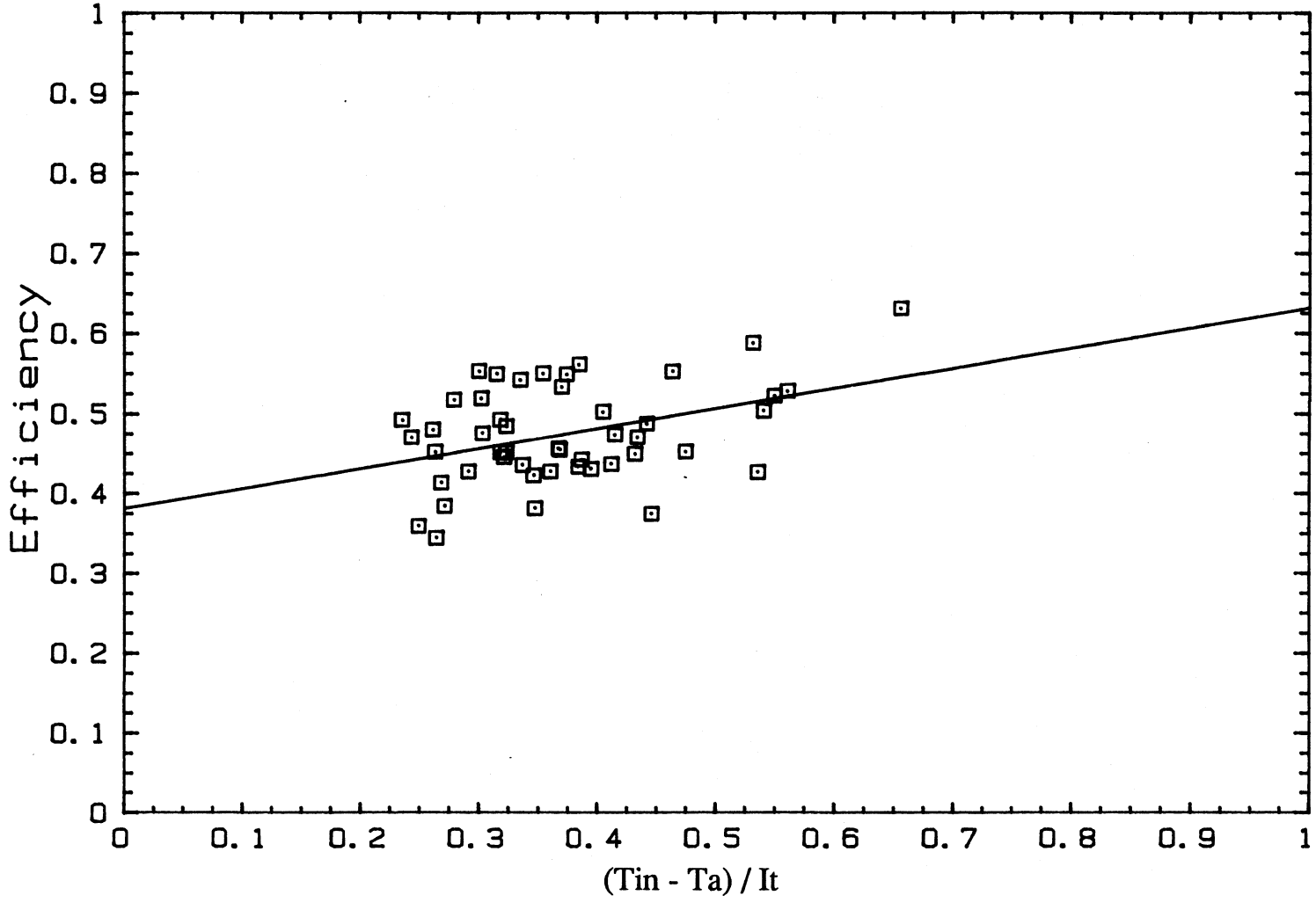

FIGURE 6.3.2b Curvefit of the efficiency - operating point values calculated for August using screening method (1b) in the efficiency method. (Honeywell)

TABLE 6.3.9 Data on the beam radiation incidence angle for timesteps when the experimental data would be used in the efficiency methods 1,2, and 3.

Month	Honeywell			Trident		
	Avg	# over 60	total	Avg	# over 60	total
Oct	41	13	854	42	137	1264
Nov	31	1	426	48	72	404
Dec	27	0	782	48	77	795
Jan	31	0	628	44	15	869
Feb	37	10	1077	40	45	1507
Mar	48	92	973	35	86	2251
Apr	58	537	1496	31	54	1618
May	65	1394	1474	30	57	1647
Jun	73	1408	1408	33	147	956
Jul	72	1026	1026	36	246	1676
Aug	60	730	1404	33	286	2107
Sep	53	49	308	40	302	1740

VI.3.5 Collector Model Method Results

Again, as in the last subsection, the results using this method are presented here even though the experimental data is poor. The main purpose for showing the results in this subsection is to show how "bad" data affects this method.

Section (IV.2.2) describes the theory and approach used to obtain the results given in this subsection. This method differs from the efficiency method since the

$F_R(\tau\alpha)_n$ and F_RU_L values are not calculated for each individual month. Instead an equation is found which gives all of the $F_R(\tau\alpha)_n$ - F_RU_L pairs that cause the collector model to gain the same monthly total energy that was actually gained by the Honeywell system.

The ten $F_R(\tau\alpha)_n$ - F_RU_L relation lines (April and September were not done) calculated from the experimental data are plotted in figure (6.3.3) and have the form:

$$F_RU_L = A\,(F_R(\tau\alpha)_n) + B \qquad (6.3.2)$$

where (A) and (B) for each month are given in table (6.3.10). As stated in section (IV.2.2) theoretically all of the lines should cross at a single point if the collector characteristics are the same for every month. However figure (6.3.3) shows no grouping of the lines for F_RU_L greater than zero. There are two groups formed for F_RU_L less than zero but they have no meaning since F_RU_L must be positive. The large variation is due to using T202 as the collector input temperature for the collector model and since it is used to calculate the experimental collector energy gain, which will cause the $F_R(\tau\alpha)_n$ - F_RU_L relationship lines to intercept the y-axis at a different point. Also the large beam radiation incidence angles that occur during the summer months may have had an effect on the results for May thru August. Another possible reason for some of the variance could be due to the change in collector flow scheme starting on April 16th.

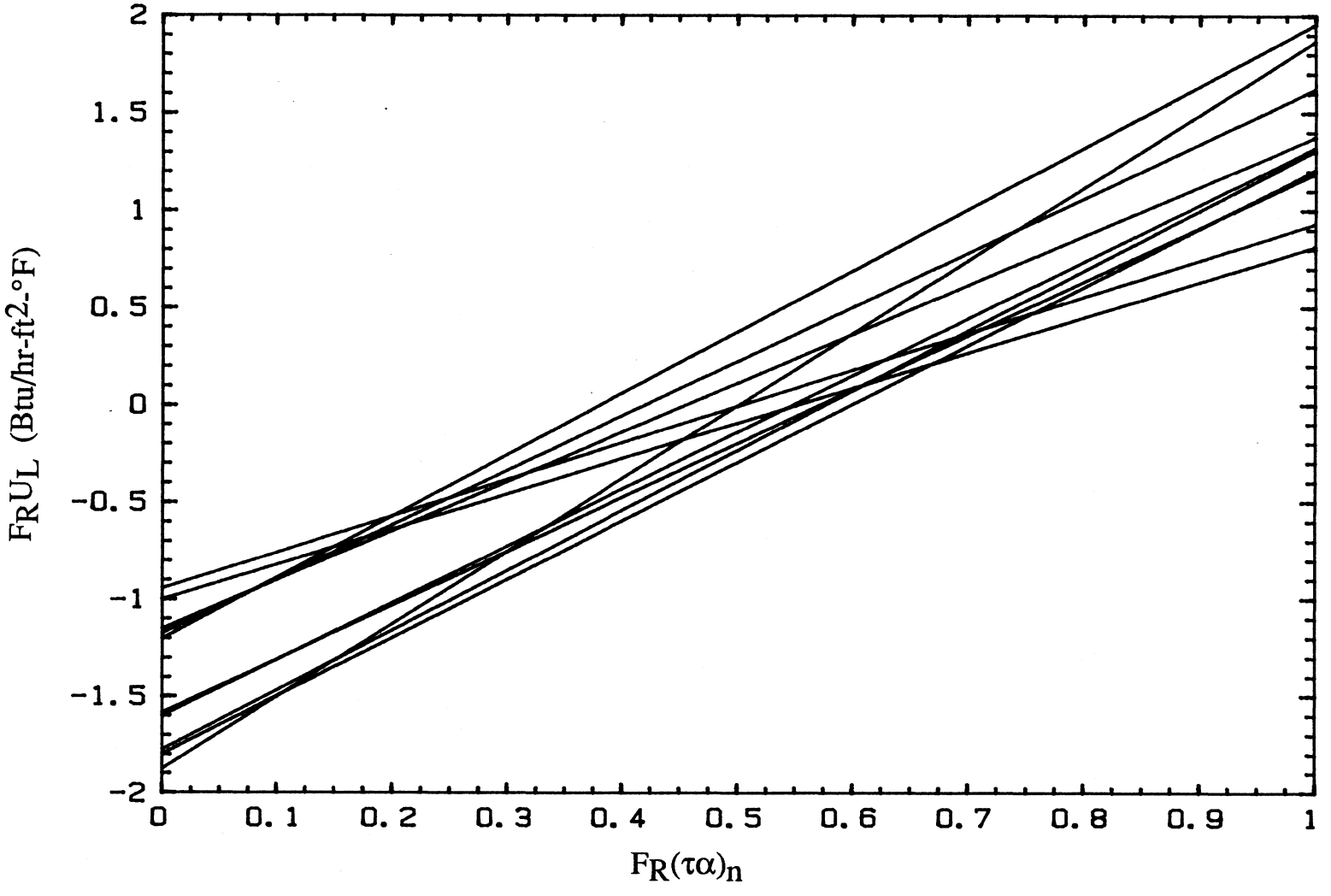

FIGURE 6.3.3 Monthly $F_R(\tau\alpha)_n$ - F_RU_L relationship lines calculated using the collector model method. (Honeywell)

TABLE 6.3.10 Constants used in equation (6.3.1) for each month to give the $F_R(\tau\alpha)_n$ - F_RU_L relationships for the collector model method. (Honeywell)

Month	A	B
Oct	3.16	-1.21
Nov	3.75	-1.88
Dec	2.80	-1.18
Jan	2.93	-1.60
Feb	3.09	-1.78
Mar	2.78	-1.59
Apr	*	*
May	3.01	-1.80
Jun	1.82	-1.00
Jul	1.88	-0.95
Aug	2.53	-1.15
Sep	*	*

* April and September were not done.

VI.4 SYSTEM MODEL RESULTS

VI.4.1 Model

The entire Honeywell system is modeled except the space heating load components. This means that the space heating loop only includes a pump and the

water-to-air heat exchanger. The reason for not including the space heating load (house) in the model is that it is very hard to accurately model a house unless the dimensions, wall heat loss values, etc. are known. These values were not known and there were not any data, other than indoor temperature, that could have been used to estimate the required values. The auxiliary furnace was also excluded due to the uncertainty in the air flow measurements and also since it adds nothing useful to the model if the house is not included.

The DHW and space heating loads were included in TRNSYS by inputting the experimental data. The DHW draw (WT300) and the city mains water temperature (T300) were input to the DHW tank model so that the model sees the same load that occurred in the actual system. The space heating load was included by inputting the air flow rate (W400) and temperature (T410) into the water-to-air heat exchanger model. Beginning in March the air flow rate meter (W400) started recording inaccurate readings; therefore, the sensor readings could not be used as input to the simulation model. Therefore, a constant value of 700 fpm (average flow rate over the previous months) was used for months after March. Flow through the water side of the space heating loop was set equal to the experimental flow (WT400).

The simulation was run for March, June, and August since 99 percent of the data records were available for them. The ASHRAE test values ($F_R(\tau\alpha)_n$, F_RU_L, and b_o) were used in the collector model. Their values are 0.787, 1.25 (Btu/hr-ft^2-°F), and 0.236. The effectiveness values for the space heating and the DHW heat exchangers were 0.35 and 0.45, respectively. (These values were calculated by Vitro from the experimental data as average effectiveness values for the two heat exchangers.) The upper and lower dead band temperatures used to control the DHW pump were 20° and 10° F, respectively. A copy of the TRNSYS deck used to run the simulations is listed in Appendix (D).

VI.4.2 Results

The energy values compared are listed and defined in table (6.3.11). The results for the three months are shown in table (6.3.12) along with the experimental values.

TABLE 6.3.11 Listing and definition of the monthly energy values calculate by the Honeywell system model. All values are measured in Btu.

Q_{in}	-	energy from the collector into the main storage tank
Q_{sp}	-	energy supplied to the air stream by the water-to-air heat exchanger in the space heating loop
Q_D	-	energy transferred from the main storage tank to the DHW tank
Q_{aux}	-	energy supplied by the the auxiliary heater in the DHW tank
$Q_{D,L}$	-	energy supplied to the load by the DHW tank
Q_L	-	$(Q_D + Q_{sp})$ - total energy supplied to the loads
T_D	-	average water temperature delivered to the load by the DHW tank
T_M	-	average water temperature in the main storage tank

The experimental values listed in table (6.3.12) show for June and August that the energy into the main storage tank is incorrect since it is larger than the amount of energy delivered to the load ($Q_{sp} + Q_D$). As explained in section (VI.2.2), the reason for the incorrect values is that temperature sensor T100 went bad in January and T202 had to be substituted.

TABLE 6.3.12 Honeywell simulation results.

Method	Q_{in}	Q_{sp}	Q_D	$Q_{D,L}$	Q_{aux}	Q_L	T_D	T_M
March								
Exp.	1.74	0.55	0.76	1.73	1.25	1.30	92	132
Sim	1.14	0.86	~0	1.51	1.70	0.86	96	127
June								
Exp.	0.72	0.01	0.81	1.50	1.02	0.82	104	140
Sim	0.12	0.02	0.0	1.55	1.74	0.02	85	122
August								
Exp.	1.32	0	1.57	1.57	0.2	1.57	135	137
Sim	0.63	~0	0.14	2.22	2.27	0.14	109	126

For all three months the simulated energy gain is much lower than the experimental energy gain (compare the simulated values to the total energy supplied to the load (Q_L) since at worst the collector energy would have to be greater than the energy supplied to the load). As explained in section (VI.3.4), two possible explanations for the low energy gains during June and August are based on the beam radiation incidence angle on the pyranometer and on the collector, each of which is larger than 60 degrees during most of the months (see table (6.3.9)). The reason for the low energy supplied to the DHW tank (Q_D) is due to the low collector gain resulting in a low storage tank temperature. Since the upper dead band temperature for the DHW tank pump is 20° F, the main storage tank temperature, at a minimum, must be greater than 140° F for energy to be transferred to the DHW tank.

The amount of energy transferred to the DHW tank depends on the effectiveness of the heat exchanger used in the tank and on the dead band temperatures used to run

the pump DHW loop pump (P3 in figure (6.1.1)). To show what effect the dead band temperature has on the amount of energy transferred to the DHW tank the simulation was run using 0 as the upper and lower dead band temperatures (i.e. zero dead band). This means that the DHW pump will run whenever the DHW tank temperature is lower than the storage tank temperature. Using this scheme for August the amount of energy supplied to the DHW tank increased to 0.65 million Btu and the collector energy gain increased to 1.28 million Btu. So decreasing the dead band temperature will increase the total amount of energy transferred. However, the energy consumed by the pump increases as the dead band decreases.

Due to the high incidence angles during the spring and summer months the results from the simulation runs and from the collector results given in section (VI.3) indicate that a TRNSYS model would not do an accurate job predicting the system results. However, the final results for the Honeywell system are very dependent on the collector model since the amount of energy available to the loads is the main factor on how well the system does. For example, it does not matter how efficient the DHW heat exchanger is if the main storage tank temperature never gets high enough for the DHW pump to turn on. Therefore, for energy systems that collect low amounts of energy (where the definition of "low" depends on the size of the storage system and the size of the loads) the system simulation results will be dependent on how well the field collector is modeled. If large amounts of energy are available, then the system simulation results (and in this case the actual field systems performance) will depend on the methods used to transfer energy from the storage tank to the loads (i.e. using a once through pre-heat for the DHW subsystem or the supply-side heat exchanger loop used in the Trident and Honeywell systems, respectively). The results will also depend on the size of the equipment and its efficiency. For example, using too large a pump will result in larger electricity consumption which may not be offset by a larger heat transfer rate if the other components are not correspondingly sized.

VII. CONCLUSIONS AND RECOMMENDATIONS

VII.1 CONCLUSIONS

The results from this study can be summarized as follows:

A: Collector Parameters

The ASHRAE test parameters do not seem to adequately describe the collector characteristics of the field panels. When used in the TRNSYS model they underpredicted the collector gain during all months for the Trident system. The reason for the difference between the experimental and "predicted" (ASHRAE) energy gains cannot be determined since there is no way to verify the experimental collector fluid flow or the collector inlet or outlet temperatures.

The efficiency method (used to calculate $F_R(\tau\alpha)_n$ and $F_R U_L$ from the experimental data) does a better job than the ASHRAE results even if the incidence angle modifier ($K_{\tau\alpha}$) was not included in the efficiency and operating point calculations. This indicates that either the ASHRAE test values do not describe the field collector characteristics or else that the experimental data is not accurate. Again there is no way to determine if the experimental data is accurate.

The incidence angle modifier $K_{\tau\alpha}$ should always be included when calculating the collector parameters from the experimental data. Using $K_{\tau\alpha}$ increased the collector performance providing closer results to the actual collector energy gains. However the results indicate that this may not be true if the incidence angle is larger than 60 degrees

during most of the month, as was the case during the summer months for the Honeywell system. The problem could also have been due to the large incidence angles of the beam radiation on the pyranometer since it was mounted in the plane of the collector (i.e vertically).

The collector model method did the best job calculating an $F_R(\tau\alpha)_n$ and F_RU_L pair that approximated the actual collector gain during every month. Using this method it was also possible to see that the collector characteristics had changed for the Trident system, whereas the efficiency method did not show this. The reason the collector model method results did not give worthwhile results for the Honeywell system was due to the large incidence angles, the fact that accurate collector energy gains could not be calculated, and/or errors in the data measurements. Also, in addition to being able to show abrupt changes in the collector characteristics, this method also calculates a single $F_R(\tau\alpha)_n$ and F_RU_L pair (more than one if the collector characteristics change as in the Trident system) which can be used in TRNSYS models. This eliminates the need to have separate decks for every month so that the collector parameters can be changed which would have been required with the monthly efficiency method results. (A single $F_R(\tau\alpha)_n$ and F_RU_L pair was also calculated using the efficiency method and would probably also have done a good job predicting the collector energy gain if the collector characteristics had not changed significantly as they did for the Trident system.)

B: Immersed Heat Exchanger

Modeling the immersed heat exchanger externally destroys stratification in the storage tank. It was not possible to determine for sure how this would affect the overall performance of the system since the experimental energy provided to the load

was not accurate. However, comparing the inlet energy to the tank with the experimental inlet energy indicated that the loss of stratification would reduce the performance of the system.

The immersed heat exchanger model could not be adequately tested, but comparing the inlet energy calculated using the model with the experimental inlet energy indicated that the immersed model would do a better job than the external model.

C: System Modeling

Modeling the loads in a system will increase the error in the model if accurate parameters (i.e. heat loss coefficients for the house, size, etc.) are not known about the load. A better method (at least as a preliminary step) is to model the system without the load comparing the model results with the experimental values calculated at the cutoff point.

When modeling systems that collect low amounts of energy (where the definition of low depends on the size of the storage system and loads) the accuracy of the collector model will determine how much energy is delivered to the loads. If the energy gain by the collector is high then the configuration, control strategies, and size of the components will determine the amount of energy delivered to the load.

The setup used to supply energy from the main storage tank to the DHW tank (like in the Honeywell system) will not work well if the solar energy gain by a system is so small that the temperature of the main storage tank stays below the set point of the storage tank. When the main storage tank temperature remains low in temperature an immersed heat exchanger (like that use in the Trident system) should be used since

some energy gain will occur since the city mains water supply will almost always be less than the storage tank temperature.

VII.2 GENERAL USEFULNESS OF THE NSDN DATA

The comments provided in this subsection are meant to summarize the advantages and disadvantages of using the NSDN data and its usefulness for further studies. (In no way are the following comments meant to criticize the way the data was taken, the condition of the data and documentation, or the methods used by Vitro to analyze the data. The comments are only meant to point out the present state of the data which would be encountered by someone trying to use the data.)

Advantages:

1) The data was taken at 5 minute 20 second time intervals so that considerable data are available, which can be very helpful when making comparisons between system and component models.

2) Many different sensors are located throughout the systems providing information at entry and exit points of the components. Again this would be very helpful when checking component models or to look at the performance of a specific component in the actual system.

Disadvantages:

1) The documentation on some systems is very poor. Usually the manufacturers specifications are not known for the system components (i.e.

pump and fan sizes, heat exchanger effectiveness values, furnaces and hot water heater sizes and effectiveness values, etc.). These types of values are needed to run simulation models. Also the the rated values are needed so that comparisons can be made between the rated and actual performance. Using the experimental data (which will always have some error) to calculate parameters as the heat exchanger effectiveness values, tank heat loss coefficients, etc. may not give accurate values, and their use in simulations can lead to errors.

2) There are many gaps in the data ranging from a single timestep to most of a month (meaning no sensor readings are available during the gap). This makes it very hard to run TRNSYS simulations and make comparisons with the experimental data since TRNSYS requires equally spaced data input. The data gaps can be filled in but this adds error to the comparison results since the data used to fill the gaps are only approximated.

Additional items:

1) In the back of Vitro's reports on the systems they list the equations that were used to calculate the different energy values they list in their report; however, if a problem occurs during the data collection period and the equation used changes this is not always indicated in the report and the person using the data must refer to the computer code used by Vitro to generate each months data to determine what form of the equation was actually used.

2) Vitro had problems with some of the data measurements. These problems were indicated in their reports for sensors that they used to calculate energy

values given in their report; however, if they did not use the sensor, it is not always documented. For example, they had trouble with the timer measurements used to indicate how long a pump or fan had been running. Since they did not use the timer measurements in any of their calculations they did not indicate in their documentation that the timer measurements were inaccurate. This problem was discovered when making comparisons between the timer and flowmeter data and verified through conversations with Vitro that they had a problem with the timer values. This means that someone using the data must be careful about what data should and should not be used.

3) Throughout this work the author was able to contact Vitro for information on how the data was collected, why a sensor was bad, etc. This was very helpful in understanding the data results and made it much easier to use the data tapes. Given the lack of documentation for many of the systems someone trying to use the tapes without contact with Vitro could be very frustrating.

From the above list it should be obvious that many problems were encountered when using the NSDN data from the two systems in this study. Based on the authors experience and the lack of documentation for the systems, use of the NSDN data is not recommended for system simulations. Also due to the questions raised about the accuracy of the data (regarding the collector energy gains as noted in section (V.3.7)) it is recommended that when comparing experimental and predicted results the work should be done at the same time as the data is being collected so that data measurements can be verified. However, since some systems are documented better than others the data may be useful to someone who needs experimental data to develop or verify a

component model, determine the performance of a component over short periods of time (depending on the amount of continuous data available), etc. However, the systems must be looked at on an individual basis to determine the amount of documentation and data available, and any sensor problems that were encountered.

VII.3 RECOMMENDATIONS FOR FURTHER WORK

The following recommendations are made for future work based on the results presented in this work:

1) The collector model method should be tried on more collectors to determine how well it works. The systems looked at should have collectors at various slopes so that the effect of the incidence angle on the results can be studied.

2) The immersed heat exchanger model should be tested against experimental data from a load-side, immersed heat exchanger that has a significant amount of stratification in the tank. The tank temperature should be measured at many different levels so that the model results can be compared assuming different numbers of tank nodes.

APPENDIX A.1

This appendix contains a listing of the significant events sheet provided by Vitro for the Trident system.

TRIDENT SYSTEM SIGNIFICANT EVENTS

DATE	EVENT
May 18, 1984	System installation completed.
May 19, 1984	Instrumentation installation completed.
May 19, 1984	Vitro site checkout completed. F300 gas meter and ET200 and T150 were defective.
June 2, 1984	During DHW usage, there is reverse flow in space heating loop. DHW usage in "summer" mode 100% usage.
June 10, 1984	Trident's sensor in storage tank caused a short and all pumps were activated. Approximately 10,000 gallons of cold water were added to storage tank and overflowed on the basement floor.
June 11, 1984	Trident's TINA controller turned off all pumps and fans.
June 26, 1984	Temperature sensor T150 is reading extremely high values, using T151 as an alternate sensor.
June 27, 1984	DHW mode was changed to "preheat" mode.
June 29, 1984	New gas meter F300 was installed and ET200 was replaced. Both were verified as operational. Also, check valve installed in space heating loop to prevent backflow.
June 30, 1984	Used a work-a-round to filter out extraneous flow during testing and problem times in June for solar energy collected and solar energy to storage.
July 1, 1984	Low DHW usage of approximately 18 gallons per day.

July 13, 1984	High DHW usage of 350 gallons per day.
September 11, 1984	T150 repaired during site visit. Prior to this date, T151 substituted for T150 in computer code.
September 15, 1984	DHW consumption level adjusted to approximately 127 gallons per day.
September 26, 1984	Auxiliary space heating unit not responding to demand for heating. (Suspect natural gas turned off.)
October 10, 1984	Gas line was opened and operating O.K.
October 14, 1984	Auxiliary space heating unit not responding to a heating demand.
October 24, 1984	Auxiliary unit now working properly again.
October 31, 1984	A problem with Trident's TINA controller resulting in continuous DHW consumption, collector pump being off, and no space heating during a large period of the month.
November 1, 1984	The same problem mentioned above continued through the month.
December 6, 1984	No DHW usage. Collector pump damaged and was replaced. Very low solar space heating usage. This is due to control problems.
January 10, 1985	Temperature sensor T401 reading high. Using alternate sensor T251. (No action planned for replacement.)
January 1985	Control problems continue with no DHW usage for the entire month and very low solar utilization for space heating.
February 4, 1985	System now using DHW usage. Control problems continue.
March 22, 1985	Trident personnel corrected the control problems which were causing the furnace to shut off on high limit and stay in auxiliary mode.
June 10, 1985	SDAS removed from site and no further data collection for Trident PSM.

APPENDIX A.2

This appendix contains a listing of the system/instrumentation failure and work-around sheet provided by Vitro for the Honeywell system.

SYSTEM/INSTRUMENTATION FAILURE AND WORK-AROUNDS USED: HONEYWELL SYSTEM

DATE	EVENT
T100, T101	Starting in January, these sensors appeared to read low. The reason for the apparent low readings could not be determined, although several things were tried:

2/8/84	Sensors were replaced.
7/17/84	The stems of the sensors were insulated.
9/17/84	Sensors and SDAS system fully checked and recalibrated.

Since the problem was never resolved, other sensors were substituted for T100 and T101 as follows. (Sensor T202 appears to provide the most satisfactory results):

1/1/84	- 1/26/84	-	T200
2/1/84	- 2/7/84	-	T200
2/7/84	- 9/30/84	-	T202

T150 — There appeared to be a problem with T150 during the last part of January and the first part of February. Although the sensor was checked in 2/8/84 and again 9/17/84, no problem could be found. In the end it was decided that T100 and T101 were a fault. For the period 2/1/84 - 2/7/84, T151 was substituted for T150.

T300 — For some unknown reason the SDAS failed to read T300 for the period from 1/1/84 through 2/7/84. A constant value of 45° F was used during this period. The sensor was repaired 2/8/84.

WT300 — Initially this sensor was equipped with a 1000 gallon register. The register was replaced with a 100 gallon register 11/15/84. The

calibration code was not updated until 12/14/84. Therefore, values given on the data tape should be divided by 10 for this period. This was done in our computer code only for the period in January, therefore, values given in the report for November may be a little high. On the other hand, after the register was changed the energy balance for the DHW subsystem was poor. Based on a bucket test of the sensor done 5/10/84, all values from WT300 have been multiplied by 2.1 for the period from 12/1/84 through 9/30/84 when calculating hot water consumption and energy usage.
On 12/19/83 there were several power interruptions at the site. The reading recorded at 16:09:32 dropped from 84.7 to 10.1. This causes our computer code to indicate more than 100 gallons had been used unless we set the reading for this scan equal to 84.7.

W410 — Based on duct mapping done at instrumentation checkout, readings from this sensor should be multiplied by 0.85 to determine true air flow through the duct. For some reason the sensor exceeded its maximum on 10/10/83 and 10/11/84. Beginning in March, the readings of the sensor decreased form 700 fpm to between 200 and 400 fpm. After 3/1/84, W410 was set to a constant value of 700 fpm whenever the fan was on. All calculations using W410 were used for check purposes only. Other sensors were used to calculate performance factor values.

F400 — This sensor was supposed to have a 1000 cubic foot register instead of a 10,000 cubic foot register. All values through 12/14/83 when the calibration code was corrected, should be divided by 10.

APPENDIX B.1

This appendix contains a listing of the TRNSYS deck used to calculate the total collector energy gain over a month.

```
* TRIDENT SYSTEM - collector deck. Use to calculate the
* monthly total energy gain given a FR(τα)n - FRUL pair.
* Can be the ASHRAE, efficiency method, or Collector model
* method values.
*
* The CONSTANTS cards are used so that the same deck can be
* used for all 12 months. Only the CONSTANTS cards have to
* be changed.
*
* The following are examples of the constant values used.
*
* --- AUGUST ---
* CONSTANTS TSTART=5088.0888888 TEND=5832. TBEG=5088. DAYS=213.
* CONSTANTS FRTA=.637 FRUL=.245 GT=9.25 FLOW=2590. RHO=.2
*
* --- MARCH ---
* CONSTANTS TSTART=1416.0888888 TEND=2160. TBEG=1416. DAYS=60./8
* CONSTANTS FRTA=.637 FRUL=.245 GT=6.94 FLOW=1942. RHO=.4/13
*
* Use GT=8.1 for entire year efficiency method curvefits.
* FLOW is the simulation collector flow rate.
* 5.2 gpm = 2590. lbm/hr, 4 gpm = 1942. lbm/hr
**********************************************************************

CONSTANTS TSTART=5088.0888888 TEND=5832. TBEG=5088. DAYS=213.
SIMULATION    TSTART  TEND  0.0888888
WIDTH 80
LIMITS 100 4
TOLERENCES  -0.0001  -0.0001
CONSTANTS FRTA=.637 FRUL=.245 GT=9.25 FLOW=2590. RHO=.2
NOLIST

*-------------------------------------------------------
* Values read in:  Insol  Tamb  WT1  T101
*                    1      2     3    4
*-------------------------------------------------------

UNIT 1   TYPE 9   CARD READER
  PARAMETERS  16
  7.0    0.0888888  -1.0 1.0  0.0  -2.0 1.0  0.0   -3.0 1.0 0.0
  -4.0 1.0 0.0
```

```
  43.0  1.0
(T10,2(F6.2),F8.2,T48,F6.2)

*-------------------------------------------------------

UNIT 39  TYPE 15    CALCULATING INSOL/TIME
  PARAMETERS 5
  -11 -1 0.0888888 1 -4
  INPUTS 1
  1,1
  0.0

UNIT 4   TYPE 42    MODIFIED RADIATION PROCESSOR
  PARAMETERS  6
  3.0   1.0   DAYS  40.0   428.90   0.0  -1.0
  INPUTS  6
  39,1    1,19    1,20    0,0    0,0   0,0
  0.0    TBEG    TBEG    RHO    22.0  10.0

UNIT 5   TYPE  1    FLAT PLATE COLLECTOR
  PARAMETERS  12
  1.0    1.0    280.0  1.0    1.0    GT   FRTA
  FRUL  -1.0    1.0    1.0    0.162
  INPUTS  10
  1,4    0,0  0,0   1,2  1,1  4,4  4,5  0,0  4,9  0,0
  33.72  FLOW FLOW  37.93 0.0  0.0  0.0  RHO  0.0  22.0

*-------------------------------------------------------
* Data manipulations                                   |
*-------------------------------------------------------

UNIT 10  TYPE 15    CALCULATING Q BASED ON RATIO OF FLOWS
  PARAMETERS 7
  -11 -1 FLOW 2 -12 1 -4
  INPUTS 2
  1,3 5,3
  0.0 0.0

*-------------------------------------------------------
* Outputs                                              |
*-------------------------------------------------------

UNIT 48  TYPE 28    PRINT ENERGY GAIN
  PARAMETERS 7
  24.0  TBEG  TEND   102.0  2.0  -11.0 -4.0
  INPUTS 1
  10,1
  LABELS 1
  Qscol
END
```

APPENDIX B.2

This appendix contains a listing of the TRNSYS deck used to model the immersed heat exchanger as an external heat exchanger.

```
* TRIDENT SYSTEM - external heat exchanger deck.
*
* Values given are for MARCH.
*
************************************************************

SIMULATION     1416.0888888   2160.  0.0888888
WIDTH 80
LIMITS 100 4
TOLERENCES  -0.0001  -0.0001
CONSTANTS
NOLIST

*-------------------------------------------------------------
* Values read in: WT3  WT1   WT4  T300  T450  T150
*                   1     2     3     4     5     6
*-------------------------------------------------------------

UNIT 1   TYPE 9     CARD READER
  PARAMETERS  22
  6.0     0.0888888  -1.0 1.0  0.0  -2.0 1.0  0.0   -3.0 1.0 0.0
  -4.0 1.0 0.0  -5.0 1.0 0.0   -6.0 1.0 0.0
  43.0   1.0
(T10,6(F6.2))

*-------------------------------------------------------------

UNIT 14  TYPE  11   Y PIECE
  PARAMETER  1
  1.0
  INPUTS  4
  1,4   1,1   1,5    1,3
  65.1  0.0   91.87   0.0

UNIT 9   TYPE 3    COLL PUMP (#1)
  PARAMETERS  1
  1.0
  INPUTS  3
  13,1    13,2    1,2
  104.2   0.0     0.0

UNIT 13  TYPE 4    STRATIFIED FLUID TANK
```

```
  PARAMETERS 6
  1.0    54.5    1.0    62.4    0.176    -4.25
  INPUTS 5
  1,6     9,2    16,1    16,2    0,0
  67.81   0.0    79.0    0.0     65.0
  DERIVATIVES 3
  115.0  110.5  104.2

UNIT 15  TYPE 3    PUMP FOR HX
  PARAMETERS 1
  1.0
  INPUTS 3
  13,3  13,4  14,2
  0.0   0.0  0.0

UNIT 16  TYPE 5    HX
  PARAMETERS 4
  4.0  EFF  1.0  1.0
  INPUTS 4
  15,1  15,2  14,1  14,2
  0.0   0.0   0.0   0.0

*-------------------------------------------------
* Outputs                                        |
*-------------------------------------------------

UNIT 45  TYPE 15    AVERAGING TEMPS
  PARAMETERS 15
  -11 -1 0.0888888 2 -4  -12 -1 0.0888888 2 -4
  -13 -1 0.0888888 2 -4
  INPUTS 3
  13,3 13,11 13,1
  0.0  0.0  0.0

UNIT 46  TYPE 28    PRINTER
  PARAMETERS 13
  24.  1416.0888888  2160.0    104.0  2.0
  -11 -4 -12 -4 -13 -4 -14 -4
  INPUTS 4
  45,1 45,2 45,3 13,6
  LABELS 4
  T200 T201 T202 QT

UNIT 47  TYPE 15    AVERAGING TEMPS
  PARAMETERS 12
  -11 -12 -13 3 3 -1 3.0 2 -1 0.0888888 2 -4
  INPUTS 3
  13,1 13,3 13,11
  0.0  0.0  0.0
```

```
UNIT 48  TYPE 28     PRINT
  PARAMETERS 16
  24.  1416.0888888  2160.0    102.0  2.0  1
  -11 -4 -12 -4 -13 -4 -14 -4 -15 -4
  INPUTS 5
  13,7 13,5 13,9 13,6 47,1
  LABELS  5
  DE Qenv Qin Qs Tavg

CHECK .10 -1,-2,+3,-4

END
```

APPENDIX B.3

This appendix contains a listing of the changes that must be made to the type 4 TRNSYS tank model so that it contains an immersed heat exchanger.

```
* Modifications to type 4 tank model to include the immersed heat exchanger.

* The converted component can use up to 10 nodes. To increase this you must
  increase the size of the storage matrices.

* INPUT 5 is used to input the heat exchanger effectiveness instead of the
  environmental temperature. The environmental temperature must be changed inside
  this program.
**********************************************************************
Replace line:
    DIMENSION U(16),V(16),QB(16),H(15)                          TY040011
with:
    DIMENSION U(16),V(16),QB(16),H(15),TCOIL(11),Q(10)
C-------------------------------------------------------------------------------------
Replace lines:
    TL=XIN(3)                                                   TY040100
    FLWLL=XIN(4)                                                TY040101
    TENV=XIN(5)                                                 TY040102
with:
    TL = 0.0
    FLWLL = 0.0
    TCOIL(NEQ+1) = XIN(3)
    FCOILL = XIN(4)
    TENV= 65.0
    FCOIL = FCOILL * CPF
     IF(FCOIL.GT.0.0) THEN
        EFF = XIN(5)
    ELSE
        EFF = 0.0
    END IF
C-------------------------------------------------------------------------------------
Delete line: (since must solve the equations starting with the last node)
    NODE = NSTART                                               TY040203
C-------------------------------------------------------------------------------------
Add the following line between lines TY040205 and TY040206:
    NODE = NEQ - N + 1
C-------------------------------------------------------------------------------------
Replace lines:
    AA = -(FL1 + FL2 + UA + UAFI )/MCPN                         TY040246
    BB = (FL1*T1 + FL2*T2 + UA*TENV + UAFI*TFLUE)/MCPN          TY040247
with:
    ONE = EFF*FCOIL
    TWO = EFF * FCOIL * TCOIL(NODE+1)
```

```
      AA = -(FL1 + FL2 + UA + UAFI + (EFF*FCOIL))/MCPN
      BB = (FL1*T1 + FL2*T2+UA*TENV+UAFI*TFLUE+
     +       (EFF*FCOIL*TCOIL(NODE+1)))/MCPN
C-----------------------------------------------------------------------------------------------
Add the following lines between TY040251 and TY040252:
      IF(FCOIL.GT.0.0) THEN
         Q(NODE) = EFF * FCOIL * (S(KAVG) - TCOIL(NODE+1))
         TCOIL(NODE) = Q(NODE)/FCOIL + TCOIL(NODE+1)
      ELSE
         Q(NODE) = 0.0
         TCOIL(NODE) = TCOIL(NODE+1)
      END IF
C-----------------------------------------------------------------------------------------------
Delete the following lines:
85    NODE = NODE + DIRECT                                                    TY040262
      IF (NODE .LE. NEQ) GO TO 90                                             TY040263
      DIRECT = -1                                                             TY040264
      NODE = NSTART - 1                                                       TY040265
C-----------------------------------------------------------------------------------------------
Replace lines:
      AA = -(FLWS + FLWL + UA+UAFI)/MCPN                                      TY040316
      BB = (FLWS*TIN + FLWL*TL + UA*TENV+UAFI*TFLUE)/MCPN                     TY040317
with:
      ONE = EFF*FCOIL
      TWO = EFF * FCOIL * TCOIL(2)
      AA = -(FLWS + UA + UAFI + (EFF*FCOIL))/MCPN
      BB =  (FLWS*TIN + UA*TENV + UAFI*TFLUE +
     .      (EFF*FCOIL*TCOIL(2)))/MCPN
C-----------------------------------------------------------------------------------------------
Add the following lines between TY040321 and TY040322:
      IF(FCOIL.GT.0.0) THEN
         Q(1) = EFF * FCOIL * (S(AVG+1) - TCOIL(2))
         TCOIL(1) = Q(1)/FCOIL + TCOIL(2)
      ELSE
         Q(1) = 0.0
         TCOIL(1) = TCOIL(2)
      END IF
C-----------------------------------------------------------------------------------------------
Add the following lines between TY040363 and TY040364:
      QCOILT = 0.0
      DO 47 I=1,NEQ
         QCOILT  = QCOILT + Q(I)
47    CONTINUE
C-----------------------------------------------------------------------------------------------
Replace line:
      OUT(6)=QTANK                                                            TY040372
with:
      OUT(6) = QCOILT
C-----------------------------------------------------------------------------------------------
```

APPENDIX B.4

This appendix contains a listing of the TRNSYS deck used to test the immersed heat exchanger model.

```
* TRIDENT SYSTEM - Immersed Heat Exchanger Deck.
*
* Uses constant effectiveness values (EFF).
* This deck is for the month of MARCH.
*
************************************************************

SIMULATION     1416.0888888   2160.  0.0888888
WIDTH 80
LIMITS 100 4
TOLERENCES  -0.0001  -0.0001
CONSTANTS
NOLIST

*-------------------------------------------------------------
* Values read in: WT3  WT1   WT4  T300  T450  T150
*                   1     2     3     4     5     6
*-------------------------------------------------------------

UNIT 1   TYPE 9   CARD READER (Trident Data)
  PARAMETERS  22
   6.0     0.0888888  -1.0 1.0  0.0  -2.0 1.0  0.0   -3.0 1.0 0.0
   -4.0 1.0 0.0  -5.0 1.0 0.0   -6.0 1.0 0.0  43.0   1.0
(T10,6(F6.2))

*-------------------------------------------------------------

UNIT 14  TYPE  11   Y PIECE
  PARAMETER  1
   1.0
   INPUTS  4
   2,4   2,1   2,5    2,3
   65.1  0.0   91.87   0.0

UNIT 9   TYPE 3   COLL PUMP (#1)
  PARAMETERS  1
   1.0
   INPUTS  3
   13,1    13,2   2,2
   104.2   0.0    0.0

UNIT 13   TYPE 4   STRATIFIED FLUID TANK
```

```
  PARAMETERS 6
  1.0    54.5    1.0    62.4    0.176    -4.25
  INPUTS 5
  2,6    9,2   14,1    14,2    0,0
  67.81   0.0   79.0    0.0    EFF
  DERIVATIVES 3
  115.0  110.5  104.2

*-------------------------------------------------
* Outputs                                        |
*-------------------------------------------------

UNIT 45  TYPE 15  AVERAGING TEMPS
  PARAMETERS 15
  -11 -1 0.0888888 2 -4
  -12 -1 0.0888888 2 -4
  -13 -1 0.0888888 2 -4
  INPUTS 3
  13,3 13,11 13,1
  0.0  0.0  0.0

UNIT 46  TYPE 28  PRINTER
  PARAMETERS 13
  24.  1416.0888888  2160.0    104.0  2.0
  -11 -4 -12 -4 -13 -4 -14 -4
  INPUTS 4
  45,1 45,2 45,3 13,6
  LABELS 4
  T200 T201 T202 QT

UNIT 47  TYPE 15  AVERAGING TEMPS
  PARAMETERS 12
  -11 -12 -13 3 3 -1 3.0 2 -1 0.0888888 2 -4
  INPUTS 3
  13,1 13,3 13,11
  0.0  0.0  0.0

UNIT 48  TYPE 28  PRINT STORAGE TANK VALUES
  PARAMETERS 16
  744.  1416.0888888  2160.0    102.0  2.0  1
  -11 -4 -12 -4 -13 -4 -14 -4 -15 -4
  INPUTS 5
  13,7 13,5 13,9 13,6 47,1
  LABELS 5
  DE Qenv Qin Qs Tavg

CHECK .10 -1,-2,+3,-4

END
```

APPENDIX C

This appendix outlines an unsuccessful attempt to use the experimental data to find a relationship for the effectiveness values as a function of the difference between the tank and coil water temperatures and capacitance rates. As noted in section (V.4.2.2) it is outlined here since it could be useful as a basis for future work regarding the immersed heat exchanger model.

The idea behind this method was to use the experimental tank temperatures to try and find a relationship between the node effectiveness values and the temperature difference between the "hot" and "cold" fluid flows. Determining this relationship from the experimental data was not possible without further assumptions, since only three equations can be written (eqns (5.4.9 a, b, &c)) and there are five unknowns: ε_1, ε_2, ε_3, T_{M1}, & T_{M2}. Therefore it was assumed that the node efficiencies were all equal at any given moment.

Since the temperature difference between the coil and tank fluids are the driving force for heat transfer, a relationship was sought between the fluid temperature difference (ΔT) and the effectiveness where both values are calculated from the experimental data.

The temperature difference was defined in the following manner. First, the temperature difference between the tank and average coil temperatures was found for each node. Then the average temperature difference was found by averaging the temperature differences found for each node. Referring to figure (5.4.9) the average temperature difference is written:

$$\Delta T_{avg} = \left\{ \left[T_1 - \frac{T_{M1} + T_{coil,i}}{2} \right] + \left[T_2 - \frac{T_{M2} + T_{M1}}{2} \right] + \left[T_3 - \frac{T_{coil,o} - T_{M2}}{2} \right] \right\} / 3$$

$$= \frac{T_1 + T_2 + T_3}{3} - \frac{(T_{coil,i} + 2(T_{M1}) + 2(T_{M2}) + T_{coil,o})}{6} \qquad \text{(A.1)}$$

An alternate method for defining the temperature difference would be to calculate the individual node temperature differences as the tank temperature minus the coil inlet temperature for that node. This would have slightly simplified the equations used, but equation (A.1) should better represent the heat transfer driving force.

It was not possible to calculate the temperature difference directly from the experimental data since the intermediate coil temperatures T_{M1} and T_{M2} were not known. However, these temperatures are also included in the node efficiency equations (5.4.9(a,b, &c)) which can be solved.

Three equally spaced temperature sensors were located in the tank during the data collection; therefore, three nodes were assumed. Since the assumption was made that all of the node effectiveness values are equal at any given moment, equations (5.4.9(a, b &c)) could be solved to calculate the effectiveness. By combining the three equations it was possible to get one of the variables (ε, T_{M1} or T_{M2}) in terms of known values. Once the effectiveness values had been calculated it is possible to calculate the temperature difference (ΔT). As with the collector efficiency plot data calculations, the

efficiency calculations were made with some restrictions placed on the data used. These restrictions were:

1) The collector pump must be off during the entire timestep.

2) Flow must have occurred in the heat exchanger coil during the timestep.

Figure (A.1) shows the experimental effectiveness values as a function of the temperature difference for March (Trident system). The data points with the large temperature differences occur when a DHW only draw has happened. This was expected since the city mains water temperature averaged 43° F during March. At the same time the space heating loop water pipes are all inside the house; therefore, the fluid would never go below a temperature of approximately 65° F.

Looking at the data plots it appeared that a fit of the form:

$$\varepsilon = a\,(1-e^{b\Delta T}) \qquad (A.2)$$

could be used to approximate the relationship between the effectiveness and the temperature difference. The constant "a" determines the maximum value that the effectiveness can have, and "b" determines how fast (relative to ΔT) this maximum is reached. Figure (A.1) shows the March data and the equation that will be used to represent it. The curve has values of a = 0.6 and b = -0.358.

Using this method the average temperature difference could be calculated during each timestep and the effectiveness calculated from equation (A.2). The results when using effectiveness values calculated in this manner did not do as well as when using a single constant effectiveness value in the immersed heat exchanger model. One

possible reason this method does not work as well as when using a constant effectiveness is that without being able to calculate accurate effectiveness values during times when the collector is running, figure (A.1) does not represent an accurate relationship between the effectiveness values and the tank - coil temperature difference. And since it is not possible to accurately calculate an effectiveness when the collector pump is running, due to the mixing action of the return water, a different method is needed to find the effectiveness as a function of the tank - coil temperature difference.

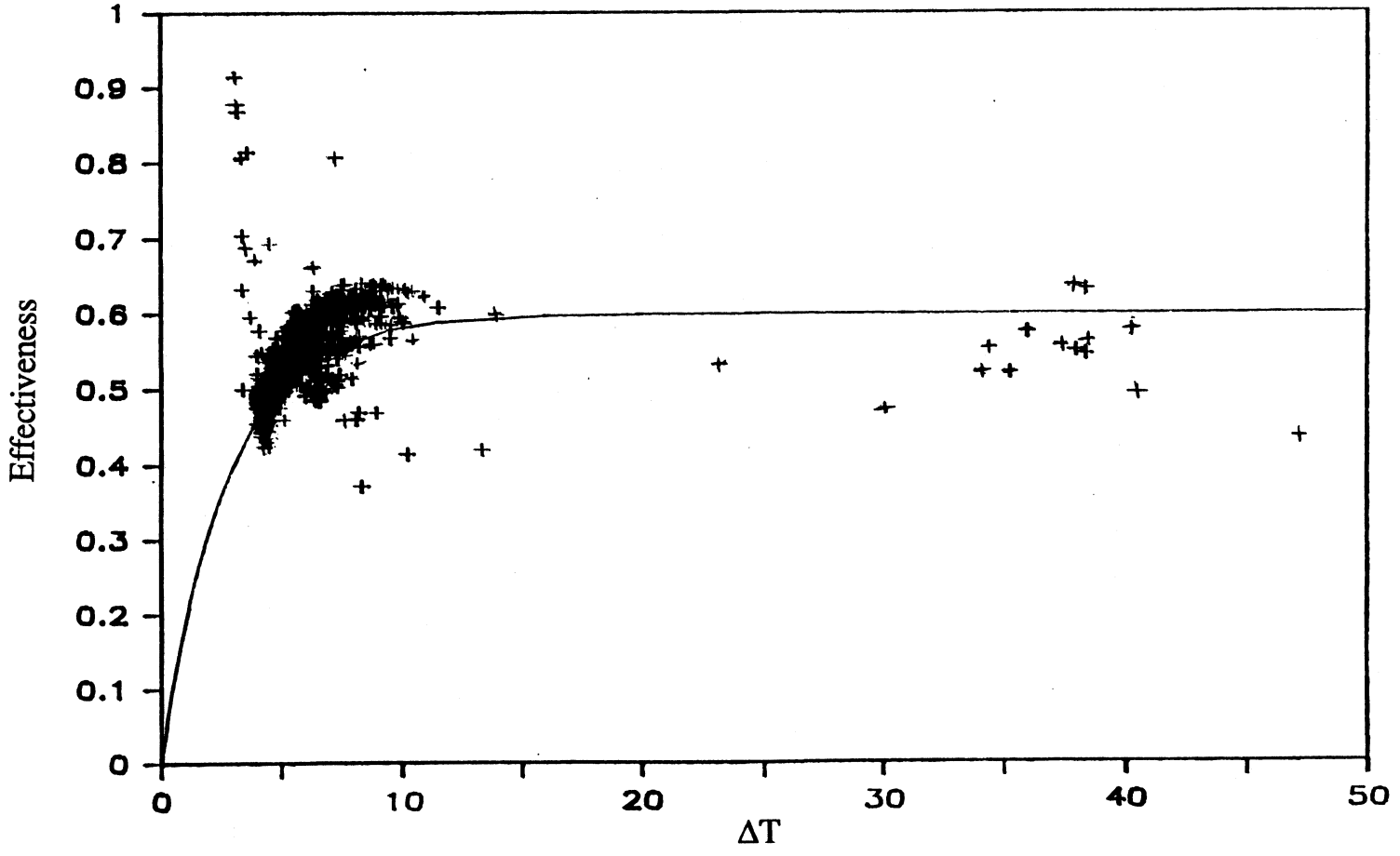

FIGURE A.1 Effectiveness versus average temperature difference (defined in equation (A.1)) calculated from the experimental data for March and the line used to approximate the relationship. (Trident)

APPENDIX D.1

This appendix contains a listing of the Honeywell system deck.

```
* HONEYWELL SYSTEM DECK - MARCH
*-------------------------------------------------------
*
* Examples of the constant cards used for June and August
*
* August
* CONSTANTS FRTA=0.787 FRUL=1.25 GT=14.69/15
* CONSTANTS DHWEFF=0.35 SPCEFF=0.45 COLP=8018./16
* CONSTANTS TOPZ=20. BOTZ=10./17
*
* June
* CONSTANTS FRTA=.787 FRUL=1.25 GT=14.69/15
* CONSTANTS DHWEFF=0.375 SPCEFF=0.45 COLP=8018./16
* CONSTANTS TOPZ=20. BOTZ=10./17
*
* DHWEFF  = Effectiveness of the heat exchanger in the DHW tank.
* SPCEFF  = Effectiveness of the space heating heat exchanger
* COLP  = Averager collector flow rate used as the collector flowrate
* TOPZ  = Upper dead band temperture
* BOTZ  = Lower dead band temperature
*************************************************************************

SIMULATION    1416.0888888  2160.  0.0888888
WIDTH 80
LIMITS 100 4
TOLERENCES  -0.00001  -0.00001
S/CONSTANTS/CONSTANTS FRTA=.787 FRUL=1.25 GT=14.69/15
S/CONSTANTS/CONSTANTS DHWEFF=0.375 SPCEFF=0.45 COLP=8018./16
S/CONSTANTS/CONSTANTS TOPZ=20. BOTZ=10./17
NOLIST

*-----------------------------------------------------------------
* Values input: Insol  Tamb  WT3  T300  WT4  T410
*                  1     2     3    4     5    6
*-----------------------------------------------------------------

UNIT 1   TYPE 9   CARD READER (Trident Data)
  PARAMETERS  22
  6.0    0.0888888  -1.0 1.0  0.0  -2.0 1.0  0.0   -3.0 1.0 0.0
  -4.0 1.0 0.0  -5.0 1.0 0.0   -6.0 1.0 0.0
  43.0   1.0
```

```
(T2,2(F6.2),2(F7.2,F6.2))

*------------------------------------------------------------------

UNIT 4  TYPE 15  Calculating Insol/time
  PARAMETERS 5
  -11 -1 0.0888888 1 -4
  INPUTS 1
  1,1
  0.0

UNIT 5   TYPE 42   MODIFIED RADIATION DATA PROCESSOR
  PARAMETERS  6
  3.0    1.0    60.0   46.78    428.897   -11.0
  INPUTS  6
  4,1    1,19   1,20     0,0    0,0   0,0
  0.0    1416.0  1416.0   0.4    90.0  0.0

UNIT 6   TYPE  1    FLAT PLATE COLLECTOR
  PARAMETERS  12
  1.0    1.0    286.0   1.0    1.0    GT    FRTA
  FRUL  -1.0    1.0    1.0     0.236
  INPUTS  10
  10,1   10,2  10,2  1,2   1,1   5,4   5,5   0,0   5,9   5,10
  33.72  0.0   0.0   37.93 0.0   0.0   0.0   0.4   0.0   0.0

UNIT 7  TYPE 8    3 STAGE CONTROLLER, SETS TANK TEMP HIGH LIMIT
  PARAMETERS 6
  4.0  0.0  0.0  200.0  0.0  0.0
  INPUTS 2
  12,3    0,0
  104.2   0.0

UNIT 8   TYPE  2    PUMP #1 CONTROLLER
  PARAMETERS  3
  4.0    20.0    2.0
  INPUTS  3
  6,1    12,1   8,1
  33.7   81.7   0.0

UNIT 9  TYPE 15    ALGEBRAIC OPERATOR
  PARAMETERS 5
  -11 -12 4 8 -4
  INPUTS 2
  8,1  7,3
  0.0  0.0

UNIT 10  TYPE 3    COLL PUMP (#1)
  PARAMETERS  1
```

```
  COLP
  INPUTS 3
  12,1    12,2    9,1
  81.72   0.0     0.0

UNIT 12  TYPE 4    STRATIFIED FLUID TANK
  PARAMETERS 6
  1.0    46.5    1.0    62.4    0.1635    -3.5
  INPUTS 5
  6,1     6,2    23,1    23,2    0,0
  67.81   0.0    79.0    0.0     65.0
  DERIVATIVES 3
  89.58  87.34  87.23

UNIT 13  TYPE 20   SPECIAL OPERATOR
  PARAMETERS 0
  INPUTS 2
  1,5  16,2
  0.0  0.0

UNIT 14   TYPE  11    FLOW DIVERTER
  PARAMETER  1
  2.0
  INPUTS  3
  12,3  12,4  13,1
  0.0   0.0   0.0

UNIT 15   TYPE  2    DHW PUMP CONTROLLER
  PARAMETERS  3
  4.0    TOPZ  BOTZ
  INPUTS  3
  12,3    18,3    15,1
  33.7    81.7    0.0

UNIT 16   TYPE 3    DHW PUMP
  PARAMETERS  1
  1369.5
  INPUTS  3
  14,1    14,2    15,1
  81.72   0.0     0.0

UNIT 17   TYPE 5    DHW TANK HEAT EXCHANGER
  PARAMETERS 4
* type   eff    Cph    Cpc
  4     DHWEFF  1      1
  INPUTS 4
  16,1  16,2  19,1  19,2
  0.0   0.0   0.0   0.0

UNIT 18   TYPE 4    DHW HX TANK
```

```
 PARAMETERS 13
 1.0   10.64   1.0   62.4   0.1509  -4.03
 14330.4 1     1    130.   10.    0   0
 INPUTS 5
 17,3   17,4  1,4   1,3   0,0
 67.81  0.0   0.0   0.0   65.0
 DERIVATIVES 1
 130.

UNIT 19  TYPE 3   DHW TANK PUMP
 PARAMETERS 1
 1369.5
 INPUTS 3
 18,1   18,2   15,1
 81.72  0.0    0.0

UNIT 21  TYPE 3   SPACE HEATING PUMP
 PARAMETERS 1
 1.0
 INPUTS 3
 14,3   14,4   1,5
 81.72  0.0    0.0

UNIT 22  TYPE 19  MODIFIED SPACE HEAT EXCHANGER
 PARAMETERS 4
* type   eff   Cph  Cpc
 4    SPCEFF   1  0.2404
 INPUTS 4
* note the last m(dot) is set to 3893.2 lbm/hr
 21,1  21,2  1,6  0,0
 0.0   0.0   0.0  3893.2

UNIT 23  TYPE 11   Y PIECE use to sum DHW and Space inputs
 PARAMETER 1
 1.0
 INPUTS 4
 17,1  17,2  22,1  22,2
 0.0   0.0   0.0   0.0

*--------------------  OUTPUT SECTION  -------------------------

UNIT 45 TYPE 15  ALGEBRAIC OPERATOR for SPACE HEATING
 PARAMETERS 8
 -11 -1 5200.0 2 -3
 -12 1 -4
 INPUTS 2
 1,5  22,5
 0.0  0.0
```

```
UNIT 46 TYPE 28   DATA SUMMARY
  PARAMETERS 19
  744.0  1416.0888888  2160.0   104.0  2.0   -11 -4
  -12 -4 -13 -4 -14 -1 8370. 2 -1 .0888888 2 -4
  INPUTS 4
  22,5  6,3  17,5, 18,10
  LABELS  4
  22_5 6_3 17_5 Tav18

UNIT 47  TYPE 28   DATA SUMMARY - DHW TANK
  PARAMETERS 16
  744.0  1416.0888888  2160.0  103.0  2.0  1
  -11 -4 -12 -4 -13 -4 -14 -4 -15 -4
  INPUTS 5
  18,7 18,5 18,9 18,6 18,8
  LABELS  5
  DE Qenv Qin Qs Qaux
CHECK  .03  -1,-2,+3,-4,+5

UNIT 48  TYPE 28   DATA SUMMARY - STORAGE TANK
  PARAMETERS 22
   744.0  1416.0888888  2160.0   102.0  2.0  1  -11 -4
  -12 -4 -13 -4 -14 -4 -15 -1 8370. 2 -1 .0888888  2 -4
  INPUTS 5
  12,7 12,5 12,9 12,6 12,10
  LABELS  5
  DE Qenv Qin Qs Tavg
CHECK  .03   -1,-2,+3,-4

END
```

APPENDIX D.2

This appendix contains a listing and explanation of the TYPE19 and TYPE20 components in the Honeywell system deck (located in Appendix E.1).

TYPE 19

```
* The TYPE19 component is a modified TYPE5 heat exchanger model. Its purpose
* is to make sure that the lower thermal capacitance is the air side at 700 fpm. This is
* done since the air flow rate measured by Vitro was in error and they used a constant
* value of 700 fpm.
*****************************************************************************
Replace lines:
    CMAX = AMAX1(CC,CH)                                          TY050036
    CMIN = AMIN1(CC,CH)                                          TY050037
    IF (CMIN .LE. 0.) GO TO 98                                   TY050038
with:
    CMAX = CH
    CMIN = CC
    IF(CMAX.EQ. 0.) GO TO 98
```

TYPE 20

```
* The TYPE20 component is used to calculate the fraction of flow
* going into the space heating part of the deck.
*****************************************************************************

    SUBROUTINE TYPE20(TIME,XIN,OUT,T,DTDT,PAR,INFO)
    DIMENSION XIN(2),PAR(15),OUT(20),INFO(10)

C  XIN(1) =  WT4,     XIN(2) =  WT301

    WT4  = XIN(1)
    WT301 = XIN(2)
    IF(WT4.EQ.0.0) THEN
       GAM = 0.0
    ELSE
       GAM = WT4/(WT4+WT301)
    END IF
    OUT(1) = GAM

    RETURN
    END
```

REFERENCES

1. Klein, S. A., *et al.*, TRNSYS 12.1 User's Manual, University of Wisconsin-Madison, Solar Energy Laboratory, Engineering Experiment Station Report 38-12, (1983).

2. American Society of Heating, Refrigerating, and Air-Conditioning Engineers, ASHRAE Standard 93-77, Methods of Testing to Determine the Thermal Performance of Solar Collectors, (1977).

3. Vitro Corp., "Packaged Residential Active-Solar Space-Conditioning System - Appendix E: System Performance Monitoring," SERI/STR-253-2620E (DE86010694), May 1986.

4. Farrington, R. B., "Collectors Tested in the Packaged Systems Program," SERI/TR-254-2838 (DE86010723), June 1986.

5. Farrington, R. B., "Test Results of Immersed Coil Heat Exchangers and Liquid Storage Tanks Used in the Packaged Systems Program," SERI/TR-254-2841 (DE86010721), June 1986.

6. Feiereisen, T. J., "An Experimental Study of Immersed Coil Heat Exchangers," M.S. Thesis, University of Wisconsin-Madison, (1982).

7. Honeywell Inc., "Packaged Residential Active-Solar Space-Conditioning System - Appendix C: Honeywell Drainback Heating and Domestic Hot Water System Using a Vertical Wall Integrated Polymer Collector," SERI/STR-253-2620C (DE86004464), May (1986).

8. Carlisle, N. A., Farrington, R. B., and Miller B. J., "Packaged Residential Active-Solar Space-Conditioning System - A Summary," SERI/TR-253-2620 (DE86010735), September (1986).

9. Trident Inc., "Packaged Residential Active-Solar Space-Conditioning System - Appendix D:," Draft Report, August (1985).

10. Duffie, J. A. and Beckman, W. A., Solar Engineering of Thermal Processes, John Wiley and Sons, Inc., New York, (1980).

ADDITIONAL REFERENCES:

Klett, D. E., Goswami, D. Y., and Saad, M. T., "Thermal Performance of Submerged Coil Heat Exchangers Used in Solar Energy Storage Tanks", Journal of Solar Energy Engineering 106, pp. 373-375, (1984).

Pollock, E., Vitro Corporation, telephone conversations, (1985-1987).